Contributions to Theory of Few and Many-Body Systems in Lower Dimensions

Tianhao Ren

Submitted in partial fulfillment of the
requirements for the degree of
Doctor of Philosophy
in the Graduate School of Arts and Sciences

COLUMBIA UNIVERSITY

2019

Abstract

Contributions to Theory of Few and Many-Body Systems in Lower Dimensions

Tianhao Ren

Few and many-body systems usually feature interesting and novel behaviors compared with their counterparts in three dimensions. On one hand, low dimensional physics presents challenges due to strong interactions and divergences in the perturbation theory; On the other hand, there exist powerful theoretical tools such as the renormalization group and the Bethe ansatz. In this thesis, I discuss two examples: three interacting bosons in two dimensions and interacting bosons/fermions in one dimension. In both examples, there are intraspecies repulsion as well as interspecies attraction, producing a rich spectrum of phenomena. In the former example, a universal curve of three-body binding energies versus scattering lengths is obtained efficiently by evolving a matrix renormalization group equation. In the latter example, exact solutions for the BCS-BEC crossover are obtained and the unexpected robust features in their excitation spectra are explained by a comprehensive semiclassical analysis.

Contents

Acknowledgments

I gratefully acknowledge the support and guidance of Prof. Igor Aleiner, from whom I learned not only almost all of my physics, but also the altitudes and methods for doing academic research.

I would like to acknowledge the help from my friends at Columbia, they are always a source of discussion and support.

I am especially grateful to my parents and my wife, without their support, my journey toward graduate study would not have been possible.

This work is dedicated to my wife Yuanwen and my son Ruicheng.

Chapter 1

Introduction

Life in lower dimensions is qualitatively different from that in three dimensions. From the few-body aspect, there is no threshold for attractive interaction to produce a bound state out of two particles. There is no Efimov effect [27, 26] for three resonantly interacting particles, thus a single quantity such as the binding energy of the shallow dimer is sufficient for the description of the few-body universality. From the many-body aspect, thermal fluctuations are enhanced since the reduced dimensionality makes the integration over the Bogoliubov $1/k^2$ law logarithmically or linearly divergent. This rules out spontaneously broken continuous symmetry for systems with short-ranged interactions in lower dimensions, known as the Hohenberg-Mermin-Wagner theorem [70, 46]. Likewise, perturbation theory breaks down in lower dimensions, and electronic transport is blocked by random disorder, both are result of similar divergences. Density wave states are favored in lower dimensions since Fermi surface nesting is more prominent. Landau theory of Fermi liquids breaks down in lower dimensions since electronic degree of freedom fractionalizes into charge and spin degrees of freedom with different velocity of propagation, giving rise to a new universality class of quantum liquid known as Tomonaga-Luttinger liquid [43]. The novel features of low dimensional physics have attracted a great deal of research interest and become one of the central topics in condensed matter physics.

Although the theory of few and many-body systems in lower dimensions poses challenges due to strong interactions and divergences, there are powerful theoretical tools to deal with a number of interesting model systems. For few-body theory, effective field theory and nonperturbative renormalization have supplemented the conventional approach of directly solving the Schrödinger equation; For many-body theory, bosonization is developed to describe the universality class of Tomonaga-Luttinger liquid, Bethe ansatz technique is extensively generalized and applied to a wide range of one dimensional

models, and numerical techniques such as quantum Monte-Carlo and density matrix renormalization group are successfully implemented to give out low energy properties with high accuracy. Nowadays, theoreticians are equipped with numerous results and tools to explore the world of low dimensional physics. Also the situation of model systems in lower dimensions as a playground for theoreticians to test ideas and gain insights has been changed recently, due to experimental realizations of quasi-one and two dimensional systems in semiconductor quantum well structures, confined cold atom gases and organic compounds. As a result, the theory of low dimensional systems has gained reignited interest and been confronted with real-world tests and applications.

In this thesis, we make several contributions to the theory of few and many-body systems in lower dimensions. In chapter 2 we investigate the few body physics of three interacting bosons in two dimensions. The bosons are classified in two species, where the interaction between same species is repulsive and between different species is attractive. Instead of solving variants of the Schrödinger equation or integral equations for the scattering amplitude, a matrix renormalization group equation is derived and efficiently evolved to search for possible three-body bound states for the system under study. Only one trimer is found and its binding energy $\epsilon_b^{(3)}$ is determined for a wide range of scattering lengths. Although there is no universal phenomenon like accumulation of Efimov trimers, a universal curve of $\epsilon_b^{(3)}/\epsilon_b^{(2)}$ ($\epsilon_b^{(2)}$ is the binding energy of the shallow dimer) is found, which depends only on the scattering lengths but not on the microscopic details of the interactions.

In chapter 3, we introduce a new type of models for two-component systems in one dimension subject to Bethe ansatz analysis. The intraspecies interaction c_1 is repulsive and the interspecies interaction c_2 is attractive, and they are tunable via Feshbach resonances. This type of models interpolates between the Lieb-Liniger model and the Yang-Gaudin model, and its integrability is obtained by fine-tuning the resonant energies. There are two interesting regimes of this type of models, showing different behaviors. In the regime with $c_1 > c_2$, the ground state is a Fermi sea of two-strings, where the Fermi momentum Q is constrained to be smaller than a certain value Q^*, and it provides an exactly solvable model of BCS-BEC crossover in one dimension. In the other regime with $c_1 < c_2$, the ground state is a single bright soliton even for fermionic atoms, which reveals itself as an embedded string solution.

In chapter 4, we develop a comprehensive semiclassical theory of solitons in one dimensional systems at BCS-BEC crossover. The exact solutions in chapter 3 show robust features of the low energy excitation spectra along the whole crossover, for example, the minimum energy of the $S = 1/2$ excitation remains exactly at $k_F = \pi n/2$, where nm_F (m_F is the mass of the fermionic atom) is the total mass density of the system. Our semiclassical theory explains them as a result of a special

feature of one dimensional systems that the conventional quasiparticle is not stable with respect to soliton formation, thus their validity is beyond integrability. The proposed semiclassical theory agrees quantitatively with the exact solutions on both the deep BCS and deep BEC side and describes qualitatively the smooth crossover. Besides, it resolves the inconsistency of existing semiclassical theory with the exact solution of soliton-like $S = 0$ excitations on the deep BCS side by a new proposal of soliton configuration.

Chapter 2

Three-Boson Bound States in Two Dimensions

2.1 Introduction

The conventional approach to the quantum three-body problem in three dimensions is introduced by Skorniakov and Ter-Martirosian for three fermions in the zero-range-interaction limit [96]. They derived an integral equation for the scattering matrix between an atom and a weakly bound dimer consisting of two atoms via the diagrammatic technique:

$$\begin{aligned} T_3(k,k',E) =& \frac{1}{E+i0-k^2/m-k'^2/m-kk'/m} \\ &+2\int \frac{d^3p}{(2\pi)^3}\frac{1}{E+i0-k^2/m-p^2/m-kp/m}T_2(E-3p^2/4m)T_3(p,k',E), \end{aligned} \tag{2.1}$$

where T_3 and T_2 are the T-matrix for atom-dimer and atom-atom scatterings respectively. It was then recognized by Danilov [17] that the Skorniakov-Ter-Martirosian equation gives a spectrum that is not bounded from below if applied to the case of three identical bosons. This pathology was then resolved by Efimov [27, 26]. He showed that in the resonant limit that the two-particle scattering length $a \to \pm\infty$, there is a condensation of three-particle bound states at the scattering threshold, whose binding energies form a discrete series:

$$\epsilon_b^{(3)}(n) \to \left(e^{-2\pi/s_0}\right)^{n-n_*}\frac{\hbar^2\kappa_*^2}{m}, \quad n \to +\infty, \tag{2.2}$$

where the consecutive binding energies have a universal ratio $e^{-2\pi/s_0} \approx 1/515$. This shows that in addition to the two-body parameter such as the scattering length a, we need to introduce yet another three-body parameter, which can be taken as the scale κ_*. More surprisingly, there are three-particle bound states even in the absence of two-particle bound state, which are referred to as the Borromean halos. These and other related three-body phenomena are collectively referred to as the Efimov physics, and they can be understood naturally from a renormalization group perspective [9, 45, 5].

In two dimensions, it is now known that there is no Efimov effect in the sense that there is no condensation of three-particle bound states or any Borromean halo [5]. As a result, there is no need to introduce any three-body parameter and the binding energy of any possible few-particle bound state is proportional to the binding energy of the shallow dimer. For example, there are only two three-particle bound states with binding energies $\epsilon_b^{(3)}(1) = 16.52\epsilon_b^{(2)}$ and $\epsilon_b^{(3)}(2) = 1.27\epsilon_b^{(2)}$ for identical bosons with zero-ranged potential [13, 12]. It is then worthwhile to generalize the scheme to more complicated systems with possible new universal features. In fact, the universal properties of three-body systems in two dimensions are readily explored in mass-imbalanced systems [6, 7, 8] and for charged particles [14, 34]. Furthermore, it is of particular interest to study systems with interspecies attraction as well as intraspecies repulsion, where few-body bound states plays an important role in determining the nature of the ground state. A primary example is provided by the exciton Bose-Einstein condensates in GaAs-based quantum well structures [18, 102, 54, 19], where there are two kinds of bright excitons with spin projection $J_z = \pm 1$ to the structural axis. The same spin projections repel each other and the opposite spin projections attract each other [72, 73, 15], as shown in Fig (2.1).

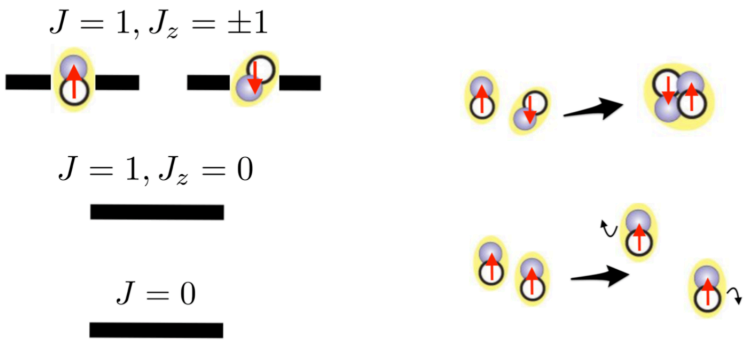

Figure 2.1: Excitons in GaAs-based quantum well structures. The excitons with spin projection $J_z = \pm 1$ are optically active, thus they are referred to as the bright excitons. The coupling between opposite spins is attractive, leading to a shallow dimer, and the coupling between like spins is repulsive.

For these bright excitons in quantum wells, formation of few-body bound states is the possible route to the instability of the condensates. A similar instability in three dimensions is resolved by

Petrov [79], whereas such instability in two dimensions is only approached from the condensation side on the mean-field level [80]. To gain a more quantitative understanding, analysis of the fate of few-body bound states is inevitable. As a first step toward such analysis, we consider three interacting bosons in two dimensions [87]. The interactions between particles are short-ranged, and we model them as contact interaction with finite radius r_0:

$$\delta^2(\boldsymbol{r}) \to \frac{1}{\pi}\delta(r^2 - r_0^2)\Big|_{r_0\to 0}. \tag{2.3}$$

This is suitable for excitonic systems in quantum well structures, where the short-ranged exchange interaction is much stronger than the direct dipole-dipole interaction [101]. We then label the three particles with numbers - particle 1 and particle 2 are of species a and repel each other; while particle 3 is of species b and attracts the other two particles. To avoid unnecessary complications, we choose the unit such that $m = \hbar = 1$. Then the system under consideration is described by the Hamiltonian

$$\mathcal{H} = -\sum_{i=1,2,3}\frac{\nabla_i^2}{2} + \lambda_1\delta^2(\boldsymbol{r}_{12}) - \lambda_2\left[\delta^2(\boldsymbol{r}_{13}) + \delta^2(\boldsymbol{r}_{23})\right], \tag{2.4}$$

where the two-dimensional δ-function is understood to have a finite radius r_0 as in Eq. (2.3). $\lambda_1 > 0$ and $\lambda_2 > 0$ represent the repulsive and attractive couplings, whose low energy scattering lengths are denoted as $\alpha_<$ and $\alpha_>$ respectively:

$$\alpha_< = e^{\mathbb{C}} r_0 \exp\left(-\frac{2\pi}{\lambda_1}\right) \;\; ; \quad \alpha_> = e^{\mathbb{C}} r_0 \exp\left(\frac{2\pi}{\lambda_2}\right), \tag{2.5}$$

where $\mathbb{C} = 0.577\cdots$ is the Euler constant and we have the relation that $\alpha_< \ll r_0 \ll \alpha_>$.

Short-ranged interactions in two dimensions is well-known to present logarithmic poles in the low-energy scattering amplitude [61, 1, 82]:

$$f_>(k) = -\frac{\sqrt{\pi/2k}}{\ln(2i/k\alpha_>)}; \quad f_<(k) = -\frac{\sqrt{\pi/2k}}{\ln(2i/k\alpha_<)}, \tag{2.6}$$

where $k = \sqrt{2\epsilon}$ is the momentum associated with the two-particle energy. The binding energy $\epsilon_b^{(2)}$ of the two-particle bound state can be determined from Eq. (2.6) as the point at which the scattering amplitude for attractive potential diverges:

$$f_>\left(i\sqrt{\epsilon_b^{(2)}}\right) \to \infty \Rightarrow \epsilon_b^{(2)} = \frac{4}{\alpha_>^2}. \tag{2.7}$$

The corresponding pole for the repulsive potential occurs at momentum $|k| \gg 1/r_0$, which is beyond the logarithmic pole approximation, and must be disregarded in the calculation as a spurious solution.

In this chapter, we will show that the system under consideration support at most one three-particle bound state. We will also determine the three-particle bound state energies $\epsilon_b^{(3)}$ for a wide range of scattering lengths $\alpha_>$ and $\alpha_<$, which traces out a universal curve of $\epsilon_b^{(3)}/\epsilon_b^{(2)}$ with no reference to microscopic details. This chapter is organized as follows. In Sec. 2.2 we introduce the parameterization scheme of the problem, and give the formal solution to the resulting one-dimensional Schrödinger equation via a boundary-matching-matrix technique. We also introduce a convenient running basis to the problem, which is suited for numerical implementations. In Sec. 2.3 we give out the explicit solutions for zero and nonzero angular momenta separately. Large scale behaviors are analyzed analytically and three-particle binding energies are calculated numerically. Finally in Sec. 2.4 we summarize the results and compare our methods with existing ones. Some technical details are relegated to the appendices.

2.2 Formalism

2.2.1 Parameterization of the Configuration Space

For the configuration space of the system under consideration, we use the Faddeev parameterization with Jacobi coordinates [29] (see Fig. 2.2)

$$\boldsymbol{r}_{12} = \boldsymbol{r}_1 - \boldsymbol{r}_2, \quad \boldsymbol{\rho}_3 = (\boldsymbol{r}_1 + \boldsymbol{r}_2 - 2\boldsymbol{r}_3)/\sqrt{3}. \tag{2.8}$$

After that, we perform the usual separation of radial and angular parts of the four dimensional vector $(\boldsymbol{r}_{12}, \boldsymbol{\rho}_3)^T$:

$$\begin{pmatrix} \boldsymbol{r}_{12} \\ \boldsymbol{\rho}_3 \end{pmatrix} = r\boldsymbol{N}, \quad \boldsymbol{N}^2 = 1. \tag{2.9}$$

This spherical separation enables us to assign a discrete set of angular level labels j for the wave function $\boldsymbol{\Phi} = (\Phi_0, \Phi_1, \cdots)^T$, due to the fact that the angular momentum operator is compact [24, 22].

Usually, the angular part of four dimensional vector is represented in terms of hyperspherical coordinate Ω in the literature [53, 21, 20, 90], where Ω is a set of three hyperangular coordinates needed to describe the surface of a four dimensional hypersphere. With the hyperspherical coordinates, the

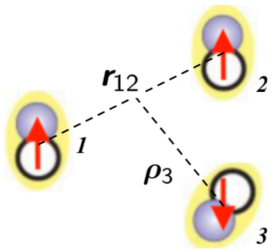

Figure 2.2: Faddeev parameterization of the configuration space of the system under consideration.

$(2j+1)$ states of the level labeled by j are all subject to influence of the interaction potential. As a result, for inclusion of N levels in the numerical calculation, the number of states needed scales as N^2, which results in slow convergence and is a serious numerical burden for large value of N. Here we adopt the Hopf coordinates instead:

$$\boldsymbol{N} = \begin{pmatrix} \sqrt{\frac{1-x}{2}}\cos\phi_1 \\ \sqrt{\frac{1-x}{2}}\sin\phi_1 \\ \sqrt{\frac{1+x}{2}}\cos\phi_2 \\ \sqrt{\frac{1+x}{2}}\sin\phi_2 \end{pmatrix}. \tag{2.10}$$

With the Hopf coordinates, as will be shown later, out of the $(2j+1)$ states of level labeled by j at most two states are affected by the interaction potential. This changes the square dependence to a linear dependence on the number of included levels, resulting in a faster convergence and making the numerical procedure more reliable.

Substituting the above parameterization of the configuration space into Eq. (2.4), the full Laplacian operator can be calculated using the covariant form

$$\nabla^2 = \frac{1}{\sqrt{g}}\nabla_i\sqrt{g}g^{ij}\nabla_j, \quad g = \det\hat{g}, \tag{2.11}$$

where Hopf variables are (r, x, ϕ_1, ϕ_2) and the metric is

$$\hat{g} = \begin{pmatrix} 1 & & & \\ & \frac{r^2}{4(1-x^2)} & & \\ & & \frac{(1-x)r^2}{2} & \\ & & & \frac{(1+x)r^2}{2} \end{pmatrix}. \tag{2.12}$$

The result is a sum of the radial term and the angular momentum term

$$-\nabla^2 = -\frac{1}{r^3}\frac{\partial}{\partial r}r^3\frac{\partial}{\partial r} + \frac{4\hat{L}^2}{r^2}, \tag{2.13}$$

where the angular momentum operator is

$$\hat{L}^2 = -\frac{\partial}{\partial x}(1-x^2)\frac{\partial}{\partial x} - \frac{\partial^2_{\phi_1}}{2(1-x)} - \frac{\partial^2_{\phi_2}}{2(1+x)}. \tag{2.14}$$

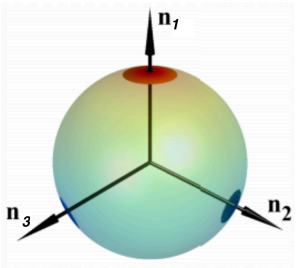

Figure 2.3: Projecting the configuration space onto the three-dimensional sphere. The north pole $\boldsymbol{n}_1$ corresponds to the repulsion and the other two poles $\boldsymbol{n}_{2,3}$ correspond to the attraction.

For the interaction terms, we first project the configuration space onto the three-dimensional unit sphere ($\phi = \phi_1 - \phi_2$):

$$\boldsymbol{n} = (\sqrt{1-x^2}\cos\phi, \sqrt{1-x^2}\sin\phi, x), \quad \boldsymbol{n}_1 = (0,0,1), \quad \boldsymbol{n}_{2,3} = (\pm\frac{\sqrt{3}}{2}, 0, -\frac{1}{2}). \tag{2.15}$$

Then we can express the distances between particles as follows:

$$|\boldsymbol{r}_{12}|^2 = \frac{r^2}{2}(1-\boldsymbol{n}\cdot\boldsymbol{n}_1), \quad |\boldsymbol{r}_{i3}|^2 = \frac{r^2}{2}(1-\boldsymbol{n}\cdot\boldsymbol{n}_{i+1}), \quad i = 1,2. \tag{2.16}$$

The short-ranged interactions are modeled as contact interaction with finite radius r_0, thus the δ function in the above expression actually depends on length scale in the following manner:

$$\delta^2(\boldsymbol{r}) \to \frac{1}{\pi}\delta\Big[\frac{r^2}{2}(1-\boldsymbol{n}\cdot\boldsymbol{n}') - r_0^2\Big] = \frac{2}{\pi r^2}\delta\Big[(1-\boldsymbol{n}\cdot\boldsymbol{n}') - \frac{2r_0^2}{r^2}\Big] \equiv \frac{2}{\pi r^2}\delta_r(1-\boldsymbol{n}\cdot\boldsymbol{n}') \tag{2.17}$$

In fact, this particular form of the cut-off via finite radius is not unique, but only observable values of $\alpha_{>,<}$ enter into the final result. Using the scale-dependent δ function, the interaction term can be

written as

$$\hat{V}_r(\boldsymbol{n}) = \frac{2}{\pi r^2} \sum_{i=1,2,3} \mu_i \delta_r (1 - \boldsymbol{n} \cdot \boldsymbol{n}_i), \tag{2.18}$$

where $\mu_1 = \lambda_1$ and $\mu_{2,3} = -\lambda_2$ are the repulsive and attractive coupling constants respectively, and the scale dependent δ-function defined in Eq. (2.17) takes care of the finite radius. Finally, we obtain a one-dimensional matrix Schrödinger equation:

$$\mathcal{H}\boldsymbol{\Phi} = \Big[-\frac{1}{r^3}\frac{\partial}{\partial r} r^3 \frac{\partial}{\partial r} + \frac{\hat{U}(r)}{r^2} \Big] \boldsymbol{\Phi} = \epsilon \boldsymbol{\Phi}, \tag{2.19}$$

where the effective potential operator $\hat{U}(r)$ is a sum of the angular momentum operator defined in Eq. (2.14) and the interaction term defined in Eq. (2.18):

$$\hat{U}(r) = 4\hat{L}^2 + r^2 \hat{V}_r(\boldsymbol{n}). \tag{2.20}$$

Under the Hopf coordinates, the separation of variable for an angular function $F(x, \phi_1, \phi_2)$ with desired symmetry is

$$F(x, \phi_1, \phi_2) = f(x) e^{i m_1 \phi_1 + i m_2 \phi_2}, \tag{2.21}$$

For free motions, the eigenstates are labeled by the quantum number set (j, m_1, m_2), where $j(j+1)$ is the eigenvalue of operator $\hat{L}^2$, and $m_{1,2}$ are integer numbers. The interaction term makes the states deviate from free motion, we then replace the operator $4\hat{L}^2$ with the effective potential operator $\hat{U}(r) = 4\hat{L}^2 + r^2\hat{V}(r)$ in Eq. (2.20). Consequently, we replace the quantum number j with effective potential $u(r)$, where $u(r)$ is the eigenvalue of operator $\hat{U}(r)$, while keeping the quantum numbers $m_{1,2}$ intact. The rotation on the four dimensional sphere will mix states with different set of (m_1, m_2), but the total angular momentum $m = m_1 + m_2$ is a good quantum number because its corresponding operator commutes with the Hamiltonian:

$$\left[-i \left(\frac{\partial}{\partial \phi_1} + \frac{\partial}{\partial \phi_2} \right), \mathcal{H} \right] = 0. \tag{2.22}$$

For each m the Hilbert state is characterized by the three-dimensional angular momentum j (integer for even m and half-integer for odd m). Also the bosonic symmetry of the system require the following symmetry property of the eigenfunction $\boldsymbol{\Phi}(\boldsymbol{n})$:

$$\boldsymbol{\Phi}(n_x, n_y, n_z) = \boldsymbol{\Phi}(-n_x, n_y, n_z). \tag{2.23}$$

The separation of variable scheme in accordance with Hopf coordinates described above enables us to consider different angular momentum m separately. For each fixed m, the three δ-functions in the interaction potential can affect at most three states for each level labeled by j. Because we are considering a bosonic system, only symmetric states are physical, which leaves us at most two affected states for each level labeled by j, all the other states can be ignored because they belong to the space orthogonal to the possible physical bound states (see Fig. 2.4 for an illustration). In short, Hopf coordinates is such a choice that enables us to identify the relevant states directly, instead of representing them as a sum of many hyperspherical harmonics, thus it greatly reduces the numerical effort. Also, as we will show in later sections, only the sector with zero angular momentum hosts the possible bound state.

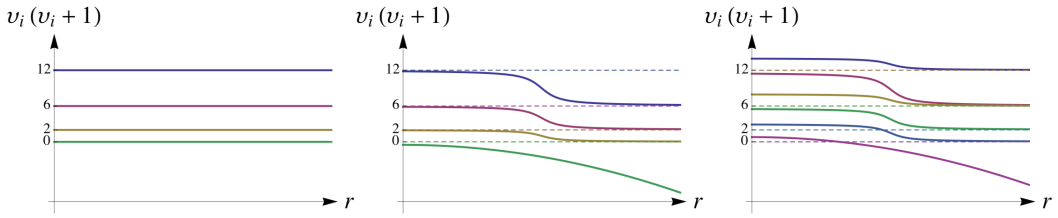

(a) $\lambda_1 = \lambda_2 = 0$ (b) $\lambda_1 = 0, \lambda_2 > 0$ (c) $\lambda_1 > 0, \lambda_2 > 0$

Figure 2.4: Schematic diagram for eigenstates of several low-lying levels within the zero angular momentum sector, where $u_i = 4\nu_i(\nu_i+1)$ is the eigenvalue of the effective potential operator $\hat{U}(r)$. In (a) with $\nu_i = i$, it is just the eigenvalue of angular momentum operator $\hat{L}^2$; In (b), only attraction is included and only one state is altered for each level, the other unaltered states are denoted as dashed lines; In (c), both attraction and repulsion is included, and unaltered states are still denoted as dashed lines.

2.2.2 Solution of the One-Dimensional Schrödinger Equation

After the effective potential operator $\hat{U}(r)$ is obtained, we are left with the problem of solving the one-dimensional matrix Schrödinger equation (2.19). Naive approach to this radial equation is to numerically solve Eq. (2.19) by limiting the basis to N functions, but it is practically inaccessible due to the exponential instability of the wave function even if one of the N boundary conditions or energies is not chosen correctly. Thus we choose another approach [34], converting the Schrödinger equation (2.19) into a first order nonlinear differential equation for the boundary-matching-matrix $\hat{\Lambda}(r)$ defined as follows:

$$r\frac{d\mathbf{\Phi}}{dr}\Big|_{r=R} = -\hat{\Lambda}(R)\mathbf{\Phi}(R). \tag{2.24}$$

Then the differential equation of $\hat{\Lambda}(r)$ is obtained by requiring the invariance of Eq. (2.24) with respect to length scale R:

$$\left[\frac{d\mathbf{\Phi}}{dr} + r\frac{d^2\mathbf{\Phi}}{dr^2}\right]_{r=R} = -\frac{d\hat{\Lambda}}{dR}\mathbf{\Phi}(R) - \hat{\Lambda}(R)\frac{d\mathbf{\Phi}}{dr}\Big|_{r=R}. \tag{2.25}$$

From the Schrödinger equation (2.19) we have

$$\frac{d^2\mathbf{\Phi}}{dr^2} = -\frac{3}{r}\frac{d\mathbf{\Phi}}{dr} + \Big(\frac{\hat{U}}{r^2} - \epsilon\Big)\mathbf{\Phi}. \tag{2.26}$$

Substitute this back into Eq. (2.25) and multiply both sides by $r = R$, then we obtain

$$\left[\Big(\hat{\Lambda}(r) - 2\Big)\, r\frac{d\mathbf{\Phi}}{dr} + (\hat{U} - r^2\epsilon)\mathbf{\Phi}\right]_{r=R} = -R\frac{d\hat{\Lambda}}{dR}\mathbf{\Phi}(R). \tag{2.27}$$

Finally refer back to definition of $\hat{\Lambda}$, which is Eq. (2.24), and we obtain the radial equation, which is a matrix renormalization equation:

$$\frac{d\hat{\Lambda}}{d\ln r} = r^2\epsilon - \hat{U}(r) - 2\hat{\Lambda} + \hat{\Lambda}^2. \tag{2.28}$$

The advantage of the boundary-matching-matrix method is its numerical stability, meaning that even if the original wave function is subject to exponential growth with respect to r, our newly defined matrix $\hat{\Lambda}(r)$ is subject to at most linear growth:

$$||\mathbf{\Phi}(r)|| \sim \exp(r) \Rightarrow ||\hat{\Lambda}(r)|| \lesssim r. \tag{2.29}$$

The initial condition for Eq. (2.28) is obtained as a solution in the region $r_0 \ll r \ll 1$, where only kinetic energy is important:

$$\frac{d\hat{\Lambda}}{d\ln r}\Big|_{r\to 0} = 0, \quad \hat{\Lambda}(r\to 0) = \Big(1 - \sqrt{4\hat{L}^2 + 1}\Big), \tag{2.30}$$

then the initial matrix $\hat{\Lambda}(r \to 0)$ is diagonal:

$$\Lambda_{ij}(r\to 0) = -2l_i\delta_{ij}, \tag{2.31}$$

where $l_i(l_i + 1)$ is the eigenvalue of angular momentum operator $\hat{L}^2$ for level i.

The large scale ($r \to \infty$) behavior of Eq. (2.28) is determined by setting $U_{ij}(r) \simeq -r^2\epsilon_b^{(2)}\delta_{i0}\delta_{j0}$, where $\epsilon_b^{(2)}$ is the two-particle threshold in application to the Hamiltonian defined in Eq. (2.19). The

equation has a stable trajectory for $\epsilon < 0$ and $j \neq 0$:

$$\Lambda_{ij} = -\delta_{ij}\sqrt{|\epsilon|}r \quad (j \neq 0). \tag{2.32}$$

While for $\epsilon > 0$ and $j \neq 0$, the trajectory shows periodic divergence jumps, typical for a spherical wave. For the lowest level $j = 0$, there are also two situations: If $\epsilon < -\epsilon_b^{(2)}$, then the solution will also goes to a stable trajectory as

$$\Lambda_0 = -\sqrt{|\epsilon + \epsilon_b^{(2)}|}r. \tag{2.33}$$

If $\epsilon > -\epsilon_b^{(2)}$, the solution again corresponds to a spherical wave, which has periodical divergence jumps at the position that are zeros of the wave function (see Fig. 2.5). These divergent solutions actually form the continuum of the states of one bound biexciton and one exciton far away.

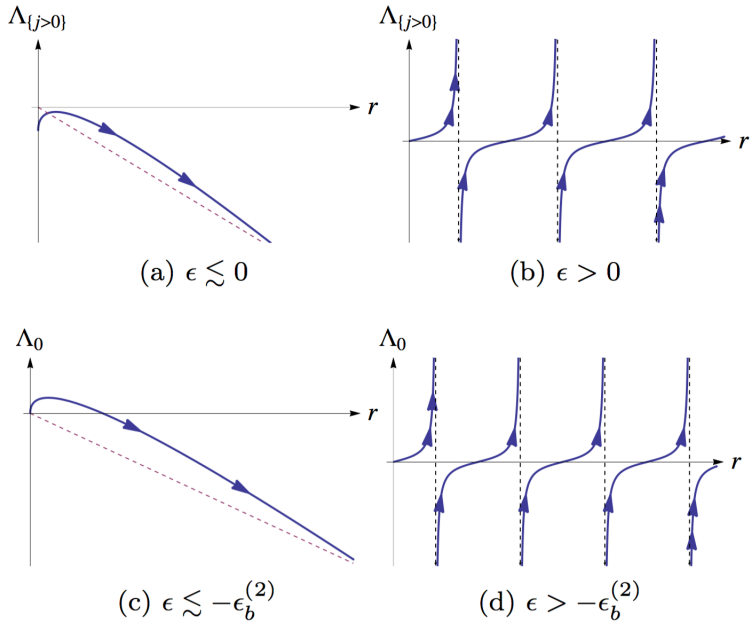

Figure 2.5: Schematic diagram for large scale behavior of Eq. (2.28), where (a) and (b) are shown for levels $j \neq 0$, (c) and (d) are shown for the lowest level $j = 0$. Left is shown for energy slightly below (a) zero for $j \neq 0$ (c) $-\epsilon_b^{(2)}$ for $j = 0$. Right is shown for energy well above (b) zero for $j \neq 0$ (d) $-\epsilon_b^{(2)}$ for $j = 0$.

In the intermediate region, we solve for the possible three-particle bound states. The bound state is determined by the way Λ_0 approaches the stable trajectory defined in Eq. (2.33), and two typical situations are shown in Fig. 2.6: (1) There is only one three-particle bound state with binding energy $\epsilon_b^{(3)}$. If the energy is between the three-particle binding energy $-\epsilon_b^{(3)}$ and the two-particle threshold $-\epsilon_b^{(2)}$, the evolution of Λ_0 will show a single jump before attracted to the stable trajectory; If the

energy is smaller than $-\epsilon_b^{(3)}$, Λ_0 will be directly attracted to the stable trajectory; The evolution of Λ_0 will diverge only when the energy is tuned exactly at the three-particle binding energy. (2) There are two three-particle bound states with binding energies $-\epsilon_{b,1}^{(3)} < -\epsilon_{b,2}^{(3)}$. The evolution of Λ_0 with different energies is similar to the previous case, but it will show two jumps before attracted to the stable trajectory if the energy is tuned to lie between $-\epsilon_{b,2}^{(3)}$ and $-\epsilon_b^{(2)}$. Following this line of reasoning, we can see the fact that the number of three-particle bound states is determined by the number of infinite jumps of Λ_0 at $\epsilon \lesssim -\epsilon_b^{(2)}$, which is exactly the content of the Levinson theorem [68, 31].

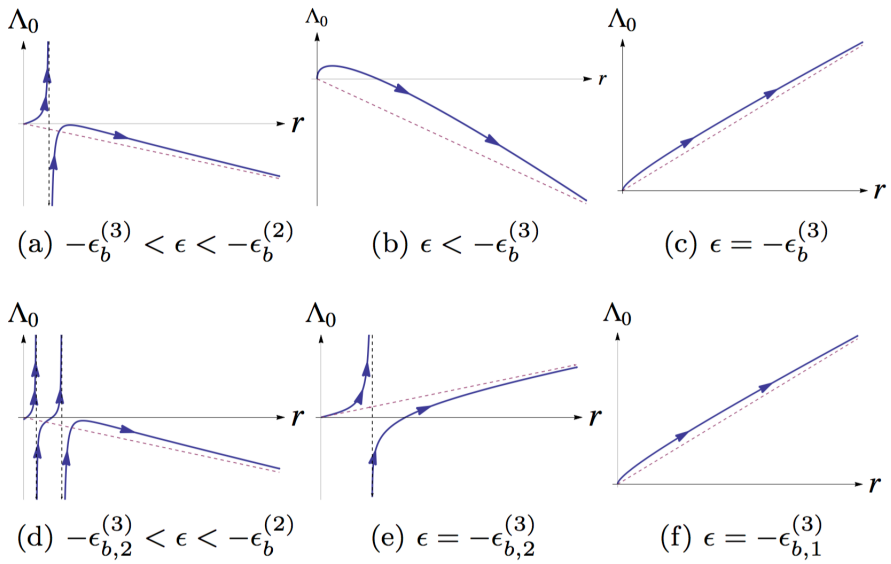

Figure 2.6: Schematic diagram for intermediate scale behavior of Eq. (2.28). Above: There is only one bound state. Below: There is two bound states, where we have $-\epsilon_{b,1}^{(3)} < -\epsilon_{b,2}^{(3)}$. Note that if only (c) or (f) is realized, bound state does not exist.

2.2.3 Running Basis

Sometimes, the following running basis that diagonalizes matrix $\hat{U}(r)$ is most convenient for both analytic and numerical calculations:

$$\hat{O} = \Big(|\chi_0\rangle, |\chi_1\rangle, \cdots \Big), \quad \hat{U}(r)\,|\chi_j\rangle = u_j(r)\,|\chi_j\rangle\,, \tag{2.34}$$

where $|\chi_j\rangle$ is the angular part of the j-th component of the normalized wave function vector $\mathbf{\Phi}(r)$, whose expression will be derived latter in Sec. 2.3 via the Green's function method. This set of basis is called running basis because it changes with the length scale r. Then we do an unitary transformation

to bring Eq. (2.28) to the running basis:

$$\hat{U} = \hat{O}\tilde{U}\hat{O}^{-1}, \quad \tilde{U}_{ij} = \delta_{ij}u_i(r), \quad \hat{\Lambda} = \hat{O}\tilde{\Lambda}\hat{O}^{-1}, \tag{2.35}$$

then the radial renormalization equation under the running basis reads (hereinafter we will drop the tilde symbol for simplicity):

$$\frac{d\hat{\Lambda}}{d\ln r} + [\hat{\Lambda}, \hat{D}] = r^2\epsilon - \hat{U} - 2\hat{\Lambda} + \hat{\Lambda}^2, \tag{2.36}$$

where the anti-symmetric matrix $\hat{D}$ is the Berry connection:

$$\hat{D} = \frac{d\hat{O}^{-1}}{d\ln r}\hat{O}, \quad \text{i.e.} \quad D_{ij} = -D_{ji} = \left\langle \frac{d\chi_i}{d\ln r} \middle| \chi_j \right\rangle. \tag{2.37}$$

It is very tempting (at least at large length scales) to neglect $\hat{D}$ altogether, which corresponds to the adiabatic approximation with a diagonal matrix $\hat{\Lambda}$. However it is not correct because of the following reason. Consider the lowest order correction $\delta\Lambda_{ij}$ to the adiabatic result $\Lambda^{(0)}_{ij} = \Lambda_i\delta_{ij}$ for the lowest level ($i = 0$), then the renormalization group equation for $\Lambda_0(r)$ reads:

$$\frac{d\Lambda_0}{d\ln r} = r^2\epsilon - u_0(r) - 2\Lambda_0 + \Lambda_0^2 - \sum_{j\neq 0}(\delta\Lambda_{0j}D_{j0} + D_{0j}\delta\Lambda_{j0}) + \sum_{j\neq 0}\delta\Lambda_{0j}\delta\Lambda_{j0}, \tag{2.38}$$

where $\delta\Lambda_{0j}$ can be obtained from the first order correction to the adiabatic approximation of Eq. (2.36):

$$\Lambda_0 D_{0j} - D_{0j}\Lambda_j = -2\delta\Lambda_{0j} + \Lambda_0\delta\Lambda_{0j} + \delta\Lambda_{0j}\Lambda_j, \tag{2.39}$$

which gives us the expression for $\delta\Lambda_{0j}$ as:

$$\delta\Lambda_{0j} = \frac{\Lambda_0 - \Lambda_j}{\Lambda_0 + \Lambda_j - 2}D_{0j}. \tag{2.40}$$

Substituting the expression for $\delta\Lambda_{0j}$ into Eq. (2.38) and using the anti-symmetry of the Berry connection $\hat{D}$, we finally obtain:

$$\frac{d\Lambda_0}{d\ln r} = \left[r^2\epsilon - \left(u_0(r) + \sum_{j\neq 0}|D_{0j}|^2\right)\right] - 2\Lambda_0 + \Lambda_0^2 + \sum_{j\neq 0}|D_{0j}|^2\left[\frac{2\Lambda_0 - 2}{\Lambda_0 + \Lambda_j - 2}\right]^2. \tag{2.41}$$

The large scale behavior of the solution is determined by the following quantity:

$$\lim_{r\to\infty}\left[r^2\epsilon-\left(u_0(r)+\sum_{j\neq 0}|D_{0j}|^2\right)\right]_{\epsilon=-\epsilon_b^{(2)}}\equiv\gamma. \tag{2.42}$$

If $\gamma>1$, the solution is unstable at $\epsilon=-\epsilon_b^{(2)}$, it has infinite number of jumps, which would correspond to infinite number of three-particle bound states. If $\gamma<1$, the solution is stable, it corresponds to the power law decay of the wave function. Only for the marginal value $\gamma=1$, should the situation correspond to the non-interacting particle (one exciton and one biexciton) in two dimensions. On the physical ground we should have $\gamma=1$, thus it is important to check for the consistency by direct calculation of the quantity γ, taking into account the Berry connection as in Eq. (2.42). We will show this calculation in later sections, see Eq. (2.69).

In summary, we have shown in this section that the running basis is a convenient choice, whose leading order is the usual adiabatic approximation [90, 21] and the correction to it is the Berry connection. we have also argued that the Berry connection must be included for a physically consistent calculation, thus we will use the exact formalism in our numerical calculation shown later.

2.3 Eigenstates and Eigenvalue of Operator $\hat{U}(r)$

To obtain the full solution of the problem, we need to solve for the eigenvalues and eigenfunctions (which define our running basis) of operator $\hat{U}(r)$. We define the following Green's function for the angular Laplacian near pole $\boldsymbol{n}'$:

$$\left[4\hat{L}^2-u_j(r)\right]G_j(\boldsymbol{n},\boldsymbol{n}')=\frac{2}{\pi}\delta_r(1-\boldsymbol{n}\cdot\boldsymbol{n}'). \tag{2.43}$$

We first solve the Green's function with $\boldsymbol{n}'$ along the north pole ($\boldsymbol{n}'=\boldsymbol{n}_1$), then perform $SO(4)$ rotations to obtain the Green's functions near the other two poles. After that we can use the obtained Green's function to make the following ansatz for eigenfunctions of operator $\hat{U}(r)$, taking into account the bosonic symmetry:

$$\chi_j(\boldsymbol{n})=\alpha_j G_j(\boldsymbol{n},\boldsymbol{n}_1)+\beta_j[G_j(\boldsymbol{n},\boldsymbol{n}_2)+G_j(\boldsymbol{n},\boldsymbol{n}_3)], \tag{2.44a}$$

$$\hat{U}(r)\chi_j(\boldsymbol{n})=u_j(r)\chi_j(\boldsymbol{n}). \tag{2.44b}$$

Once the eigen-problem of operator $\hat{U}(r)$ is solved, then it is straightforward to solve Eq. (2.36) analytically or numerically.

The solution of Eq. (2.43) for $\boldsymbol{n}' = \boldsymbol{n}_1$ can be variable-separated:

$$G_j(\boldsymbol{n}, \boldsymbol{n}_1) = G_j(x) e^{im_1\phi_1 + im_2\phi_2}, \tag{2.45a}$$

$$\left[4\hat{Q}_{m_1,m_2} - u_j(r)\right] G_j(x) = \frac{2}{\pi}\delta_r(1-x), \tag{2.45b}$$

$$\hat{Q}_{m_1,m_2} = -\frac{\partial}{\partial x}(1-x^2)\frac{\partial}{\partial x} + \frac{m_1^2}{2(1-x)} + \frac{m_2^2}{2(1+x)}. \tag{2.45c}$$

In expansion of the Green's function in terms of eigenfunctions of $\hat{L}^2$, we only need to consider those that are connected to the δ function, so we require $m_1 = 0$ such that the eigenfunctions are regular around $x = -1$. Those with nonzero m_1, although present in the general solution, are scale-independent and have no contribution to the renormalization group equation.

As discussed in Sec. 2.2.1, total angular momentum $m = m_1 + m_2$ is a good quantum number, therefore we can consider different angular momentum separately. We will first discuss the case with zero angular momentum, where three-particle bound state is possible; then we will show that no three-particle bound state exists for non-zero angular momentum.

2.3.1 Zero Angular Momentum: Analytics

In this section, we will analyze the large scale behavior of the case with zero angular momentum. It can be solved in two limiting cases, one of which agrees with the perturbative result and the other one shows the importance of including the Berry connection for the system to have physical marginal value $\gamma = 1$.

For zero angular momentum we are dealing with the following Green's function:

$$\left[-4\frac{\partial}{\partial x}(1-x^2)\frac{\partial}{\partial x} - u_j(r)\right] G_j(x) = \frac{2}{\pi}\delta_r(1-x). \tag{2.46}$$

This is just the Legendre equation of degree ν_j (except near point $x = 1$) if we make the following substitution:

$$u_j = 4\nu_j(\nu_j + 1). \tag{2.47}$$

Then the solution can be obtained by comparing the singularities [37] near point $x = 1$, which gives us the following expression for the Green's function (here we use subscript ν_j instead of j for Green's

function to emphasize the dependence on degree ν_j):

$$G_{\nu_j}(x) = \frac{1}{4\cos\left[(\nu_j + 1/2)\pi\right]} P_{\nu_j}(-x), \tag{2.48}$$

and it is regularized at point $x = 1$ by the finite radius r_0:

$$G_{\nu_j}(1) = \frac{1}{4\pi}\left[\ln\frac{16}{\delta} - \Psi(-\nu_j) - \Psi(\nu_j + 1) + 2\Psi\left(\frac{1}{2}\right)\right], \tag{2.49}$$

where $\delta = r_0^2/r^2$ and $\Psi(x)$ is the digamma function.

In the sector of zero angular momentum, only scalar-like combinations will enter the wave function, thus the specification of Eq. (2.44a) to zero angular momentum is

$$\chi_j(\boldsymbol{n}) = \alpha_j G_{\nu_j}(\boldsymbol{n}\cdot\boldsymbol{n}_1) + \beta_j\left[G_{\nu_j}(\boldsymbol{n}\cdot\boldsymbol{n}_2) + G_{\nu_j}(\boldsymbol{n}\cdot\boldsymbol{n}_3)\right]. \tag{2.50}$$

Substitute this ansatz into Eq. (2.44b), we will obtain the following constraints on the coefficients:

$$\begin{pmatrix} \frac{1}{\lambda_1} + G_{\nu_j}(1); & 2G_{\nu_j}\left(-\frac{1}{2}\right) \\ -G_{\nu_j}\left(-\frac{1}{2}\right); & \frac{1}{\lambda_2} - G_{\nu_j}(1) - G_{\nu_j}\left(-\frac{1}{2}\right) \end{pmatrix} \begin{pmatrix} \alpha_j \\ \beta_j \end{pmatrix} = 0. \tag{2.51}$$

By setting the determinant to zero we obtain the equation of the spectrum:

$$\left[\ln\frac{r}{\alpha_<} - F(\nu_j) + 2\pi G_{\nu_j}\left(-\frac{1}{2}\right)\right]\left[\ln\frac{r}{\alpha_>} - F(\nu_j) + 4\pi G_{\nu_j}\left(-\frac{1}{2}\right)\right] = 2\left[2\pi G_{\nu_j}\left(-\frac{1}{2}\right)\right]^2, \tag{2.52}$$

where the function $F(\nu_j)$ is defined as:

$$F(\nu_j) = \frac{1}{2}\Big[\Psi(-\nu_j) + \Psi(\nu_j + 1)\Big] + 2\pi G_{\nu_j}\left(-\frac{1}{2}\right). \tag{2.53}$$

Here $\alpha_{>,<}$ are the scattering lengths for attractive and repulsive coupling respectively, see Eq. (2.5).

The solution to the equation of spectrum can be solved analytically in the following two limiting cases: $u_0 \to 0$ and $|u_0| = -u_0 \to \infty$; while for general cases we will solve it numerically. In case of $u_0 \to 0$, we have $u_0 \sim 4\nu_0 \to 0$ from Eq. (2.47). We first rewrite Eq. (2.52) into a more convenient form:

$$\frac{2}{\ln\frac{r}{\alpha_>} - F(\nu_j)} + \frac{1}{\ln\frac{r}{\alpha_<} - F(\nu_j)} = -\frac{1}{2\pi G_{\nu_j}(-\frac{1}{2})}, \tag{2.54}$$

then we substitute the following behaviors for relevant functions into the above equation:

$$F(\nu_0 \to 0) \sim -\mathbb{C} - \ln\frac{\sqrt{3}}{2} + O(\nu_0), \tag{2.55a}$$

$$2\pi G_{\nu_0}\left(-\frac{1}{2}\right)\Big|_{\nu_0\to 0} \sim -\frac{1}{2\nu_0} - \ln\frac{\sqrt{3}}{2} + O(\nu_0). \tag{2.55b}$$

Finally, we obtain the following solution:

$$\frac{u_0}{2} \sim 2\nu_0 = \frac{2}{\ln\frac{r}{\alpha_>} - F(0)} + \frac{1}{\ln\frac{r}{\alpha_<} - F(0)}, \tag{2.56}$$

that is just the perturbative result of the effective potential $u_0(r)$.

In the case of $|u_0| \to \infty$, we have the following asymptotic behaviors:

$$\nu_0 = -\frac{1}{2} + i\lambda, \quad \lambda = \frac{1}{2}\sqrt{|u_0+1|} \to \infty, \tag{2.57a}$$

$$F(\nu_0) \sim \ln\lambda - \frac{1}{24\lambda^2} + O\left(\frac{1}{\lambda^3}\right), \tag{2.57b}$$

$$G_{\nu_0}\left(-\frac{1}{2}\right) \sim \frac{1}{2\sqrt{\pi}3^{1/4}}\exp\left(-\frac{2\pi}{3}\lambda\right), \tag{2.57c}$$

then using Eq. (2.52) we obtain the following solution:

$$\ln\frac{r}{\alpha_>} = \frac{1}{2}\ln|u_0| - \ln 2 - \frac{2}{3|u_0|}. \tag{2.58}$$

The other solution associated with $\alpha_<$ corresponds to the spurious state discussed previously in the introduction section and should be dropped. Solving Eq. (2.58) iteratively we will obtain the large scale behavior of the effective potential:

$$u_0(r \to \infty) = -r^2\epsilon_b^{(2)} - 4/3 + O(r^{-2}), \tag{2.59}$$

where $\epsilon_b^{(2)} = 4/\alpha_>^2$ is the two-particle threshold. According to the discussion at the end of Sec. 2.2.3, this result will give us $\gamma = \frac{4}{3} > 1$ in the adiabatic approximation, which leads to an infinite number of bound states and is physically inconsistent. In this sense, it is necessary to include the Berry connection D_{ij} [see Eq. (2.37)].

The integral expression for the Berry connection D_{ij} is:

$$D_{ij} = \frac{1}{8\pi^2\sqrt{N_iN_j}}\int_{-1}^{1}dx\int_0^{2\pi}d\phi_1 d\phi_2\ \frac{d\chi_i(\boldsymbol{n})}{d\ln r}\chi_j(\boldsymbol{n}). \tag{2.60}$$

Using the ansatz for $\chi_i(\boldsymbol{n})$ of Eq. (2.50) and the Green's function in Eq. (2.48), we will find that the Berry connection matrix $\hat{D}$ is given by:

$$D_{ij} = \frac{(\alpha_i\alpha_j + 2\beta_i\beta_j)}{8\pi^2\sqrt{N_iN_j}(\nu_i - \nu_j)(\nu_i + \nu_j + 1)}, \tag{2.61}$$

where the normalization factor N_i of the angular eigenfunctions is calculated to be

$$N_i = \frac{\left[(\alpha_i^2 + 2\beta_i^2)\partial_{\nu_i}G_{\nu_i}(1) + [2\beta_i^2 + 4\alpha_i\beta_i]\partial_{\nu_i}G_{\nu_i}(-\frac{1}{2})\right]}{(4\pi)(2\nu_i + 1)}. \tag{2.62}$$

The details of the derivation of these results can be found in Appendix A. According to Eq. (2.41), we have the correction to the effective potential of the lowest level as:

$$\Delta u_0(r \to \infty) = \sum_{j\neq 0} |D_{0j}|^2. \tag{2.63}$$

This can be calculated using the following trick. Firstly, Eq. (2.51) for the eigenstate coefficients (α, β) can be rewritten in a more compact form:

$$\hat{H}(\nu)\vec{\alpha} = 0, \quad \vec{\alpha} = \begin{pmatrix} \alpha \\ \sqrt{2}\beta \end{pmatrix}, \tag{2.64}$$

where the 2×2 matrix Hamiltonian $\hat{H}(\nu)$ is

$$\hat{H}(\nu) = 2\pi \begin{pmatrix} \frac{1}{\lambda_1} + G_\nu(1); & \sqrt{2}G_\nu\left(-\frac{1}{2}\right) \\ \sqrt{2}G_\nu\left(-\frac{1}{2}\right); & G_\nu(1) + G_\nu\left(-\frac{1}{2}\right) - \frac{1}{\lambda_2} \end{pmatrix}. \tag{2.65}$$

From Eq. (2.47) and the fact that u_j is real, it is easy to verify that $\hat{H}(\nu)$ is a real, symmetric two by two matrix. Then we must have

$$\det \hat{H} \cdot \hat{H}^{-1} = \sigma_y \hat{H} \sigma_y. \tag{2.66}$$

Since $\hat{H}(\nu)$ has zero eigenvalues, then $\det \hat{H}$ have zeros and $\hat{H}^{-1}$ have pole structures:

$$\hat{H}^{-1}(\nu) = \sum_j \frac{\vec{\alpha}_j \otimes \vec{\alpha}_j^T}{\nu - h_j}, \tag{2.67}$$

where h_j is the j-th pole and $\vec{\alpha}_j$ is the properly normalized eigenvector of $\hat{H}(\nu)$ corresponding to the

j-th pole. As a result, the normalization condition for the eigenstate $\vec{\alpha}$ can be chosen as:

$$\vec{\alpha} \otimes \vec{\alpha}^T = \sigma_y \hat{H} \sigma_y = \det \hat{H} \cdot \hat{H}^{-1}. \tag{2.68}$$

Using the matrix Hamiltonian $\hat{H}(\nu)$ and the normalization condition defined above, we can express the righthand side of Eq. (2.63) as a contour integration on the complex plane of variable ν:

$$\sum_{j\neq 0} |D_{0j}|^2 = \frac{1}{2}\left\{ \frac{1}{2\pi i}\oint_{\mathcal{C}} d\nu \frac{\mathrm{Tr}[\mathrm{Res}\ \hat{K}(\nu_0)\cdot\hat{K}(\nu)]}{(\nu_0-\nu)^2} + \frac{1}{2\pi i}\oint_{\mathcal{C}} d\nu \frac{\mathrm{Tr}[\mathrm{Res}\ \hat{K}(\nu_0^*)\cdot\hat{K}(\nu)]}{(\nu_0^*-\nu)^2} \right\}, \tag{2.69}$$

where the matrix function $\hat{K}(\nu)$ is formally defined as $\hat{K}(\nu) = \hat{H}^{-1}(\nu)$. It has poles at where the matrix Hamiltonian has zeros, and decays rapidly enough when $|\nu|$ goes to infinity. The derivation of this result can be found in Appendix B, and the integration contour is shown in Fig. 2.7.

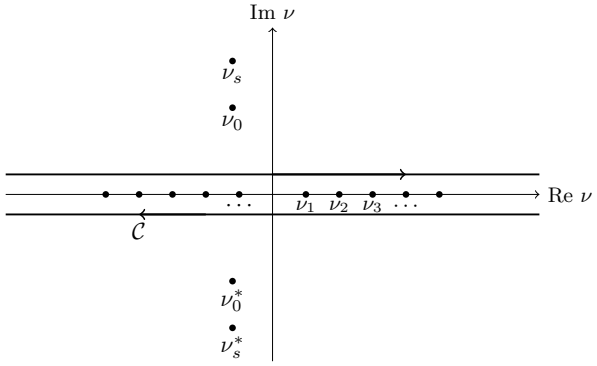

Figure 2.7: Integration contour for the calculation of Δu_0. The contour is along real axis, where the first order poles reside. There are four extra poles far off the real axis, which correspond to true bound state (ν_0) and spurious bound state (ν_s) respectively. The physical meaning of true bound state and spurious bound state is discussed at the end of the Sec. 2.1

The integration contour can be deformed to enclose the other four poles off the real axis and the integration can be easily carried out (see Appendix B), leading to the following result:

$$\Delta u_0 = \sum_j |D_{0j}|^2 = \frac{1}{3}, \tag{2.70}$$

which combined with Eq. (2.59) gives us the marginal result $\gamma = 1$. This shows the importance of including Berry connection matrix $\hat{D}$ and the physical consistency. With this marginal situation, the existence and property of the three-particle bound state must be handled numerically.

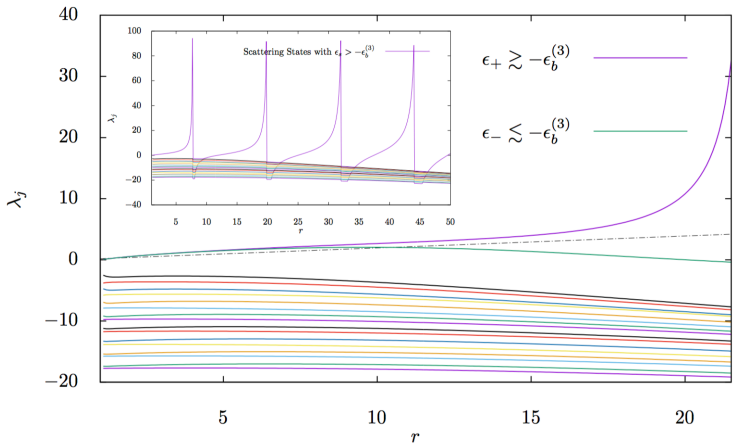

Figure 2.8: Eigenvalues of matrix $\hat{\Lambda}$, calculated for energy slightly above (ϵ_+) and below (ϵ_-) the binding energy $\epsilon_b^{(3)}$. Inset shows result for energy well above $\epsilon_b^{(3)}$, which is the typical behavior for spherical waves.

2.3.2 Zero Angular Momentum: Numerics

The numerical implementation of the renormalization group equation (2.36) is simple, it is just a set of first-order ordinary differential equations and the second-order numerical integration algorithm is efficient enough for our purpose. The initial matrix Eq. (2.30) is diagonal, the first-order correction matrix $\hat{D}$ is anti-symmetric and the effective potential matrix $\hat{u}$ is diagonal, these conditions guarantee that during the evolution all eigenvalues of matrix $\hat{\Lambda}$ are real as they should be. The algorithm is divided into two steps: firstly we run the renormalization process at energy slightly below the two-particle threshold, the existence of three-particle bound state is reflected in the divergence of the highest eigenvalue of $\hat{\Lambda}$ and the number of bound states equals to the number of jumps of the highest eigenvalue [1] by Levinson's theorem [68, 31], as discussed at the end of Sec. 2.2.2. Secondly, if the bound state exists, we further run the renormalization process with varying energies to determine the binding energy of the three-particle bound state. Typical behaviors of different energies are shown in Fig. 2.8, where energy slightly above the three-particle binding energy shows a single jump and energy slightly below the three-particle binding energy shows no divergence. If the energy is well above the three-particle binding energy, the situation corresponds to a spherical wave, where periodic jumps will occur at the zeros of the wave function.

The calculation is carried out using MATLAB [69] on a laptop with number of levels included $N = 40$. Each run of the renormalization process takes less than 10 minutes [2] and inclusion of more

[1] Mathematically the divergence is positive on one side of the vertical asymptote and negative on the other side, thus there is jump from one side to the other side. These jumps are numerically realized by inverting the highest eigenvalue while keep the other eigenvalues intact when the former hits a sufficiently large value.

[2] In the numerical calculation we need to carefully exclude the spurious level as discussed in the introduction section.

Table 2.1: Critical values of $\alpha_>$ corresponding to different $\alpha_<$ when the three-particle bound state disappear into the two-particle threshold.

$\alpha_<$	0.80	0.82	0.85	0.90	0.95
$\alpha_>^c$	1.82	1.85	1.90	1.99	2.09

levels only changes the result by less than 1%. For zero angular momentum, there exists at most one three-particle bound state. At large $\alpha_>/\alpha_<$ ratio, the ratio between three-particle binding energy and the two-particle threshold versus $\alpha_>/\alpha_<$ falls on a universal curve, as illustrated in Fig. 2.9. A similar universal curve also appears in the case of three-boson all interacting attractively [6, 7, 8]. According to the result for vanishing intraspecies interaction [6, 12], the universal curve in Fig. 2.9 should approach 1.39 asymptotically at infinite $\alpha_>/\alpha_<$ ratio. Curiously, the convergence to 1.39 is extremely slow: it only reaches 0.4 for $\alpha_>/\alpha_< = 250$, the largest scattering length ratio shown in Fig. 2.9. In fact, the curve reaches ~ 1 only for $\alpha_>/\alpha_< \sim 10^8$ and the correction to 1.39 in the large $\alpha_>/\alpha_<$ limit scales as $1/\ln(\alpha_>/\alpha_<)$. This curious fact can be partially understood from the first order perturbation theory with respect to the small parameter $f_<$ from Eq. (2.6). It seems that the result $(\epsilon_b^{(3)} - \epsilon_b^{(2)})/\epsilon_b^{(2)} = 1.39$ is practically inaccessible due to the logarithmic slow convergence. Into the region with small $\alpha_>/\alpha_<$ ratio, universality breaks and the three-particle binding energy merges into the two-particle threshold at critical values, we listed several critical values in Table 2.1. It's notable that our calculation only takes the two scattering lengths $\alpha_<$ and $\alpha_>$ as input parameters (see Eq. (2.52)). The microscopic cut-off r_0 only appears in the initial condition, where the kinetic energy dominates and the limit $r \to 0$ can be safely taken (see Eq. (2.30)). These indicate that the property of the three-particle bound state depends only on the scattering lengths $\alpha_>, \alpha_<$, but not on the microscopic details of the interactions.

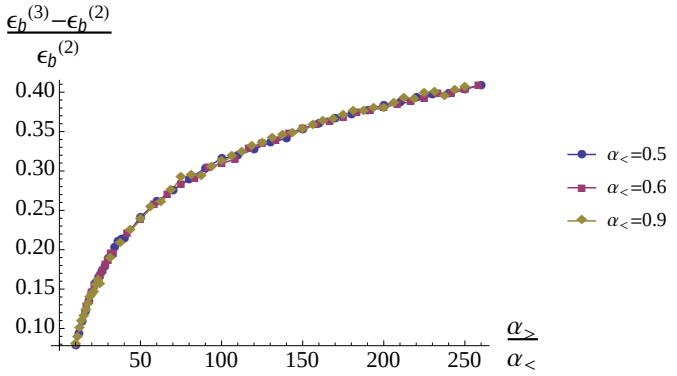

Figure 2.9: The universal curve of $(\epsilon_b^{(3)} - \epsilon_b^{(2)})/\epsilon_b^{(2)}$ versus $\alpha_>/\alpha_<$ at large scattering length ratios. Data points are collected in the region $\alpha_>/\alpha_< \geqslant 10$, and with three different values of $\alpha_<$. They fall on the same curve within the numerical accuracy.

2.3.3 Non-Zero Angular Momentum

For the solution to Eq. (2.43) with total angular momentum $m \neq 0$, we first solve for the north pole $\boldsymbol{n}' = \boldsymbol{n}_1$ and then rotate the solution to the other two poles. The construction of the Green's function can be carried out following the standard procedure of separation of variables:

$$\begin{aligned} &G(\boldsymbol{n}, \boldsymbol{n}_1) = G(x) \exp(i m_1 \phi_1 + i m_2 \phi_2), \\ &\hat{L}^2 = \left[-\frac{\partial}{\partial x}(1-x^2)\frac{\partial}{\partial x} + \frac{m_1^2}{2(1-x)} + \frac{m_2^2}{2(1+x)} \right]. \end{aligned} \tag{2.71}$$

In expansion of Green's function in terms of eigenfunctions of $\hat{L}^2$, we only need to consider those that are connected to the δ-function, thus we require $m_1 = 0$ and the eigenfunctions to be regular around $x = -1$. These eigenfunctions then can be represented in terms of hypergeometric functions [37]:

$$\begin{aligned} &\hat{L}^2 X_j^{(m)}(x) = \left(j + \frac{m}{2}\right)\left(j + \frac{m}{2} + 1\right) X_j^{(m)}(x), \\ &X_j^{(m)}(x) = \left(\frac{1+x}{2}\right)^{m/2} R_j^{(m)}\left(\frac{1+x}{2}\right), \\ &R_j^{(m)}(x) = {}_2F_1(-j, j+m+1; m+1; x), \end{aligned} \tag{2.72}$$

where $m = m_1 + m_2 = m_2$ and j takes the value $0, 1, 2, \cdots$. By using the representation of δ-function

$$\delta(x) = \frac{1}{2}\sum_{j=0}^{\infty} \frac{(-)^j (2j+m+1)\Gamma(j+m+1)}{\Gamma(m+1)\Gamma(j+1)} X_j^{(m)}(x), \tag{2.73}$$

we immediately obtain the expression for Green's function:

$$G_{\nu_j}^{(m)}(\boldsymbol{n}, \boldsymbol{n}_1) = (\boldsymbol{N} \cdot \boldsymbol{B_1})^m \frac{1}{4\cos\pi\left(\nu_j + \frac{1}{2}\right)} \frac{\Gamma(\nu_j + m + 1)}{\Gamma(\nu_j + 1)\Gamma(m+1)} R_{\nu_j}^{(m)}(1 - \boldsymbol{N}^T \hat{A}_1 \boldsymbol{N}) \tag{2.74}$$

where the four-dimensional vector $\boldsymbol{B}_1$ and 4×4 matrix $\hat{A}_1$ are defined as

$$A_1 = \begin{pmatrix} 1 & & & \\ & 1 & & \\ & & 0 & \\ & & & 0 \end{pmatrix}, \quad \boldsymbol{B}_1 = (0, 0, 1, i)^T, \tag{2.75}$$

and $\boldsymbol{N}$ is the following four-dimensional unit vector:

$$\boldsymbol{N} = \begin{pmatrix} \sqrt{\frac{1-x}{2}}\cos\phi' \\ \sqrt{\frac{1-x}{2}}\sin\phi' \\ \sqrt{\frac{1+x}{2}}\cos\phi' \\ \sqrt{\frac{1+x}{2}}\sin\phi' \end{pmatrix}, \tag{2.76}$$

where ϕ' is an arbitrary phase. To obtain the Green's function with $\boldsymbol{n}'$ along the other two poles, we rotate vector $\boldsymbol{B}_1$ and matrix $\hat{A}_1$ by $2\pi/3$ on three-dimensional unit sphere, which corresponds to $\pi/3$ rotation in four-dimensions. The rotation matrices are as follows:

$$\mathcal{R}_{2,3} = \begin{pmatrix} \frac{1}{2} & 0 & \mp\frac{\sqrt{3}}{2} & 0 \\ 0 & \frac{1}{2} & 0 & \mp\frac{\sqrt{3}}{2} \\ \pm\frac{\sqrt{3}}{2} & 0 & \frac{1}{2} & 0 \\ 0 & \pm\frac{\sqrt{3}}{2} & 0 & \frac{1}{2} \end{pmatrix}. \tag{2.77}$$

Applying the rotation matrices to the four-dimensional vector $\boldsymbol{B}_1$ and 4×4 matrix $\hat{A}_1$ we get:

$$\begin{aligned} \hat{A}_{2,3} &= \mathcal{R}_{2,3}\hat{A}_1\mathcal{R}_{2,3}^{-1} = \begin{pmatrix} \frac{1}{4} & 0 & \pm\frac{\sqrt{3}}{4} & 0 \\ 0 & \frac{1}{4} & 0 & \pm\frac{\sqrt{3}}{4} \\ \pm\frac{\sqrt{3}}{4} & 0 & \frac{3}{4} & 0 \\ 0 & \pm\frac{\sqrt{3}}{4} & 0 & \frac{3}{4} \end{pmatrix}, \\ \boldsymbol{B}_{2,3} &= \mathcal{R}_{2,3}\boldsymbol{B}_1 = \left(\mp\frac{\sqrt{3}}{2}, \mp\frac{\sqrt{3}}{2}i, 1/2, i/2\right)^T. \end{aligned} \tag{2.78}$$

Substituting the ansatz for eigenfunctions in Eq. (2.44a) with the above specification into Eq. (2.44b), we will obtain the following constraints on the coefficients (here we add the superscript to emphasize the dependence on the angular momentum m):

$$\begin{pmatrix} \frac{1}{\lambda_1} + G^{(m)}_{\nu_j}(11); & G^{(m)}_{\nu_j}(12) + G^{(m)}_{\nu_j}(13) \\ -G^{(m)}_{\nu_j}(21); & \frac{1}{\lambda_2} - G^{(m)}_{\nu_j}(22) - G^{(m)}_{\nu_j}(23) \end{pmatrix} \begin{pmatrix} \alpha_j \\ \beta_j \end{pmatrix} = 0, \tag{2.79}$$

where we have used the shortened notation $G^{(m)}_{\nu_j}(lm) \equiv G^{(m)}_{\nu_j}(\boldsymbol{n}_l, \boldsymbol{n}_m)$. Still the equation of spectrum is obtained via setting the determinant to zero. In order to calculate the involved quantities $G^{(m)}_{\nu_j}(lm)$, we need to put the three-dimensional unit vectors in Eq. (2.15) back on the four-dimensional unit

sphere. This can be done using the following correspondence:

$$\begin{aligned}
&\boldsymbol{n}_1 \to \boldsymbol{N}_1 = (0, 0, \cos\phi', \sin\phi')^T, \\
&\boldsymbol{n}_{2,3} \to \boldsymbol{N}_{2,3} = \left(\mp\frac{\sqrt{3}}{2}\cos\phi', \mp\frac{\sqrt{3}}{2}\sin\phi', \frac{1}{2}\cos\phi', \frac{1}{2}\sin\phi' \right)^T,
\end{aligned} \tag{2.80}$$

where ϕ' is an arbitrary phase. By direct calculation we will obtain the following results

$$\begin{cases} G_\nu^{(m)}(11) = e^{im\phi'} f(\nu, m) R_\nu^{(m)}(1) \\ G_\nu^{(m)}(12) = \frac{1}{2^m} e^{im\phi'} f(\nu, m) R_\nu^{(m)}(\frac{1}{4}) \\ G_\nu^{(m)}(13) = \frac{1}{2^m} e^{im\phi'} f(\nu, m) R_\nu^{(m)}(\frac{1}{4}) \end{cases}, \begin{cases} G_\nu^{(m)}(21) = \frac{1}{2^m} e^{im\phi'} f(\nu, m) R_\nu^{(m)}(\frac{1}{4}) \\ G_\nu^{(m)}(22) = e^{im\phi'} f(\nu, m) R_\nu^{(m)}(1) \\ G_\nu^{(m)}(23) = \frac{(-)^m}{2^m} e^{im\phi'} f(\nu, m) R_\nu^{(m)}(\frac{1}{4}) \end{cases}, \tag{2.81}$$

where the factor $f(\nu, m)$ is defined as

$$f(\nu, m) = \frac{1}{4\cos\left[\left(\nu + \frac{1}{2}\right)\pi\right]} \frac{\Gamma(\nu + m + 1)}{\Gamma(\nu + 1)\Gamma(m + 1)}, \tag{2.82}$$

and $R_\nu^{(m)}(x)$ has a singularity at $x = 1$ which is regularized by the finite radius r_0:

$$f(\nu, m) R_\nu^{(m)}(1) = \frac{1}{4\pi} \left[\ln\frac{16}{\delta} - \Psi(-\nu) - \Psi(\nu + m + 1) + 2\Psi\left(\frac{1}{2}\right) \right],$$

where $\delta = r_0^2/r^2$ and the $\Psi(x)$ is the digamma function [37]. Putting all these results together, we finally obtain the equation of spectrum for general value of m:

$$\left[\ln\frac{r}{\alpha_<} - \frac{1}{2} M(\nu_j, m) \right] \left[\ln\frac{r}{\alpha_>} - \frac{1}{2} M(\nu_j, m) + 2\pi(-)^m N(\nu_j, m) \right] = 2\left[2\pi N(\nu_j, m) \right]^2, \tag{2.83}$$

with the following definition of the relevant quantities:

$$\begin{aligned}
M(\nu, m) &= \Psi(-\nu) + \Psi(\nu + m + 1), \\
N(\nu, m) &= \frac{1}{2^m} \frac{1}{4\cos\left[\left(\nu + \frac{1}{2}\right)\pi\right]} \frac{\Gamma(\nu + m + 1)}{\Gamma(\nu + 1)\Gamma(m + 1)} R_\nu^{(m)}\left(\frac{1}{4}\right),
\end{aligned} \tag{2.84}$$

where $\mathbb{C} = 0.577\cdots$ is the Euler constant. Specification of Eq. (2.83) to the case $m = 0$ is just what we got previously in Eq. (2.52).

We then analyze the large scale behavior of the lowest level. With increasing length scale r, the angular eigenvalue u_0 becomes more and more negative, and the imaginary part of ν_0 becomes larger.

In the limit $|u_0| = -u_0 \to \infty$, the asymptotic behaviors of the relevant functions [37] are:

$$M(\nu_0, m) \sim \ln|u_0| - 2\ln 2 - \frac{4-3m^2}{3|u_0|}, \quad N(\nu_0, m) \sim \frac{\exp\left(-\frac{2\pi}{3}\sqrt{|u_0|}\right)}{|u_0|^{1/4}}. \tag{2.85}$$

Then asymptotically, the equation of spectrum 2.83 reduces to

$$\ln\frac{r}{\alpha_>} = \frac{1}{2}\ln|u_0| - \ln 2 - \frac{4-3m^2}{6|u_0|}, \tag{2.86}$$

where only the solution associated with $\alpha_>$ is chosen because the other solution associated with $\alpha_<$ corresponds to the spurious state discussed previously in the introduction section. Solving this equation iteratively we will get the large scale behavior of the effective potential:

$$u_0^{(m)}(r \to \infty) = -r^2\epsilon_b^{(2)} + (3m^2-4)/3 + O(r^{-2}), \tag{2.87}$$

where $\epsilon_b^{(2)} = 4/\alpha_>^2$ is the two-particle threshold binding energy. This is the result under adiabatic approximation.

By performing the asymptotic analysis similar to those for zero angular momentum, we will obtain the following solution to the effective potential $u_0^{(m)}(r)$ up to first order correction (Appendix B):

$$u_0^{(m)}(r \to \infty) = -r^2\epsilon_b^{(2)} + (m^2-1) + O(r^{-2}) \tag{2.88}$$

thus for non-zero angular momentum, the wave function we will obtain is subject to power-law decay, and no three-particle bound state is guaranteed at large length scale. To confirm the absence of three-particle bound state, we need the calculation not only at large length scale, but also in the intermediate region, which we will still investigate numerically.

The numerical implementation for nonzero angular momentum is essentially the same as that for zero angular momentum, if we substitute the proper angular eigenfunctions into the corresponding formulas. Result shows that there is no three-particle bound state for nonzero angular momentum. To get a sense of what is happening among different m values, we also calculated the effective potential $u_0(r)/r^2$ for the lowest level, the curve has minimum in case of $m = 0$ while for $m > 0$ the potential is monotonously decreasing with increasing r (Fig. 2.10), then it is straightforward to see the possibility of getting three-particle system bounded for $m = 0$ and its unlikeness for $m > 0$.

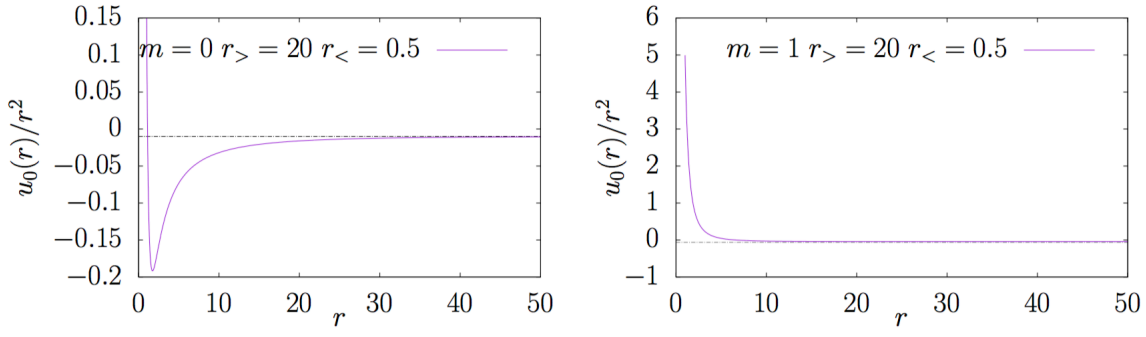

Figure 2.10: Effective Potential $u_0(r)/r^2$ for $m = 0, 1$ with input parameters $\alpha_> = 20$ and $\alpha_< = 0.5$. The dashed line indicates the position of the two-particle threshold.

2.4 Conclusion

In summary, we investigated the existence of three-particle bound states in a two-species, interacting bosonic system in two dimensions where coupling between like bosons is repulsive and otherwise attractive. We developed a simple and efficient algorithm via choice of proper parameterization and base functions. Large scale behavior of the system is handled analytically and interaction region is handled numerically. Our result shows that there is only one three-particle bound state for zero angular momentum, and it will merge into the two-particle threshold at small ratio between scattering lengths (the critical ratio $\alpha_>^c/\alpha_<$ is about $2.2 \sim 2.3$). In contrast, there exist two three-particle bound states when the couplings between all the three bosons with equal masses are attractive, as investigated in the literature [13, 6, 7, 8, 12]. For non-zero angular momentum, there is no three-particle bound state. The two scattering lengths provide enough information to determine the three-particle binding energy, while the microscopic cut-off r_0 and the interaction constants $\lambda_{1,2}$ do not enter any way other than through the scattering lenghts. Our result is in agreement with the previous investigations [6, 64] in the sense that there are only finite number of three-particle bound states in two dimensions, in contrast to the condensation of infinite number of three-particle bound states in three dimensions, and we showed this fact both analytically (the parameter γ define in Eq. (2.42) is equal to or smaller than unity, which excludes the possibility of infinite number of bound states) and numerically.

Existing approaches for this kind of quantum three-body problem in the literature are mainly different variations of the Skorniakov-Ter-Martirosian methods. It can be implemented in real space and solved via the integral equations for the scattering amplitude [78, 81]; or be implemented in momentum space and solved via the diagrammatic techniques for scattering matrix [12, 63, 52]. It

can also be converted into a series of solvable differential equations [77]. All these approaches involve several numerical integrations over unbounded spaces or kernel inversion, some of them are limited to s-wave resonant scattering. Here we provide an alternative approach to the quantum three-body problems, simple and efficient, involving only direct root finding and evolving of a first-order ordinary differential equation to an intermediate length scale (for example, the divergence behavior showing the existence of bound state is already clear at a relatively small length scale $r \sim 20$ in Fig. 2.8, and there is no need to evolve the equation further to any larger length scale). It is capable of handling both short- and long- range physics, free of numerical instability and converges fast enough to avoid parallelism on clusters. Also our choice of basis via Hopf coordinates reduces the squared proliferation of hyperspherical harmonics to a linear one with increasing number of included levels, which saves greatly in numerical endeavor.

Chapter 3

Exact Solutions to Two-Component Many-Body Systems in One Dimension

3.1 Introduction

In the previous chapter, we have investigated the instability of the condensation in a two-component system with interspecies attraction and intraspecies repulsion in two dimensions, which is from a few-body aspect. To gain more insight from the complementary many-body aspect, especially beyond mean-field and perturbative results, it is worthwhile to construct corresponding models in one dimension that is subject to exact solutions. Apart from the theoretical interest, these exactly solvable models are also of practical value due to the tremendous advances in the experimental realization of quasi-one dimensional interacting quantum systems using confined cold atoms.

The prototype of one-dimensional exactly solvable models is the famous Lieb-Liniger model [67, 66], which is now accessible to experimentalists [74, 56, 83, 106]. The two-component models we shall discuss in the current chapter are multicomponent extensions of the Lieb-Liniger type system [88], which host a rich spectrum of many-body physics. On the experimental side, such systems have been realized using different hyperfine states of cold atoms, which provide us with the desired pseudospin degrees of freedom [108, 71, 3, 65]. The intra- and inter-species interactions can then be tuned via the Feshbach resonances [16, 28] or external potentials confining the system in one dimension [23, 44].

On the theoretical side, the study of exactly solvable models for multicomponent systems begins with spin 1/2 fermions, which is now known as the Yang-Gaudin model [35, 109, 110]. Sutherland [98] and Schlottmann [93, 92] then made the generalization to arbitrary spins. The bosonic counterpart was also studied by various groups [38, 57].

In spite of extensive studies of two-component exactly solvable models in the literature, they are all limited to the case with a single type of coupling. This is probably due to the fact that models of simple δ-contact interactions with two different coupling constants fail to fulfill the Yang-Baxter equation. Here we propose a new type of models for two-component systems with tunable interspecies interactions, where the Yang-Baxter equation can be fulfilled by fine-tuning the resonant energies. Although the strict exact solvability beyond the level of two-body scatterings would require the introduction of extra singular counterterms, the models proposed here can still be well described by the Bethe ansatz, at least for relatively small densities. It is of relevance not only to experimentally accessible systems such as bosonic ^{87}Rb quantum gases but also to fundamental theoretical problems such as BCS-BEC crossover, since, unlike the Yang-Gaudin model, it connects regimes of weakly attractive atoms to weakly repulsive molecules. Besides, it presents exotic many-body physics of which in one case the solution is a Fermi sea of two-strings. The remarkable feature is that the Fermi momentum Q characterizing this sea is limited by the value Q^*, as the increase of the mass density at fixed interaction is accommodated by the growing density of states of two-strings. A similar phenomenon was noticed by Gurarie [42] for a single component model with Feshbach resonance, where the system becomes unstable for small or large interactions. In the other case, an embedded string solution emerges, which means that the uniform system is unstable and it collapses into a bright soliton. This collapsing instability happens for fermionic atoms, which is contrary to the intuition that fermions won't collapse due to the Pauli exclusion principle.

The remainder of this chapter is organized as follows: In Sec. 3.2 we present the models and discuss their integrability, then their exact solutions are worked out via the quantum inverse scattering method [105, 58]. Both bosonic and fermionic cases are considered and we will discover two different regimes, depending on the competition between inter- and intra-species couplings. In Sec. 3.3 we discuss the uniform regime with repulsion overcoming attraction, where the ground state properties and low energy excitations are derived. We also analyze the system with an external magnetic field in this regime, where a considerable portion of the phase diagram is occupied by the Fulde-Ferrel-Larkin-Ovchinnikov (FFLO) state [33, 62] and a lower critical magnetic field is found even for large densities. In Sec. 3.4 we turn to the other regime where the ground state is a bright soliton. Finally, we summarize the results and discuss possible experimental realizations and extensions.

3.2 Models and Their Integrability

3.2.1 Models

Firstly, we review two famous examples of integrable models, which are relevant in our subsequent discussion of BCS-BEC crossover in one dimension. One of them, the prototype for spin 1/2 fermions, is the Yang-Gaudin model [35, 109, 110] defined by the Hamiltonian:

$$\hat{\mathcal{H}} = \int dx \left[\partial_x \hat{\psi}^\dagger(x) \partial_x \hat{\psi}(x) - c_F \hat{\psi}^\dagger(x) \hat{\psi}^\dagger(x) \hat{\psi}(x) \hat{\psi}(x) \right], \tag{3.1}$$

where $\hat{\psi} = \begin{pmatrix} \hat{\psi}_\uparrow \\ \hat{\psi}_\downarrow \end{pmatrix}$ represents the spin-1/2 fermions with mass $m_F = 1/2$, and we have made the choice that $c_F > 0$ corresponds to the attraction between particles. We also adopt the convention that $\hbar = 1$ in this paper. It is well known that the ground state configuration of this attractive Yang-Gaudin model is a Fermi sea of singlet bound pairs, where the effective interaction between these bound pairs is still characterized by the attractive coupling c_F. In the limit $c_F \to 0$, the Yang-Gaudin model describes weakly bound pairs within BCS mechanism, while in the limit $c_F \to \infty$, it describes hardcore bosons instead of weakly interacting bosons.

The second example of integrable models, the prototype for spinless bosons, is the Lieb-Liniger model [67, 66] defined by the Hamiltonian:

$$\hat{\mathcal{H}} = \int dx \left[\partial_x \hat{\varphi}^\dagger(x) \partial_x \hat{\varphi}(x) + c_B \hat{\varphi}^\dagger(x) \hat{\varphi}^\dagger(x) \hat{\varphi}(x) \hat{\varphi}(x) \right], \tag{3.2}$$

where $\hat{\varphi}$ represents the spinless bosons with mass $m_B = 1/2$, and we have the opposite choice that $c_B > 0$ corresponds to repulsion between particles, contrary to the Yang-Gaudin model. Now there is an interesting connection between the Yang-Gaudin model and the Lieb-Liniger model - If we identify the spinless boson as the singlet bound state of two fermions (accordingly we need to impose the mass relation such that $m_B = 2m_F$), then the Yang-Gaudin model and the Lieb-Liniger model can be formally connected by just a change of sign of the coupling constant c. This seemingly artificial construction was proposed to be an exactly solvable model for BCS-BEC crossover in one dimension, where the connection between the two models is realized by geometric resonances [32, 103]. The Lieb-Liniger model is necessarily needed for the BEC side, because the strong coupling limit of the Yang-Gaudin model is a gas of hardcore bosons (which is also known as the fermionic super Tonks-Girardeau gas [39]) instead of weakly interacting bosons. Although this provides a smooth crossover

between the two pairing schemes, it is not satisfactory because there is no single Hamiltonian governing the behavior of the system from Eq. (3.1) with $c_F \ll 1$ to Eq. (3.2) with $c_B \ll 1$. Moreover, the molecule on the BEC side is unbreakable due to the quasi-1D confinement, thus the information of spin excitations is lost.

To connect the Lieb-Liniger model and the Yang-Gaudin model by a single Hamiltonian, we consider two-component interacting bosons and fermions with tunable interspecies interactions, which will provide an ideal scenario for one dimensional BCS-BEC crossover without the drawbacks mentioned above. Generally, the tunable interspecies interaction is realized via Feshbach resonances, where atoms are bound into molecules. Exact solutions to models with Feshbach resonances are studied in the literature for one-component interacting particles [42, 51] and for noninteracting fermions in the so-called quantum three-wave interaction model [107, 85]. Here we make a further step to two-component interacting systems, where the applicability of Bethe ansatz is obtained by fine-tuning the resonant energies.

We start by introducing the bosonic model, where the resonance can be viewed as a singlet bound state (molecule) of two participating bosons. It is defined by the Hamiltonian:

$$\hat{\mathcal{H}} = \int dx \Big\{ \partial_x \hat{\psi}^\dagger \partial_x \hat{\psi} + \frac{\partial_x \hat{\Pi}^\dagger \partial_x \hat{\Pi}}{2m_\Pi} - \epsilon_0 \hat{\Pi}^\dagger \hat{\Pi} + g \hat{\psi}^\dagger \hat{\psi}^\dagger \hat{\psi} \hat{\psi} + \left[\frac{t}{2} \left(i \partial_x \hat{\psi}^T \sigma_y \hat{\psi} \right) \hat{\Pi}^\dagger + h.c. \right] \Big\}, \tag{3.3}$$

where $\hat{\psi} = \begin{pmatrix} \hat{\psi}_\uparrow \\ \hat{\psi}_\downarrow \end{pmatrix}$ represents the two-component bosons and $\hat{\Pi}$ represents the molecules with binding energy ϵ_0. The matrix σ_y is the y component of the Pauli matrix $\boldsymbol{\sigma} = (\sigma_x, \sigma_y, \sigma_z)$. The introduction of spatial derivatives into the resonant coupling is due to the fact that the spatial part of the bosonic wave function in the singlet channel has odd parity. Also, we have adopted the convention that $m_\psi = 1/2$, and we have left m_Π unspecified. In fact, the relation between m_Π and m_ψ is dictated by Galilean invariance: Under the Galilean transformation

$$\partial_t \to \partial_t - v\partial_x, \quad \hat{\psi} \to \hat{\psi} e^{-i\left(m_\psi v x + \frac{m_\psi v^2}{2} t \right)}, \quad \hat{\Pi} \to \hat{\Pi} e^{-i\left(m_\Pi v x + \frac{m_\Pi v^2}{2} t \right)}, \tag{3.4}$$

the action $S = \int dx dt \ \left(i \hat{\psi}^\dagger \partial_t \hat{\psi} + i \hat{\Pi}^\dagger \partial_t \hat{\Pi} \right) - \int dt \ \hat{\mathcal{H}}$ of the system will remain unchanged apart from a constant shift, provided we impose the relation that $m_\Pi = 2m_\psi$. Thus we can simply substitute $m_\Pi = 1$ into Eq. (3.3). There is one more point that we need to pay attention to, which is the conservation of particle number. This means that the operator $\hat{N}$ defined below commutes with the

Hamiltonian $\hat{\mathcal{H}}$:

$$\hat{N} = \int dx \ \left(\hat{\psi}^\dagger\hat{\psi} + 2\hat{\Pi}^\dagger\hat{\Pi}\right), \quad [\hat{N}, \hat{\mathcal{H}}] = 0. \tag{3.5}$$

The definition of $\hat{N}$ takes into account the resonant coupling processes where two bosons with opposite pseudospin transform into one molecule or vice versa. This commutability can be achieved by imposing the following commutation relations:

$$\begin{aligned} &[\hat{\psi}_\sigma(x), \hat{\psi}^\dagger_{\sigma'}(x')] = \delta_{\sigma\sigma'}\delta(x-x'), \quad \sigma, \sigma' = \uparrow, \downarrow \\ &[\hat{\Pi}(x), \hat{\Pi}^\dagger(x')] = \delta(x-x'), \end{aligned} \tag{3.6}$$

and all the other commutators give out zero.

The fermionic model can be constructed similarly, with the introduction of both scalar and vector resonances. It is defined by the Hamiltonian:

$$\begin{aligned} \hat{\mathcal{H}} = \int dx \Bigg\{ &\partial_x\hat{\psi}^\dagger\partial_x\hat{\psi} + \frac{1}{2}\partial_x\hat{\mathbf{\Xi}}^\dagger\cdot\partial_x\hat{\mathbf{\Xi}} + \frac{1}{2}\partial_x\hat{\Pi}^\dagger\partial_x\hat{\Pi} - \epsilon_\Xi\hat{\mathbf{\Xi}}^\dagger\cdot\hat{\mathbf{\Xi}} - \epsilon_\Pi\hat{\Pi}^\dagger\hat{\Pi} + g\hat{\psi}^\dagger\hat{\psi}^\dagger\hat{\psi}\hat{\psi} \\ &+ \left[\frac{t_\Xi}{2}\left(i\partial_x\hat{\psi}^T\boldsymbol{\sigma}\sigma_y\hat{\psi}\right)\cdot\hat{\mathbf{\Xi}}^\dagger + h.c.\right] + \left[\frac{t_\Pi}{2}\left(i\hat{\psi}^T\sigma_y\hat{\psi}\right)\cdot\hat{\Pi}^\dagger + h.c.\right]\Bigg\}, \end{aligned} \tag{3.7}$$

where $\hat{\psi} = \begin{pmatrix}\hat{\psi}_\uparrow \\ \hat{\psi}_\downarrow\end{pmatrix}$ represents the spin-1/2 fermions, $\hat{\mathbf{\Xi}}$ represents the vector resonances with binding energy ϵ_Ξ and $\hat{\Pi}$ represents the scalar resonances with binding energy ϵ_Π. Also we adopt the convention that $m_\psi = 1/2$, then $m_\Xi = m_\Pi = 1$ is required by the Galilean invariance, just as what we have discussed previously. Again we need to be careful about the conservation of particle number:

$$\hat{N} = \int dx \ \left(\psi^\dagger\psi + 2\hat{\mathbf{\Xi}}^\dagger\cdot\hat{\mathbf{\Xi}} + 2\hat{\Pi}^\dagger\hat{\Pi}\right), \quad [\hat{N}, \hat{\mathcal{H}}] = 0. \tag{3.8}$$

This can be achieved by imposing the following commutation and anticommutation relations:

$$\begin{aligned} &\{\hat{\psi}_\sigma(x), \hat{\psi}^\dagger_{\sigma'}(x')\} = \delta_{\sigma\sigma'}\delta(x-x'), \\ &\{\hat{\psi}^\dagger_\sigma(x), \hat{\psi}^\dagger_{\sigma'}(x')\} = 0, \quad \{\hat{\psi}_\sigma(x), \hat{\psi}_{\sigma'}(x')\} = 0 \\ &[\hat{\Xi}_\mu(x), \hat{\Xi}^\dagger_{\mu'}(x')] = \delta_{\mu\mu'}\delta(x-x'), \\ &[\hat{\Pi}(x), \hat{\Pi}^\dagger(x')] = \delta(x-x'), \end{aligned} \tag{3.9}$$

and all the other commutators give out zero. In the above equations, the spin labels σ, σ' take values of $\uparrow, \downarrow$, and the polarization labels μ, μ' take values of $+, -, z$. The relation between polarization labels

and vector labels is as follows:

$$\hat{\Xi}_+ = \frac{1}{\sqrt{2}}(\hat{\Xi}_x + i\hat{\Xi}_y), \quad \hat{\Xi}_- = \frac{1}{\sqrt{2}}(\hat{\Xi}_x - i\hat{\Xi}_y). \tag{3.10}$$

The bosonic and fermionic models introduced here can be solved via Bethe ansatz if we fine tune the resonant energies $\epsilon_0, \epsilon_\Xi, \epsilon_\Pi$, and both of them can be effectively described as a two-component system with intraspecies repulsion and interspecies attraction. By tuning the strength of attraction from vanishingly small toward the strength of repulsion, the system first shows BCS-type pairing behavior, then it develops toward the fermionic super Tonks-Girardeau gas regime, and finally, it turns into the weakly interacting bosons regime and shows BEC-type pairing behavior. Thus we can have a single Hamiltonian governing the whole range of BCS-BEC crossover, and there is no geometric confinement preventing the breaking of bound pairs. What is more, if we tune the strength of attraction beyond repulsion, we will enter into a new regime where the uniform configuration is unstable and the system collapses into a bright soliton. Now let us discuss these interesting physics one by one, starting from the integrability.

3.2.2 Integrability

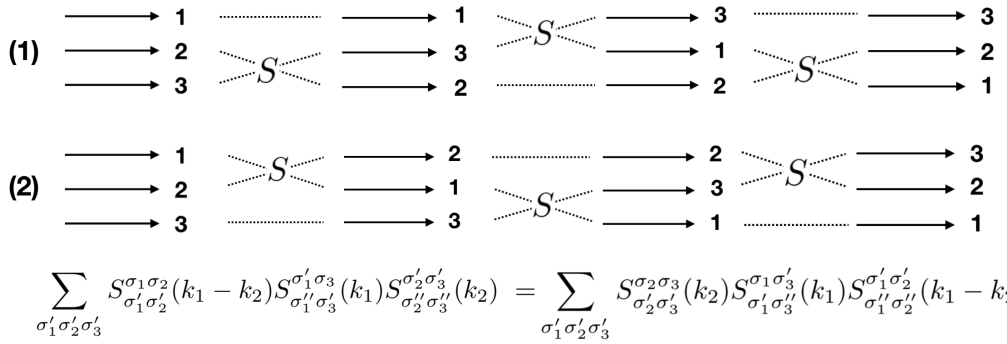

$$\sum_{\sigma_1'\sigma_2'\sigma_3'} S^{\sigma_1\sigma_2}_{\sigma_1'\sigma_2'}(k_1-k_2) S^{\sigma_1'\sigma_3}_{\sigma_1''\sigma_3'}(k_1) S^{\sigma_2'\sigma_3'}_{\sigma_2''\sigma_3''}(k_2) = \sum_{\sigma_1'\sigma_2'\sigma_3'} S^{\sigma_2\sigma_3}_{\sigma_2'\sigma_3'}(k_2) S^{\sigma_1\sigma_3'}_{\sigma_1'\sigma_3''}(k_1) S^{\sigma_1'\sigma_2'}_{\sigma_1''\sigma_2''}(k_1-k_2)$$

Figure 3.1: Illustration of the Yang-Baxter equation. It is essentially a requirement of consistency such that the two different scattering paths in (1) and (2) give out the same result.

Integrable models with internal degrees of freedom can be solved using the quantum inverse scattering method [105, 58]. The essential point is to construct the two-body S-matrix which fulfills the Yang-Baxter equation (see Fig. 3.1 for an illustration). For a time inversion and space inversion invariant and species-conserving model in free space, the two-body S-matrix in pseudospin subspace

$\{\uparrow,\downarrow\}$ assumes the following general form:

$$S(k)=\begin{pmatrix} a(k) & 0 & 0 & 0 \\ 0 & b(k) & c(k) & 0 \\ 0 & c(k) & b(k) & 0 \\ 0 & 0 & 0 & a(k) \end{pmatrix}, \tag{3.11}$$

where the relative momentum $k=k_2-k_1$ is the difference in momentum between the two scattering particles. The requirement of unitarity

$$S^\dagger(k)S(-k)=S(k)S^\dagger(-k)=I \tag{3.12}$$

together with the Yang-Baxter equation

$$\sum_{\sigma_1'\sigma_2'\sigma_3'} S^{\sigma_1\sigma_2}_{\sigma_1'\sigma_2'}(k_1-k_2)S^{\sigma_1'\sigma_3}_{\sigma_1''\sigma_3'}(k_1)S^{\sigma_2'\sigma_3'}_{\sigma_2''\sigma_3''}(k_2)=\sum_{\sigma_1'\sigma_2'\sigma_3'} S^{\sigma_2\sigma_3}_{\sigma_2'\sigma_3'}(k_2)S^{\sigma_1\sigma_3'}_{\sigma_1'\sigma_3''}(k_1)S^{\sigma_1'\sigma_2'}_{\sigma_1''\sigma_2''}(k_1-k_2) \tag{3.13}$$

then put severe constraints on the S-matrix elements:

$$\begin{aligned} &a(k)a(-k)=1, \quad a(k)=b(k)+c(k), \quad \frac{a(k)}{b(k)}+\frac{a(-k)}{b(-k)}=2, \\ &\frac{a(k_1)b(k_2)-a(k_2)b(k_1)}{b(k_2-k_1)}=\frac{c(k_1)c(k_2)}{c(k_2-k_1)}. \end{aligned} \tag{3.14}$$

As a result, the integrability can be checked by identifying the S-matrix elements in Eq. (3.11) and checking the validity of Eq. (3.14). Then the exact solutions can be explicitly constructed using the algebraic Bethe ansatz [105, 58], and the resulting Bethe ansatz equations for an eigenstate with M out of N particles placed spin-down are as follows (for a short summary of the standard derivation, see Appendix C):

$$\begin{aligned} &\prod_{n=1}^{N}\frac{a(\Lambda_\alpha-k_n)}{b(\Lambda_\alpha-k_n)}=\prod_{\substack{\beta=1\\ \beta\neq\alpha}}^{M}\frac{a(\Lambda_\alpha-\Lambda_\beta)b(\Lambda_\beta-\Lambda_\alpha)}{a(\Lambda_\beta-\Lambda_\alpha)b(\Lambda_\alpha-\Lambda_\beta)}, \quad \alpha=1,2,\cdots,M; \\ &(\mp)^{N-1}\exp(-ik_jL)=\prod_{n=1}^{N}a(k_j-k_n)\prod_{\alpha=1}^{M}\frac{a(\Lambda_\alpha-k_j)}{b(\Lambda_\alpha-k_j)}, \quad j=1,2,\cdots,N, \end{aligned} \tag{3.15}$$

where L is the size of the system, the charge rapidities $k_n, n=1,2,\cdots,N$ are the physical momenta, and the spin rapidities $\Lambda_\alpha, \alpha=1,2,\cdots,M$ are auxiliary parameters (thus the ansatz is also called nested Bethe ansatz). Also in the second set of equations, the upper sign is for bosons, and the lower

sign is for fermions.

We first review the Bethe ansatz equations for the Yang-Gaudin model and the Lieb-Liniger model and then turn to the present models defined in Eqs. (3.3) and (3.7). The S-matrix elements for the Yang-Gaudin model described in Eq. (3.1) are [105, 58]:

$$a(k) = 1, \quad b(k) = \frac{k}{k - ic_F}, \quad c(k) = \frac{-ic_F}{k - ic_F}. \tag{3.16}$$

This clearly fulfills the integrability criterion as specified in Eq. (3.14). Then it is straightforward to substitute Eq. (3.16) into Eq. (3.15) to obtain the Bethe ansatz equations:

$$\begin{aligned} \prod_{j=1}^{N} \left(\frac{\Lambda_\alpha - k_j - ic'_F}{\Lambda_\alpha - k_j + ic'_F} \right) &= - \prod_{\beta=1}^{M} \left(\frac{\Lambda_\alpha - \Lambda_\beta - ic_F}{\Lambda_\alpha - \Lambda_\beta + ic_F} \right), \\ \exp(ik_j L) &= \prod_{\alpha=1}^{M} \left(\frac{k_j - \Lambda_\alpha - ic'_F}{k_j - \Lambda_\alpha + ic'_F} \right), \end{aligned} \tag{3.17}$$

where $c'_F = c_F/2$ and we have made the conventional shift $\Lambda_\alpha \to \Lambda_\alpha + ic'_F$. The ground state configuration of this attractive Yang-Gaudin model (with even number of particles) is known to be a Fermi sea of two-string solutions with the structure:

$$k_{\alpha,1} = \Lambda_\alpha + ic'_F, \quad k_{\alpha,2} = \Lambda_\alpha - ic'_F, \tag{3.18}$$

where $\alpha = 1, 2, \cdots, M$ with $M = N/2$, and the Bethe ansatz equations reduce into equations for the center momenta Λ_α:

$$\exp(2i\Lambda_\alpha L) = (-) \prod_{\beta=1}^{M} \left(\frac{\Lambda_\alpha - \Lambda_\beta - ic_F}{\Lambda_\alpha - \Lambda_\beta + ic_F} \right). \tag{3.19}$$

Because the center momenta Λ_α in the ground state configuration are all real, we can take the logarithm of the above equations:

$$2\Lambda_\alpha L = 2\pi J_\alpha - \sum_{\beta=1}^{M} \theta(\Lambda_\alpha - \Lambda_\beta), \tag{3.20}$$

where J_αs are consecutive integers or half-odd integers depending on:

$$J_\alpha = \frac{M + 1 - 2\alpha}{2}, \quad \alpha = 1, 2, \cdots, M. \tag{3.21}$$

The phase-shift function $\theta(\Lambda - \Lambda')$ is defined as:

$$\theta(\Lambda - \Lambda') = -2 \arctan\left(\frac{\Lambda - \Lambda'}{c_F}\right). \tag{3.22}$$

In the thermodynamic limit where $N \to \infty, L \to \infty$ with fixed density $n_F = N/L$, Eq. (3.20) can be replaced by an integral equation for the density of state $\sigma(\Lambda_j) = 1/L(\Lambda_{j+1} - \Lambda_j)$, following Hultén's continualization procedure [48]:

$$\sigma(\Lambda) + \frac{c_F}{\pi} \int_{-Q}^{Q} d\Lambda' \frac{\sigma(\Lambda')}{(\Lambda - \Lambda')^2 + c_F^2} = \frac{1}{\pi}, \tag{3.23}$$

where Q is the Fermi momentum of the ground state, and it is determined by the density n_F via the relation:

$$\frac{n_F}{2} = \int_{-Q}^{Q} d\Lambda \ \sigma(\Lambda). \tag{3.24}$$

After solving the above integral equation, the physical quantities of the ground state can then be calculated in terms of the density of states $\sigma(\Lambda)$.

The Lieb-Liniger model as described in Eq. (3.2) in fact has simpler structure compared with the Yang-Gaudin model, because it is a single-component model. The resulting ground state configuration with N particles fulfills the Bethe ansatz equations:

$$k_j L = 2\pi I_j - \sum_{n=1}^{N} \theta(k_j - k_n), \tag{3.25}$$

where I_js are consecutive integers or half-odd integers depending on:

$$I_j = \frac{N + 1 - 2j}{2}, j = 1, 2, \cdots, N. \tag{3.26}$$

The corresponding phase-shift function is defined as

$$\theta(k - k') = 2 \arctan\left(\frac{k - k'}{c_B}\right), \tag{3.27}$$

and the integral equation for the density of states $\rho(k) = 1/L(k_{j+1} - k_j)$ in the thermodynamic limit is:

$$\rho(k) - \frac{c_B}{\pi} \int_{-q}^{q} dk' \frac{\rho(k')}{(k - k')^2 + c_B^2} = \frac{1}{2\pi}. \tag{3.28}$$

Similarly q is the Fermi momentum of the ground state [1], and it is determined by the density $n_B = N/L$ via the relation:

$$n_B = \int_{-q}^{q} dk\ \rho(k). \tag{3.29}$$

Now it is clear from Eqs. (3.23) and (3.28) that we can formally connect the Yang-Gaudin model and the Lieb-Liniger model by just a change of sign of the coupling constant c, where the spinless boson in the Lieb-Liniger model is identified with the singlet bound pair in the Yang-Gaudin model (thus the requirement that $m_B = 2m_F$ and $n_B = 2n_F$).

Now we consider the model defined in Eq. (3.3). It can be intuitively understood as follows: The two-component bosonic atoms denoted by $\hat{\psi}$ live on hyperplanes corresponding to different ordering sectors X, where $x_{X_1} < x_{X_2} < \cdots < x_{X_N}$. Without resonant couplings as in the case of the Yang-Gaudin and the Lieb-Liniger model, we only need to require the continuity of wave functions when these hyperplanes intersect. With Feshbach resonances as in our model, the molecules denoted by $\hat{\Pi}$ can be viewed as living on the intersections of the hyperplanes, which play the role of boundary conditions. As a result, we can describe the system with atomic S-matrices, where the molecules only enter as appropriate boundary conditions for the atomic wave functions. Next, we calculate the corresponding S-matrix elements to check the integrability of the present model.

In the triplet channel for ψ-bosons, the Π-boson is not excited, and we have both configuration $(\uparrow\uparrow)$ and $(\uparrow\downarrow + \downarrow\uparrow)/\sqrt{2}$. The two-atom states for them are

$$\begin{aligned} |\text{two atom}\rangle^{\text{tri},1} &= \int dx_1 dx_2\ \phi(x_1,x_2)\hat{\psi}^\dagger_\uparrow(x_1)\hat{\psi}^\dagger_\uparrow(x_2)\,|0\rangle\,, \\ |\text{two atom}\rangle^{\text{tri},0} &= \int dx_1 dx_2\ \phi(x_1,x_2)\frac{\hat{\psi}^\dagger_\uparrow(x_1)\hat{\psi}^\dagger_\downarrow(x_2)+\hat{\psi}^\dagger_\uparrow(x_2)\hat{\psi}^\dagger_\downarrow(x_1)}{2}\,|0\rangle\,. \end{aligned} \tag{3.30}$$

By acting the S-matrix in Eq. (3.11) on both wave functions, we obtain

$$\begin{aligned} S(k)\,|\text{two atom}\rangle^{\text{tri},1} &= a(k)\,|\text{two atom}\rangle^{\text{tri},1}\,, \\ S(k)\,|\text{two atom}\rangle^{\text{tri},0} &= \Big(b(k)+c(k)\Big)\,|\text{two atom}\rangle^{\text{tri},0}\,, \end{aligned} \tag{3.31}$$

which leads to the result that $a(k) = b(k) + c(k)$. Taking into account that the spatial part of the wave functions has even parity, we can make the ansatz for $\phi(x_1, x_2) = \phi_{\text{tri}}(x_2 - x_1)$ such that:

$$\phi_{\text{tri}}(x) = \cos(kx/2 + \delta_{\text{tri}}\text{sgn}x), \tag{3.32}$$

[1] Interacting one dimensional system has the interesting properties that both bosons and fermions obey the exclusion principle: identical particles cannot have the same momentum, otherwise the wave function will vanish. For a detailed discussion, see Ref. [58].

where $\delta_{\rm tri}$ is the scattering phase shift. The corresponding Schrödinger equation for $\phi_{\rm tri}(x)$ can then be derived from the model Hamiltonian in Eq. (3.3):

$$(-2\partial_x^2 - k^2/2)\phi_{\rm tri}(x) + 2g\delta(x)\phi_{\rm tri}(0) = 0, \tag{3.33}$$

where $\phi_{\rm tri}(0) \equiv [\phi_{\rm tri}(0^+) + \phi_{\rm tri}(0^-)]/2 = \cos\delta_{\rm tri}$. Integration of Eq. (3.33) around $x = 0$ gives out

$$a(k) = b(k) + c(k) = e^{i2\delta_{\rm tri}} = \frac{k - ig}{k + ig}. \tag{3.34}$$

In the singlet channel for ψ-bosons, the Π-boson is also excited. The general form of the two-atom state in this case can be expressed as:

$$|\text{two atom}\rangle^{\rm sin} = \int dy\ \Phi(y)\hat{\Pi}^\dagger(y)\,|0\rangle + \int dx_1 dx_2\ \phi(x_1,x_2)\frac{\hat{\psi}_\uparrow^\dagger(x_1)\hat{\psi}_\downarrow^\dagger(x_2) - \hat{\psi}_\uparrow^\dagger(x_2)\hat{\psi}_\downarrow^\dagger(x_1)}{2}\,|0\rangle\,. \tag{3.35}$$

Based on symmetry considerations, the following ansatz for $\phi(x_1, x_2)$ and $\Phi(y)$ is appropriate:

$$\phi(x_1,x_2) = \phi_{\rm sin}(x_2 - x_1)e^{iK(x_1+x_2)}, \quad \Phi(y) = \Phi\ e^{2iKy}, \tag{3.36}$$

where K is the momentum of the mass center and the singlet wave function has odd parity

$$\phi_{\rm sin}(x) = \sin(kx/2 + \delta_{\rm sin}{\rm sgn}x). \tag{3.37}$$

Then the corresponding Schrödinger equation is:

$$\begin{aligned} &(-2\partial_x^2 - k^2/2)\phi_{\rm sin}(x) + t^*\delta'(x)\Phi = 0, \\ &-\epsilon_0\Phi - t\partial_x\phi(x)\Big|_{x\to 0^+} = k^2\Phi/2, \end{aligned} \tag{3.38}$$

which gives the expression for the S-matrix element in the singlet channel

$$b(k) - c(k) = e^{2i\delta_{\rm sin}} = \frac{4(k^2 + 2\epsilon_0) - i|t|^2k}{4(k^2 + 2\epsilon_0) + i|t|^2k}. \tag{3.39}$$

Equation (3.39) together with Eq. (3.34) give us the expression of matrix elements specified in Eq. (3.11). Substituting them into the requirement in Eq. (3.14), we finally arrive at the follow-

ing condition for integrability of the present model defined in Eq. (3.3):

$$2\epsilon_0 = g(g - |t|^2/4). \tag{3.40}$$

This can be achieved by fine tuning the resonant energy ϵ_0. We further introduce new coupling constants c_1, c_2 as:

$$c_1 = g, \quad c_2 = 2\epsilon_0/g, \tag{3.41}$$

such that the S-matrix elements take the simple form

$$a(k) = \frac{k - ic_1}{k + ic_1}, \quad \frac{b(k)}{a(k)} = \frac{k}{k - ic_2}. \tag{3.42}$$

In the case with repulsive intraspecies coupling $c_1 > 0$, the sign of c_2 is controlled by the resonant energy ϵ_0. The choice $c_2 > 0$ introduces a interspecies attraction resulting a physical pole in the singlet channel, which is exactly the singlet bound state with binding energy $\epsilon_0 > 0$ that we have in mind when proposing the model. Furthermore from Eq. (3.40) we can infer the competition between the two coupling constants:

$$c_1 - c_2 = |t|^2/4 > 0. \tag{3.43}$$

Above we only considered two-body scatterings defined by the Hamiltonian in Eq. (3.3) and we showed that the model can be made integrable by fine-tuning the resonant energy if only two-body scatterings are important. Strictly speaking, this is not sufficient for the integrability when we consider three-body and four-body scatterings (in particular, the resulting wave functions for the three-atom sector have discontinuities when a Π particle sits right on top of a ψ particle). In another word, the Π-ψ and Π-Π scatterings cannot be factorized into successive two-body scatterings. Practically, at least for relatively small densities of the system, the effect of three-body and four-body scatterings is negligible compared with two-body scatterings, since Π particles live only on the intersections of the hyperplanes and their scatterings are of measure zero. This is in the spirit of the so-called asymptotic Bethe ansatz [98, 42, 51]. It is also possible to save the factorizability by introducing counterterms to the quadratic spectrum, as what has been done for the exact solution to the multichannel Kondo model [91, 4]. This recipe can be made local and Galilean invariant, for example, the counter terms to be added to the Hamiltonian are

$$\hat{\mathcal{H}}_{\text{counter}} = \frac{1}{2}\int dx \ \left[\mathcal{T}_x\left(\partial_x\hat{\Pi}^\dagger\hat{\psi}^\dagger\hat{\psi}\hat{\Pi} - 2\hat{\Pi}^\dagger\partial_x\hat{\psi}^\dagger\hat{\psi}\hat{\Pi} + \partial_x\hat{\Pi}^\dagger\hat{\Pi}^\dagger\hat{\Pi}\hat{\Pi}\right) + h.c.\right], \tag{3.44}$$

where the jumping operator $\mathcal{T}_x$ on two-body interaction terms is defined as

$$\mathcal{T}_x\left[\hat{A}^\dagger\hat{B}^\dagger\hat{C}\hat{D}\right] \equiv \left[\hat{A}^\dagger(x)\hat{B}^\dagger(x')\hat{C}(x)\hat{D}(x')\right]_{x'=x-0} - \left[\hat{A}^\dagger(x)\hat{B}^\dagger(x')\hat{C}(x)\hat{D}(x')\right]_{x'=x+0}. \tag{3.45}$$

Although these counterterms save the factorizability when the resonance is turned on ($t \neq 0$), they pose the problem of producing a continuum of bound states when the resonance is turned off ($t = 0$), and we don't know what will become of these bound states once the resonance is turned on. Here we disregard all these complexities and use the S-matrix specified in Eq. (3.42) to construct the Bethe ansatz. We believe this captures the essential features of the model as the corresponding Bethe ansatz equations give out physically sensible results.

Before entering into the standard process of quantum inverse scattering method of solving the bosonic model, we also check the integrability of the fermionic model described in Eq. (3.7) on the two-body scattering level, disregarding the complexities discussed above. Then the same S-matrix elements in Eq. (3.42) are obtained for the fermionic model but with the possibility of $c_1 < c_2$. We follow the same procedure as the bosonic case. The corresponding Schrödinger equation in the triplet channel is then

$$\begin{aligned} (-2\partial_x^2 - k^2/2)\phi_{\rm tri}(x) + t_\Xi^*\delta'(x)\Phi_\Xi = 0, \\ -\epsilon_\Xi\Phi_\Xi - t_\Xi\partial_x\phi_{\rm tri}(x)_{x\to 0^+} = k^2\Phi_\Xi/2, \end{aligned} \tag{3.46}$$

where $\phi_{\rm tri}(x) = \sin(kx/2 + \delta_{\rm tri}{\rm sgn}x)$ is the spatial part of the triplet wave function and Φ_Ξ is the amplitude of the vector resonance wave function. We then obtain the S-matrix element in the triplet channel:

$$a(k) = b(k) + c(k) = e^{2i\delta_{\rm tri}} = \frac{4(k^2 + 2\epsilon_\Xi) - i|t_\Xi|^2 k}{4(k^2 + 2\epsilon_\Xi) + i|t_\Xi|^2 k}. \tag{3.47}$$

Similarly, in the singlet channel we have the following Schrödinger equation:

$$\begin{aligned} (-2\partial_x^2 - k^2/2)\phi_{\rm sin}(x) + [2g\phi_{\rm sin}(0) + t_\Pi^*\Phi_\Pi]\delta(x) = 0, \\ -\epsilon_\Pi\Phi_\Pi + t_\Pi\phi_{\rm sin}(0) = k^2\Phi_\Pi/2, \end{aligned} \tag{3.48}$$

where $\phi_{\rm sin}(x) = \cos(kx/2 + \delta_{\rm sin}{\rm sgn}x)$ is the spatial part of the singlet wave function and Φ_Π is the amplitude of the scalar resonance wave function. We then obtain the S-matrix element in the singlet channel:

$$b(k) - c(k) = e^{2i\delta_{\rm sin}} = \frac{k(k^2 + 2\epsilon_\Pi) - i[gk^2 + 2g\epsilon_\Pi + |t_\Pi|^2]}{k(k^2 + 2\epsilon_\Pi) + i[gk^2 + 2g\epsilon_\Pi + |t_\Pi|^2]}. \tag{3.49}$$

Equation (3.47) together with Eq. (3.49) produce the same S-matrix elements in Eq. (3.42) if the following fine tuning is applied:

$$\epsilon_\Xi = 0, \quad \frac{|t_\Xi|^2}{4}\left(\frac{|t_\Xi|^2}{4} - g\right) = -\frac{|t_\Pi|^2}{g} = 2\epsilon_\Pi, \tag{3.50}$$

and the coupling constants c_1, c_2 are defined as:

$$c_1 = |t_\Xi|^2/4, \quad c_1 - c_2 = -|t_\Pi|^2/(2\epsilon_\Pi). \tag{3.51}$$

If the scalar resonance is made a singlet bound state with binding energy $\epsilon_\Pi > 0$, then we realize the possibility of $c_1 < c_2$ mentioned above.

Since both the bosonic and fermionic model present the same form of S-matrix elements in Eq. (3.42), we can discuss their exact solutions together by substituting Eq. (3.42) into Eq. (3.15). The resulting algebraic Bethe ansatz equations in the sector where M out of N atoms are placed spin-down are:

$$\begin{aligned}
(-)\prod_{n=1}^{N}\frac{\Lambda_\alpha - k_n - ic_2'}{\Lambda_\alpha - k_n + ic_2'} &= \prod_{\beta=1}^{M}\frac{\Lambda_\alpha - \Lambda_\beta - ic_2}{\Lambda_\alpha - \Lambda_\beta + ic_2}, \\
(\mp)^{N-1}e^{-ik_jL} &= \prod_{n=1}^{N}\frac{k_j - k_n - ic_1}{k_j - k_n + ic_1}\prod_{\alpha=1}^{M}\frac{\Lambda_\alpha - k_j - ic_2'}{\Lambda_\alpha - k_j + ic_2'},
\end{aligned} \tag{3.52}$$

where L is the size of the system, $c_2' = c_2/2$, $j, n = 1, 2, \cdots, N$ and $\alpha, \beta = 1, 2, \cdots, M$. The conventional shift $\Lambda_\alpha \to \Lambda_\alpha + ic_2'$ is introduced. Also the upper sign is for bosons, and the lower sign is for fermions. In the following sections we discuss the two cases with $c_1 > c_2 > 0$ and $c_2 > c_1 > 0$ respectively.

3.3 Uniform Regime with $c_1 > c_2 > 0$

In this section, we discuss the present model in the parameter regime $c_1 > c_2 > 0$, where the ground state is a Fermi sea of the two-atom bound pair. Firstly, we derive the equation for the density of states in the thermodynamic limit, where we analyze its singular behavior due to level condensation and find that the Fermi momentum is bounded from above. Then we discuss the physics of BCS-BEC crossover in the context of the present model, where we find that the extremes of the excitation spectra have robust features and the system develops a collapsing instability in the limit $c_2 \to c_1$. After that, we discuss the zero temperature phase diagram of the present model with an external magnetic field,

of which a considerable part is occupied by the one dimensional analog of the FFLO state. Besides, a critical magnetic field arises due to the presence of the upper bound for the Fermi momentum. This is in contrast to the situation for the Yang-Gaudin model, where an arbitrarily small external magnetic field can polarize the ground state as long as the particle density of the system is large enough.

3.3.1 Level Condensation and Limiting Fermi Momentum Q^*

Let us start with the system with even number of atoms. Then the ground state is a Fermi sea of two-strings with the same structure as in the Yang-Gaudin model:

$$k_{\alpha,1} = \Lambda_\alpha + ic_2', \quad k_{\alpha,2} = \Lambda_\alpha - ic_2', \tag{3.53}$$

where $\alpha = 1, 2, \cdots, M = N/2$ and the Bethe ansatz equations in Eq. (3.52) reduce to the equations for the center momenta Λ_α:

$$\begin{aligned} e^{i2\Lambda_\alpha L} = (-)\prod_{\beta=1}^{M} &\left(\frac{\Lambda_\alpha - \Lambda_\beta - ic_2}{\Lambda_\alpha - \Lambda_\beta + ic_2}\right)\left(\frac{\Lambda_\alpha - \Lambda_\beta + ic_1}{\Lambda_\alpha - \Lambda_\beta - ic_1}\right)^2 \\ &\left(\frac{\Lambda_\alpha - \Lambda_\beta + i(c_1+c_2)}{\Lambda_\alpha - \Lambda_\beta - i(c_1+c_2)}\right)\left(\frac{\Lambda_\alpha - \Lambda_\beta + i(c_1-c_2)}{\Lambda_\alpha - \Lambda_\beta - i(c_1-c_2)}\right). \end{aligned} \tag{3.54}$$

Because the center momenta Λ_α in the ground state are all real, we can take the logarithm of the above equations:

$$2\Lambda_\alpha L = 2\pi J_\alpha - \sum_{\beta=1}^{M} \theta(\Lambda_\alpha - \Lambda_\beta), \tag{3.55}$$

where J_αs are consecutive integers or half-odd integers depending on:

$$J_\alpha = \frac{M+1-2\alpha}{2}, \quad \alpha = 1, 2, \cdots, M. \tag{3.56}$$

The phase-shift function $\theta(\Lambda - \Lambda')$ is defined as:

$$\begin{aligned} \theta(\Lambda-\Lambda') = &-2\arctan\left(\frac{\Lambda-\Lambda'}{c_2}\right) + 4\arctan\left(\frac{\Lambda-\Lambda'}{c_1}\right) \\ &+ 2\arctan\left(\frac{\Lambda-\Lambda'}{c_1+c_2}\right) + 2\arctan\left(\frac{\Lambda-\Lambda'}{c_1-c_2}\right). \end{aligned} \tag{3.57}$$

We can see that Eq. (3.57) reduces to Eq. (3.22) in the limit $c_2 \ll 1 \ll c_1$, and to Eq. (3.27) in the limit $0 < c_1 - c_2 \ll 1 \ll c_1$, so the present model has the Yang-Gaudin model and the Lieb-Liniger model as its two limiting models. Also the total energy and momentum of the system can then be

expressed as:

$$E=\sum_{\alpha=1}^{M}\left[\left(\Lambda_\alpha+\frac{ic_2}{2}\right)^2+\left(\Lambda_\alpha-\frac{ic_2}{2}\right)^2\right],\quad P=\sum_{\alpha=1}^{M}2\Lambda_\alpha. \tag{3.58}$$

In the thermodynamic limit, Eq. (3.55) can be replaced by an integral equation for the density of state $\sigma(\Lambda_j)=1/[L(\Lambda_{j+1}-\Lambda_j)]$, just like what we have discussed previously:

$$\sigma(\Lambda)-\int_{-Q}^{Q}d\Lambda'\ K(\Lambda-\Lambda')\sigma(\Lambda')=\frac{1}{\pi},\quad K(\Lambda-\Lambda')=\frac{1}{2\pi}\theta'(\Lambda-\Lambda'), \tag{3.59}$$

where Q is the Fermi momentum of the ground state, and it is determined by the density $n=N/L$ via the relation:

$$\frac{n}{2}=\int_{-Q}^{Q}d\Lambda\ \sigma(\Lambda). \tag{3.60}$$

Also the total energy and momentum of the system in the thermodynamic limit can be expressed using the density of state $\sigma(\Lambda)$:

$$E=\int_{-Q}^{Q}d\Lambda\left(2\Lambda^2-\frac{c_2^2}{2}\right)\sigma(\Lambda),\quad P=\int_{-Q}^{Q}d\Lambda\ 2\Lambda\sigma(\Lambda). \tag{3.61}$$

For further analysis of Eq. (3.59), it is useful to rescale the parameters with respect to Q:

$$x\equiv\frac{\Lambda}{Q},\quad \lambda\equiv\frac{c_1}{Q},\quad \xi\equiv\frac{c_2}{c_1}. \tag{3.62}$$

Correspondingly, the integral equation for the density of states with the rescaled parameters is:

$$\sigma(x)-\int_{-1}^{1}dx'\ K(x-x')\sigma(x')=\frac{1}{\pi}, \tag{3.63}$$

where $K(x)$ expressed in the rescaled parameters is

$$K(x)=\frac{1}{\pi}\left(-\frac{\xi\lambda}{x^2+(\xi\lambda)^2}+\frac{2\lambda}{x^2+\lambda^2}+\frac{(1+\xi)\lambda}{x^2+(1+\xi)^2\lambda^2}+\frac{(1-\xi)\lambda}{x^2+(1-\xi)^2\lambda^2)}\right), \tag{3.64}$$

and Eq. (3.60) is equivalent to

$$\int_{-1}^{1}dx\ \sigma(x)=\frac{n}{2Q}. \tag{3.65}$$

By construction, the density of states $\sigma(x)\geqslant 0$ for $x\in[-1,1]$. Correspondingly, the kernel

$$\mathcal{L}(x,x')=\delta(x-x')-K(x-x') \tag{3.66}$$

in Eq. (3.63) must also be a positive definite operator, with its smallest eigenvalue bigger than $1/(\pi\sigma_{\max})$, where $\sigma_{\max}$ is the maximum value of $\sigma(x)$ on the interval $x \in [-1, 1]$ [58]. This is indeed the case in the Lieb-Liniger model and the Yang-Gaudin model for any coupling strength.

However, in the present model, the kernel $\mathcal{L}(x, x')$ in Eq. (3.66) is positive definite only for $\lambda > \lambda^* = \lambda^*(\xi)$, where $\lambda^*(\xi)$ will be found later. Equivalently, Eq. (3.62) yields an upper bound for the Fermi momentum:

$$Q < Q^* = c_1/\lambda^*. \tag{3.67}$$

Then, the apparent conflict appears: How do we satisfy the conservation of the mass density of the system in Eqs. (3.60) and (3.65) while the Fermi momentum Q is limited by Q^*? Solution of this problem is to have $\sigma(x) \to \infty$ at $n \to \infty$ while keeping Q^* fixed. The only way to have such a result is to require the operator $\mathcal{L}(x, x')$ to have an almost zero mode at $\lambda \to \lambda^* + 0$:

$$\int_{-1}^{1} dx' \mathcal{L}_{\lambda^*}(x, x')\sigma^0(x) = 0. \tag{3.68}$$

This phenomenon reminds us the condensation of levels which is characteristic for weakly interacting bosons (see Fig. 3.2).

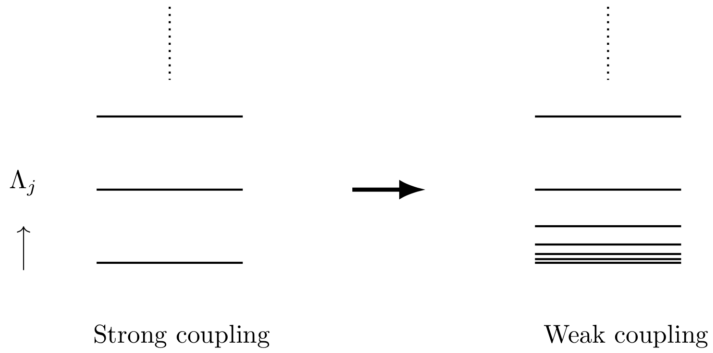

Figure 3.2: Condensation of levels for weakly interacting bosons in one dimension. Left pane is drawn for strong coupling and right pane is draw for weak coupling.

For a fixed value of ξ and different values of λ, we solve Eq. (3.63) numerically using the modified quadrature method [86], where the usual quadrature approximation to the integral is modified to give more accurate result for a weakly singular kernel. The critical value $\lambda^*(\xi)$ is determined by the point at which the value of the solution $\sigma(x)$ to Eq. (3.63) changes from positive to negative. Accordingly, for a fixed value of ξ, the zero mode $\sigma^0(x)$ for $\mathcal{L}_{\lambda^*}(x, x')$ can be approximated by the singular part of the solution $\sigma(x)$ that grows with increasing density n when $\lambda \to \lambda^*(\xi) + 0$. The numerically determined

critical curve $\lambda^*(\xi)$ is shown in Fig. 3.3, which has the limiting behavior that $\lambda^*(\xi \to 0) \approx 0.88$ and $\lambda^*(\xi \to 1) \to \infty$. In the latter limit, the upper bound Q^* goes to zero and the system develops a collapsing instability which we will discuss in Sec. 3.4. Also the critical curve $\lambda^*(\xi)$ can be fitted by

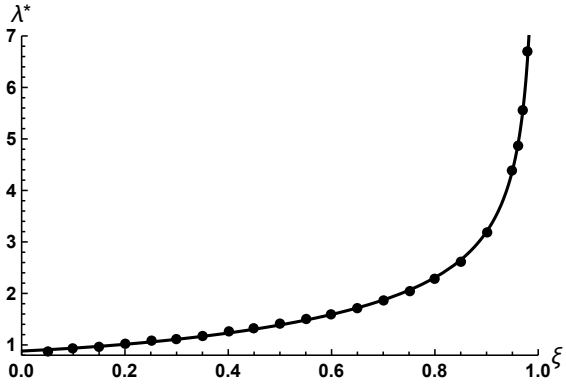

Figure 3.3: The critical value λ^* as a function of $\xi = c_2/c_1$. The dots are obtained numerically and the thick line is the curve of the fitting function in Eq. (3.69). We can see that as $\xi \to 1$, $\lambda^* \to \infty$, which means that Q^* tends to zero, this implies the instability of the system.

the following formula:

$$\lambda^*(\xi) = \sqrt{\frac{0.75}{1-\xi}} + 0.015 + 0.045\xi + 0.50\xi^2, \quad \xi \in (0,1), \tag{3.69}$$

The solution $\sigma(x)$ to Eq. (3.63) at $\lambda \to \lambda^* + 0$ for several values of ξ is shown in Fig. 3.4, and it consists of a regular and a singular part:

$$\sigma(x) = \sigma_{\rm reg}(x) + \sigma^0(x), \tag{3.70}$$

where the singular part $\sigma^0(x)$ can be viewed as the approximated zero mode defined in Eq. (3.68), thus we use the same symbol for them.

In the limit $\xi \to 1$, we can extract the analytical expression for the zero mode from Eq. (3.63). For $\xi \to 1$, we have $(1-\xi)\lambda^*(\xi) \to 0$ from Eq. (3.69), then $K(x-x')$ in Eq. (3.64) at $\lambda \to \lambda^* + 0$ can be approximated as

$$\begin{aligned} K(x-x') &\approx \frac{1}{\pi}\left(\frac{3}{2\lambda} + \frac{(1-\xi)\lambda}{(x-x')^2 + (1-\xi)^2\lambda^2}\right), \\ &\approx \frac{3}{2\pi\lambda} + \delta(x-x') - \frac{(1-\xi)\lambda}{\pi}\frac{\partial}{\partial x}\mathcal{P}\frac{1}{x-x'}, \end{aligned} \tag{3.71}$$

where the symbol $\mathcal{P}$ represents the Cauchy principle part. As a result, Eq. (3.63) can be reduced to

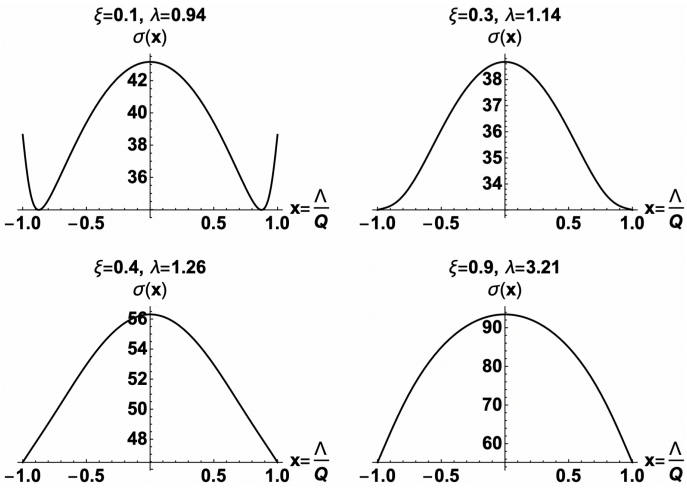

Figure 3.4: The solution $\sigma(x)$ to Eq. (3.63) for $\lambda \to \lambda^*(\xi) + 0$. $\sigma(x)$ can be separated into the regular part $\sigma_{\rm reg}(x)$ and the singular part $\sigma^0(x)$, where the latter grows with increasing n and is seen in the figure as the part near $x = 0$.

an equation for the zero mode $\sigma^0(x)$:

$$-\frac{3}{2\pi\lambda}\int_{-1}^{1} dx'\sigma^0(x') + \frac{(1-\xi)\lambda}{\pi}\frac{\partial}{\partial x}\mathcal{P}\int_{-1}^{1} dx'\frac{\sigma^0(x')}{x-x'} = \frac{1}{\pi}. \tag{3.72}$$

Using the identity that

$$\mathcal{P}\int_{-1}^{1}\frac{dx'}{x-x'}\sqrt{1-x'^2} = \pi x, \tag{3.73}$$

the solution $\sigma^0(x)$ to Eq. (3.72) can be determined as

$$\sigma^0(x) = \frac{4\lambda}{\pi}\frac{1}{4(1-\xi)\lambda^2 - 3}\sqrt{1-x^2}, \tag{3.74}$$

where the value of λ is then fixed by the normalization condition in Eq. (3.65):

$$\int_{-1}^{1} dx'\sigma^0(x') = \frac{n}{2Q} = \frac{n}{2c_1}\lambda. \tag{3.75}$$

The critical value λ^* is given by either the condition that $\sigma^0(x) \geqslant 0$ or by Eq. (3.75) in the limit $n \to \infty$:

$$\lambda^* = \sqrt{\frac{3}{4(1-\xi)}}, \tag{3.76}$$

which agrees with the fitting formula in Eq. (3.69) in the limit $\xi \to 1$. Using Eq. (3.76), we can rewrite $\sigma^0(x)$ in Eq. (3.74) as

$$\sigma^0(x) = \frac{4\lambda\lambda^{*2}}{3\pi}\frac{\sqrt{1-x^2}}{\lambda^2 - \lambda^{*2}} = \frac{2c_1}{3\pi}\frac{\sqrt{1-x^2}}{Q^* - Q}, \tag{3.77}$$

where $Q = c_1/\lambda$ and $Q^* = c_1/\lambda^*$. This square root singularity in $\sigma^0(x)$ also appears in the Lieb-Liniger model when the coupling constant c_B approaches zero from the positive side [67, 49]. Here it appears in the limit $\xi \to 1$ when Q approaches Q^* from below. The difference is that in the Lieb-Liniger model, the Fermi momentum Q grows with increasing density n, while in the present model the Fermi momentum is bounded from above with increasing density n, so the present model provides a more proper realization for BEC in one dimension.

For ξ smaller than 1, the zero mode $\sigma^0(x)$ acquires correction to the form in Eq. (3.77) near the boundaries $x = \pm 1$ (see Fig. 3.4). Numerical calculation shows that this correction is negligible up to the point $\xi = 0.4$, so the functional form in Eq. (3.77) provides a good description of the zero mode $\sigma^0(x)$ in the range $0.4 < \xi < 1$, and we only need to replace the prefactor $2c_1/(3\pi)$ with a positive function $F(Q^*)$ that depends on Q^*.

Far away from the lower bound λ^*, asymptotic behaviors for the density of state $\sigma(x)$ can be extracted from Eq. (3.63) in the limit $\lambda \to \infty$ with $\lim_{\xi\to 0} \xi\lambda \to 0$ and $\lim_{\xi\to 1}(1-\xi)\lambda \to 0$. For $\xi \to 0$, Eq. (3.63) reduces to

$$\sigma(x) + \frac{1}{\pi}\int_{-1}^{1} dx' \frac{\xi\lambda}{(x-x')^2 + (\xi\lambda)^2}\sigma(x') = \frac{1}{\pi}, \tag{3.78}$$

which coincides Eq. (3.23) for the Yang-Gaudin model if we rescale the parameters there accordingly. The asymptotic behavior for the solution $\sigma(x)$ to Eq. (3.78) in the limit $\xi\lambda \to 0$ has already been obtained in literature [36, 50]:

$$\sigma(x) = \frac{1}{2\pi}\left(1 + \frac{\xi\lambda}{\pi}\frac{1}{1-x^2} + \cdots\right). \tag{3.79}$$

For $\xi \to 1$, Eq. (3.63) reduces to

$$\sigma(x) - \frac{1}{\pi}\int_{-1}^{1} dx' \frac{(1-\xi)\lambda}{(x-x')^2 + (1-\xi)^2\lambda^2}\sigma(x') = \frac{1}{\pi}, \tag{3.80}$$

which coincides Eq. (3.28) for the Lieb-Liniger model if we rescale the parameters there accordingly. The asymptotic behavior for the solution $\sigma(x)$ to Eq. (3.80) in the limit $(1-\xi)\lambda \to 0$ has also been obtained in the literature [49, 36]:

$$\sigma(x) = \frac{1}{\pi(1-\xi)\lambda}\sqrt{1-x^2} + \frac{1}{2\pi^2}\frac{1}{\sqrt{1-x^2}}\left[x\ln\left(\frac{1-x}{1+x}\right) + \ln\frac{16\pi e}{(1-\xi)\lambda}\right] + \cdots. \tag{3.81}$$

The two asymptotic behaviors in Eqs. (3.79) and (3.81) will be of use in the next section when we

calculate the asymptotic behaviors of physical observables in the BCS and BEC limits of the present model.

3.3.2 BCS-BEC Crossover without External Magnetic Field

We will now show that the present model can provide an ideal scenario for BCS-BEC crossover in one dimension, without the drawbacks of simply connecting Yang-Gaudin model with Lieb-Liniger model. The behavior of the system is controlled by two dimensionless coupling constants:

$$\gamma_1 = c_1/n, \quad \gamma_2 = c_2/n, \tag{3.82}$$

where $m_\psi n = m_\psi N/L$ is the total mass density of the system with m_ψ being the mass of the atom. The ratio between the two dimensionless coupling constants is $\gamma_2/\gamma_1 = \xi$.

We consider the situation that $\gamma_1 \gg 1$ is kept fixed at a large value and γ_2 is varied such that ξ goes from 0 to 1. In the limit $\xi \to 0$, the dominant term in Eq. (3.57) is:

$$\theta(\Lambda - \Lambda') \approx -2 \arctan\left(\frac{\Lambda - \Lambda'}{c_2}\right), \tag{3.83}$$

which coincides with the Yang-Gaudin model (see Eq. (3.22)). Thus the BCS limit can be realized by tuning γ_2 to the limit $\xi \to 0$, where the system is weakly coupled with small dimensionless coupling γ_2. As we tune the coupling γ_2 larger, the system evolves toward the fermionic super Tonks-Girardeau gas, where the Yang-Gaudin model terminates. If we tune the coupling γ_2 even larger, the system can overcome this strong coupling limit and develop bosonic behaviors. In the limit $\xi \to 1$, the dominant term in Eq. (3.57) is:

$$\theta(\Lambda - \Lambda') \approx 2 \arctan\left(\frac{\Lambda - \Lambda'}{c_1 - c_2}\right), \tag{3.84}$$

which coincides with the Lieb-Liniger model (see Eq. (3.27)). Thus the BEC limit is realized by tuning γ_2 to the limit $\xi \to 1$, where the system is again weakly coupled with small dimensionless coupling $\delta\gamma = \gamma_1 - \gamma_2$. We can see that the present model describes the BCS-BEC crossover in a unified fashion, with a single Hamiltonian governing the evolution.

The crossover between fermionic and bosonic behaviors can be demonstrated by the evolution of density of states $\sigma(x)$ with varying γ_2. The asymptotic behaviors of $\sigma(x)$ in the BCS and BEC limits are shown in Eqs. (3.79) and (3.81), and a typical result of $\sigma(x)$ obtained by solving Eq. (3.63) together with Eq. (3.65) numerically is shown in Fig. 3.5, where the crossover between flat distribution in BCS limit and level condensation in BEC limit is transparent. Next, we discuss the ground state

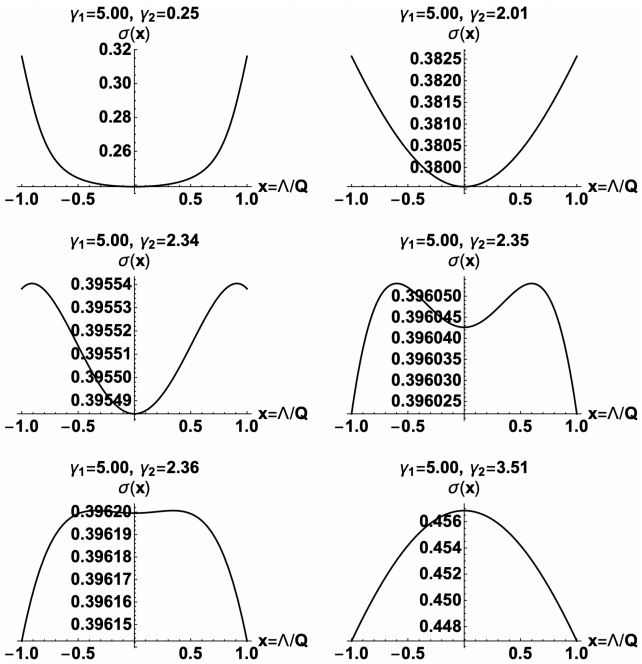

Figure 3.5: Density of states $\sigma(x)$ with fixed γ_1 and varying γ_2, where $\gamma_{1,2} \equiv c_{1,2}/n$. By tuning γ_2 toward γ_1, the behavior of the system changes from weakly attractive fermions (nearly fat at the center and sharp increase near the boundary) to fermionic super Tonks-Girardeau gas and finally to weakly interacting bosons (condensation at the center).

properties and low energy excitations of the present model at BCS-BEC crossover respectively.

3.3.2.1 Ground State Properties and Instability

We analyze the ground state energy and further the compressibility of the system. The ground state energy density ϵ and conserved density n can be calculated using the density of states $\sigma(x)$:

$$\begin{aligned} \epsilon &= \frac{E}{L} = \int_{-Q}^{Q} d\Lambda \left(2\Lambda^2 - \frac{c_2^2}{2}\right) \sigma(\Lambda) = Q^3 \int_{-1}^{1} dx \left(2x^2 - \frac{\xi^2\lambda^2}{2}\right) \sigma(x), \\ n &= \frac{N}{L} = \int_{-Q}^{Q} d\Lambda \; 2\sigma(\Lambda) = Q \int_{-1}^{1} dx \; 2\sigma(x), \end{aligned} \tag{3.85}$$

and the compressibility κ can be calculated from the energy density ϵ using the standard thermodynamic relation:

$$\frac{1}{\kappa} = n^2 \left(\frac{d^2\epsilon}{dn^2}\right). \tag{3.86}$$

The asymptotic behaviors of ϵ and κ in the BCS ($\xi \to 0$) and BEC ($\xi \to 1$) limits are obtained by

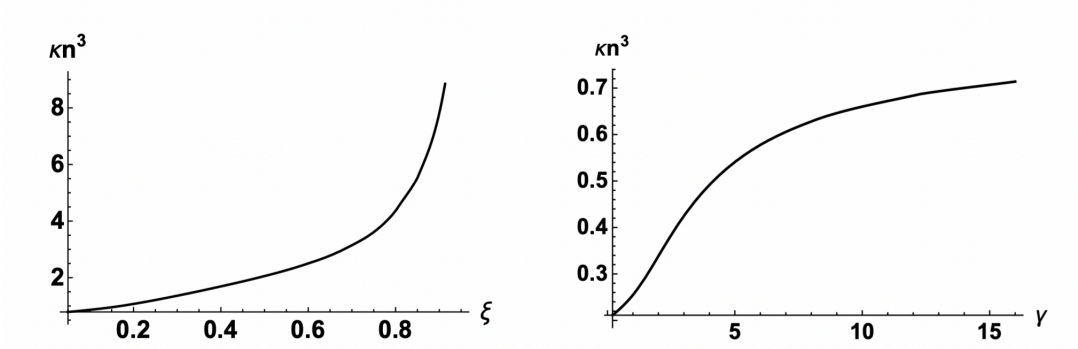

Figure 3.6: Numerical result for compressibility, where we have made it dimensionless by multiplying by n^3. Left panel is plotted for the present model with $\gamma_1 = 5$, where κn^3 changes with $\xi = c_2/c_1$. Right panel is plotted for the Yang-Gaudin model by varying dimensionless coupling constant $\gamma = c_F/n$. The difference is apparent: for the present model, there is divergence for compressibility, while for the Yang-Gaudin model, the compressibility saturates at a finite value.

substituting Eqs. (3.79) and (3.81) into Eqs. (3.85) and (3.86):

$$\begin{aligned} \frac{\epsilon + nc_2^2/4}{n\epsilon_F} &\overset{\xi\to 0}{\approx} \frac{1}{3}\left(1 - \frac{6\gamma_1}{\pi^2}\xi + \cdots\right), \quad \frac{\epsilon + nc_2^2/4}{n\epsilon_F} \overset{\xi\to 1}{\approx} \frac{\gamma_1(1-\xi)}{\pi^2}\left(1 - \frac{8\sqrt{\gamma_1(1-\xi)}}{3\pi} + \cdots\right), \\ \frac{1}{\kappa n^3} &\overset{\xi\to 0}{\approx} \frac{\pi^2}{2}\left(1 - \frac{2\gamma_1}{\pi^2}\xi + \cdots\right), \quad \frac{1}{\kappa n^3} \overset{\xi\to 1}{\approx} \frac{\gamma_1(1-\xi)}{2}\left(1 - \frac{\sqrt{\gamma_1(1-\xi)}}{\pi} + \cdots\right). \end{aligned} \tag{3.87}$$

where $\epsilon_F = \pi^2 n^2/4$ is the Fermi energy for the noninteracting Fermi gas and $c_2^2/4$ is the binding energy per atom. The results in Eq. (3.87) agree with those for the Yang-Gaudin model and the Lieb-Liniger model in the weak coupling limit respectively [67, 59, 32].

For general values of ξ, we numerically solve Eq. (3.63) for the density of states $\sigma(x)$ and numerically calculate the ground state energy and compressibility. A typical result for the compressibility is shown in Fig. 3.6, together with the result for the Yang-Gaudin model for a comparison. From Fig. 3.6, we can see that instead of saturating at a finite value as in the Yang-Gaudin model, the compressibility of the system in the present model diverges in the limit $\xi \to 1$, just as shown by the asymptotic behavior in Eq. (3.87). This means that the system becomes infinitely compressible and the spatially uniform ground state becomes unstable. In the meantime, the upper bound Q^* for the Fermi momentum goes to zero in the same limit (see Fig. 3.3). These facts signal a collapsing instability in the system, which we will discuss in the Sec. 3.4.

3.3.2.2 Excitations and Robustness of Their Extremes

We analyze the low energy excitations of the present model. There are two types of them, classified according to the spin quantum number - the $S = 0$ excitations and the $S = 1/2$ excitations. We first

summarize their features and then present the detailed analysis.

The spectrum of the $S = 0$ excitations in the present model has two branches, one of them is the usual Bogoliubov quasiparticle branch and the other is similar to the type-II branch in the Lieb-Liniger model [66]. Physically, the former can be identified as the particle branch and the latter can be identified as the hole branch (see Fig. 3.7), a classification due to the fact that the structure of the ground state is the same as that of a Fermi system. There are two robust features for the second branch: The maximum energy is achieved at $k_{\max} = k_F = \pi n/2$ and there is a periodicity of $2k_F = \pi n$, where k_F is the Fermi momentum for the noninteracting Fermi gas. These two features are robust against the variations of the dimensionless coupling strength γ_1 and γ_2.

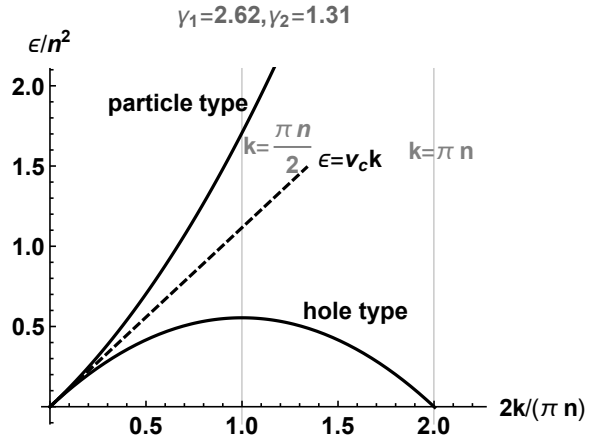

Figure 3.7: A typical spectrum for the $S = 0$ excitations. There are two branches, one for hole type and one for particle type. At long wavelength, they both reduce to the phonon branch. The maximum of the hole branch is fixed at $k_{\max} = k_F = \pi n/2$ and there is a periodicity of $2k_F = \pi n$ in the hole branch.

The spectrum of the $S = 1/2$ excitations in the present model is similar to that in the Yang-Gaudin model (see Fig. 3.8). It is gapped and also has a robust extreme: The minimum energy is achieved at $k_{\min} = k_F = \pi n/2$, robust against variations of the dimensionless coupling strength γ_1 and γ_2. This is in sharp contrast to the situation in higher dimensions, where the momentum of the minimum energy can be shifted from k_F on the deep BCS side to zero on the deep BEC side [76]. This is also counterintuitive in the sense that there is no conservation law to guarantee this robustness as in the Luttinger theorem, since there is tunneling between atoms and molecules back and forth.

The calculation of low energy excitations for exactly solvable models follows a standard procedure [105, 58]. The idea is as follows: The low energy excitations can be excited by various perturbations to the ground state. Since in the thermodynamic limit, the integral equations for the perturbations are linear, we can make a clever choice of linear combinations of the perturbations to give out phys-

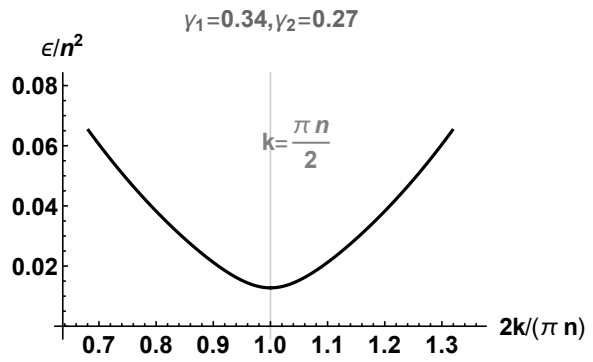

Figure 3.8: A typical spectrum for the $S = 1/2$ excitations. It is similar to that in the Yang-Gaudin model. The minimum energy is fixed at $k_{\min} = k_F = \pi n/2$.

ical relevant elementary excitations, according to their quantum numbers. Below we carry out this procedure for both $S = 0$ excitations and $S = 1/2$ excitations.

As in the Lieb-Liniger model, the $S = 0$ excitations can be classified into two categories: the hole type and the particle type. For the hole type excitation, a two-string with center momentum $|\Lambda_h| < Q$ is moved to Q. This hole type perturbation introduces a shift in the center momentum of the ground state $\Lambda \to \Lambda + \Delta(\Lambda)$. We then define a new function $\omega_h(\Lambda) \equiv \sigma(\Lambda)\Delta(\Lambda)L$, the integral equation for which can be obtained by the usual perturbation theory from Eq. (3.55):

$$\omega_h(\Lambda) - \frac{1}{2\pi}\int_{-Q}^{Q} d\Lambda'\ \theta'(\Lambda - \Lambda')\omega_h(\Lambda') = -\frac{1}{2\pi}\left[-\theta(\Lambda - \Lambda_h) + \theta(\Lambda - Q)\right]. \tag{3.88}$$

The energy ϵ_h and momentum k_h of the excitation can be expressed in terms of the function $\omega_h(\Lambda)$:

$$\begin{aligned} \epsilon_h(\Lambda_h) &= \int_{-Q}^{Q} d\Lambda'\ 4\Lambda'\omega_h(\Lambda') + 2Q^2 - 2\Lambda_h^2, \\ k_h(\Lambda_h) &= \int_{-Q}^{Q} d\Lambda'\ 2\omega_h(\Lambda') + 2Q - 2\Lambda_h. \end{aligned} \tag{3.89}$$

For the particle type excitation, a two-string with center momentum Q is moved to $\Lambda_p > Q$. Similarly we define a function $\omega_p(\Lambda)$ and express the energy ϵ_p and momentum k_p through it:

$$\begin{aligned} &\omega_p(\Lambda) - \frac{1}{2\pi}\int_{-Q}^{Q} d\Lambda'\ \theta'(\Lambda - \Lambda')\omega_p(\Lambda') = -\frac{1}{2\pi}\left[\theta(\Lambda - \Lambda_p) - \theta(\Lambda - Q)\right], \\ &\epsilon_p(\Lambda_p) = \int_{-Q}^{Q} d\Lambda'\ 4\Lambda'\omega_p(\Lambda') - 2Q^2 + 2\Lambda_p^2, \\ &k_p(\Lambda_p) = \int_{-Q}^{Q} d\Lambda'\ 2\omega_p(\Lambda') - 2Q + 2\Lambda_p. \end{aligned} \tag{3.90}$$

These integral equations and dispersion relations can be generally worked out numerically, and a

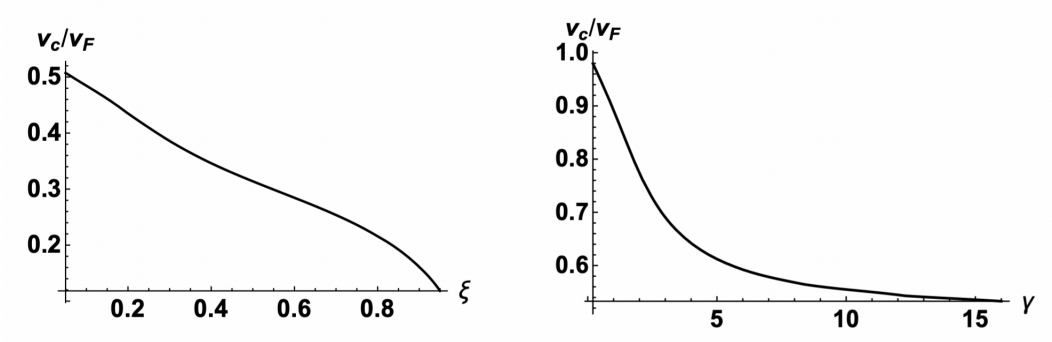

Figure 3.9: Numerical result for sound velocity scaled with v_F. Left panel is plotted for the present model with $\gamma_1 = 5$, where v_c/v_F changes with $\xi = c_2/c_1$. Right panel is plotted for the Yang-Gaudin model by varying dimensionless coupling constant $\gamma = c_F/n$. They are different in the following aspect: The present model has vanishing sound velocity at $\xi \to 1$, while the Yang-Gaudin model has a finite lower bound for the sound velocity: $v_c/v_F > 0.5$.

typical result is shown in Fig. 3.7. Just as pointed out at the beginning of this subsection, the features of the $S = 0$ spectrum are (1) There is a hole branch as well as a particle branch. (2) Both branches are gapless, and at long wavelength they are just phonons with linear dispersion $\epsilon = v_c k$, where v_c is the sound velocity. (3) There are two robust points, the momentum $k_{\max} = k_F$ of the maximum energy and the periodicity $2k_F$.

In fact, the robustness of the periodicity and $k_{\max}$ can be proved from Eqs. (3.55) and (3.58) in the thermodynamic limit. Firstly, the periodicity is fixed by the translational invariance: If we shift each Λ with the same amount π/L, then this operation will change the total energy by the amount $NL^{-2} \to 0$, while it will change the total momentum by the amount $(N/2)(2\pi/L) = \pi n$. Secondly, the momentum $k_{\max}$ is fixed by the reflection invariance: If we replace each Λ with $\pi/L - \Lambda$, then this operation will also change the total energy by the amount $NL^{-2} \to 0$, such that the spectrum has a reflection symmetry about the total momentum $\pi n/2$.

After we obtain the spectrum of the $S = 0$ excitations, we calculate the sound velocity by linearizing the dispersion $\epsilon(k)$ in the long wavelength limit $k \to 0$. Since in the BCS ($\xi \to 0$) and BEC ($\xi \to 1$) limits the present model reduces to the Yang-Gaudin model and the Lieb-Liniger model respectively (see Eqs. (3.78) and (3.80)), the asymptotic behavior of the sound velocity in these two limits can be obtained using the results for the latter two models in the weak coupling limit [66, 59, 32]:

$$\frac{v_c}{v_F} \overset{\xi\to 0}{\approx} 1 - \frac{\gamma_1}{\pi^2}\xi + \cdots, \quad \frac{v_c}{v_F} \overset{\xi\to 1}{\approx} \frac{\sqrt{\gamma_1(1-\xi)}}{\pi}\left(1 - \frac{\sqrt{\gamma_1(1-\xi)}}{2\pi} + \cdots\right), \tag{3.91}$$

where $v_F = \pi n$ is the Fermi velocity for the noninteracting Fermi gas. The sound velocity for general values of ξ is numerically calculated and presented in Fig. 3.9. We can see that the sound velocity is

monotonously decreasing with ξ, as the system goes from the BCS ($\xi \to 0$) limit to the BEC ($\xi \to 1$) limit. Also the vanishing of sound velocity in the limit $\xi \to 1$ is consistent with the divergence of compressibility in the same limit. This is in sharp contrast to the Yang-Gaudin model, where the system can never reach the weakly interacting BEC limit.

Let us turn to the analysis of the gapped $S = 1/2$ excitations. Unlike the $S = 0$ excitations, the lowest spin excited state is a triplet state, described by the continuum of two $S = 1/2$ excitations and one $S = 0$ hole excitation. In this triplet state, we break a two-string with center momentum $|\Lambda_h| < Q$ and add two unpaired atoms with momentum $k_{1,2}$ into the system. The corresponding function $\omega_{\rm tri}(\Lambda)$ satisfies the following integral equation:

$$\omega_{\rm tri}(\Lambda) - \frac{1}{2\pi}\int_{-Q}^{Q} d\Lambda'\ \theta'(\Lambda-\Lambda')\omega_{\rm tri}(\Lambda') = \frac{1}{2} - \frac{1}{2\pi}\left[-\theta(\Lambda-\Lambda_h) + \theta_s(\Lambda-k_1) + \theta_s(\Lambda-k_2)\right], \quad (3.92)$$

where the newly defined phase-shift function $\theta_s(\Lambda-k)$ corresponds to the scattering between a molecule and an unpaired atom:

$$\theta_s(\Lambda-k) = -2\arctan\left(\frac{\Lambda-k}{c_2'}\right) + 2\arctan\left(\frac{\Lambda-k}{c_1+c_2'}\right) + 2\arctan\left(\frac{\Lambda-k}{c_1-c_2'}\right). \quad (3.93)$$

The extra term $1/2$ on the righthand side of Eq. (3.92) comes from the fact that the J_α in Eq. (3.55) will change from integer to half-odd integer (or from half-odd integer to integer) if an odd number of two-strings or an odd number of unpaired atoms is added into the system (see Fig. 3.10).

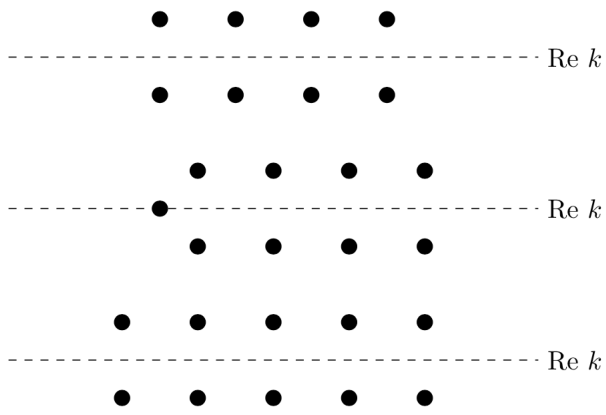

Figure 3.10: The schematic picture for the distribution of the roots k. For two-strings with center momentum Λ_α, the two roots $k_{\alpha,1}$ and $k_{\alpha,2}$ are separated by a distance c_2 along the imaginary axis. For unpaired atoms, the roots lie on the real axis. We can see that when a single two-string or a single unpaired atom is added into the system, the J_α in Eq. (3.55) will be shifted by half of unity.

The energy $\epsilon_{\rm tri}$ and momentum $k_{\rm tri}$ can be once again expressed using the function $\omega_{\rm tri}(\Lambda)$:

$$\begin{aligned}\epsilon_{\rm tri} &= \int_{-Q}^{Q} d\Lambda'\ 4\Lambda'\omega_{\rm tri}(\Lambda') - 2\Lambda_h^2 + k_1^2 + k_2^2 + \frac{c_2^2}{2},\\ k_{\rm tri} &= \int_{-Q}^{Q} d\Lambda'\ 2\omega_{\rm tri}(\Lambda') - 2\Lambda_h + k_1 + k_2.\end{aligned} \tag{3.94}$$

As we discussed before, Eqs. (3.92) and (3.94) are all linear, and this triplet state in fact includes three elementary excitations - one hole type $S = 0$ excitation and two $S = 1/2$ excitations. By subtracting the $S = 0$ component, we are left with the sum of two $S = 1/2$ components. There are two ways to define the single $S = 1/2$ excitations (we denote them with subscript s), both are physically relevant:

$$\begin{aligned}\omega_s^{(1)}(\Lambda) - \frac{1}{2\pi}\int_{-Q}^{Q} d\Lambda'\ \theta'(\Lambda-\Lambda')\omega_s^{(1)}(\Lambda') &= \frac{1}{2\pi}\theta(\Lambda - Q) - \frac{1}{2\pi}\theta_s(\Lambda - k),\\ \omega_s^{(2)}(\Lambda) - \frac{1}{2\pi}\int_{-Q}^{Q} d\Lambda'\ \theta'(\Lambda-\Lambda')\omega_s^{(2)}(\Lambda') &= \frac{1}{2} - \frac{1}{2\pi}\theta_s(\Lambda - k),\end{aligned} \tag{3.95}$$

The corresponding expressions for energies and momenta are:

$$\begin{aligned}\epsilon_s^{(1)} &= \int_{-Q}^{Q} d\Lambda'\ 4\Lambda'\omega_s^{(1)}(\Lambda') - 2Q^2 + k^2 + \frac{c_2^2}{4} + \mu,\\ k_s^{(1)} &= \int_{-Q}^{Q} d\Lambda'\ 2\omega_s^{(1)}(\Lambda') - 2Q + k,\\ \epsilon_s^{(2)} &= \int_{-Q}^{Q} d\Lambda'\ 4\Lambda'\omega_s^{(2)}(\Lambda') + k^2 + \frac{c_2^2}{4} - \mu,\\ k_s^{(2)} &= \int_{-Q}^{Q} d\Lambda'\ 2\omega_s^{(2)}(\Lambda') + k,\end{aligned} \tag{3.96}$$

For the first definition, we remove a two-string and add an unpaired atom, so the net result corresponds to subtraction of one atom. For the second definition, we only add an unpaired atom (the extra term $1/2$ in the equation for $\omega_s^{(2)}(\Lambda)$ comes from the shift of J_α in Eq. (3.55), see Fig. 3.10), so it corresponds to addition of one atom. Both of them change the number of atoms by one, thus we need to shift their energies by the chemical potential μ, such that the minimum of the two spectra coincides to ensure the particle-hole symmetry of the $S = 1/2$ excitations.

Solving the above sets of integral equations numerically we will obtain the spectrum for the $S = 1/2$ excitations. Typical results are shown in Fig. 3.11, where the notable features are: (1) The $S = 1/2$ excitations have their lowest energy at momentum $k_{\rm min} = k_F$, robust against variations of the dimensionless coupling strength γ_1 and γ_2. (2) The $S = 1/2$ excitations are gapped, where the gap $\Delta(\xi)$ grows with increasing ξ (see Fig. 3.12 for $\Delta(\xi)$ with general values of ξ). (3) In the limit

$\xi \to 0$, the spectrum is of BCS type, where a small region of quadratic dispersion is followed by an intermediate region of linear dispersion, before the dispersion reaches another quadratic region of large momentum. (4) In the limit $\xi \to 1$, the spectrum is of BEC type, where the dispersion is quadratic all the way.

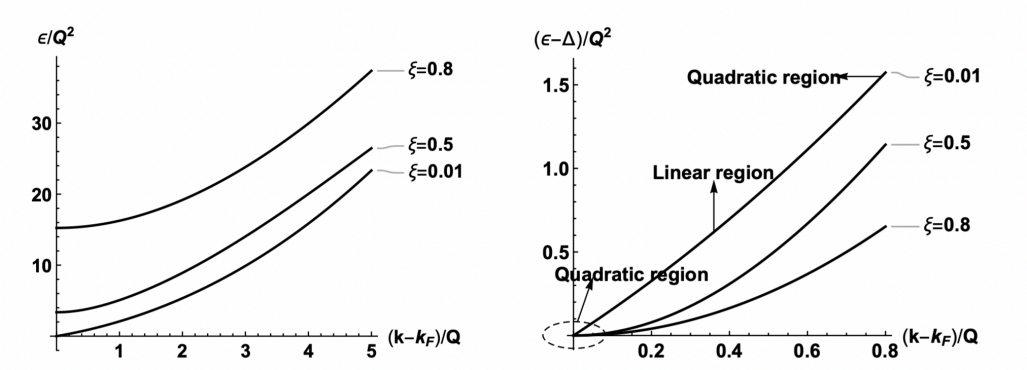

Figure 3.11: Typical spectra for the $S = 1/2$ excitations, where the momentum is shifted by k_F. Three different choices of ξ are shown. Right panel is obtained from left panel by offsetting the spin gap. For very small ξ, the dispersion curve has three parts: a narrow quadratic region near the minimum, a intermediate linear region and finally a quadratic region at large energy. For ξ close to 1, the dispersion is purely quadratic.

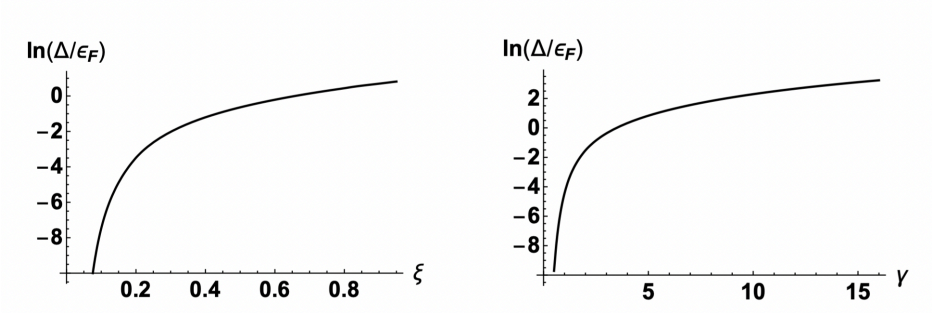

Figure 3.12: Numerical result for spin gap scaled with ϵ_F. Left panel is plotted for the present model with $\gamma_1 = 5$, and right panel is plotted for the Yang-Gaudin model. They appear practically the same, but with the following difference: the present model terminates at $\xi = 1$, while the Yang-Gaudin model will continue the logarithmic behavior with ever growing $\gamma = c_F/n$.

The robustness of $k_{\min}$ can be verified analytically. For addition of one atom, we can determine the lowest energy configuration by the following condition:

$$\frac{d\epsilon_s^{(2)}}{dk}\Big|_{k=k_{\min}} = 0. \tag{3.97}$$

This can by solved by variation of the function $\omega_s^{(2)}$ with respect to parameter k, and the result is quite simple: $k_{\min} = 0$. Now we can calculate the corresponding momentum by substitute $k = 0$ into

Eqs. (3.95) and (3.96):

$$\begin{aligned}
&\omega_s^{(2)}(\Lambda) - \frac{1}{2\pi}\int_{-Q}^{Q} d\Lambda'\ \theta'(\Lambda-\Lambda')\omega_s^{(2)}(\Lambda') = \frac{1}{2} - \frac{1}{2\pi}\theta_s(\Lambda), \\
&k_s^{(2)} = \int_{-Q}^{Q} d\Lambda'\ 2\omega_s^{(2)}(\Lambda').
\end{aligned} \tag{3.98}$$

The second term $-\theta_s(\Lambda)/2\pi$ on righthand side of Eq. (3.98) is odd in Λ, which has no contribution to the momentum $k_s^{(2)}$, thus we have an alternative expression for $k_s^{(2)}$:

$$\begin{aligned}
&\tilde{\omega}_s(\Lambda) - \frac{1}{2\pi}\int_{-Q}^{Q} d\Lambda'\ \theta'(\Lambda-\Lambda')\tilde{\omega}_s(\Lambda') = \frac{1}{2}, \\
&k_s^{(2)} = \int_{-Q}^{Q} d\Lambda'\ 2\tilde{\omega}_s(\Lambda'),
\end{aligned} \tag{3.99}$$

This alternative function $\tilde{\omega}_s(\Lambda)$ fulfills the same integral equation as the density of states $\sigma(\Lambda)$, if we make a simple change of the constant inhomogeneous term (see Eq. (3.59)). As a result we have:

$$\tilde{\omega}_s(\Lambda) = \frac{\pi}{2}\sigma(\Lambda) \Rightarrow k_s^{(2)} = \pi\int_{-Q}^{Q} d\Lambda'\ \sigma(\Lambda') = \frac{\pi n}{2}, \tag{3.100}$$

which means that the minimum of the $S = 1/2$ spectrum resides at $k_s^{(2)} = \pi n/2 = k_F$ in the case of addition of one atom.

Usually, the fixed momentum k_F appears in the context of Luttinger theorem, which contributes the robustness even in presence of interactions to the conservation of the particle number. In contrast, our result that the minimum of the $S = 1/2$ spectrum is fixed at momentum k_F is somewhat surprising, in the sense that the non-conserving nature of the operator $\hat{N}_\psi \equiv \int dx\ \hat{\psi}^\dagger\hat{\psi}$ (see Eqs. (3.5) and (3.8)) would in principle lead to a changing minimum position in momentum. In fact, the robustness discussed here is due to a special feature of the one dimensional system that the quasiparticle excitation is not stable with respect to soliton formation. A full explanation from a comprehensive semiclassical analysis is presented in the next chapter [89].

Now we discuss the asymptotic behaviors of the $S = 1/2$ excitations in the BCS ($\xi \to 0$) and BEC ($\xi \to 1$) limits. In the BCS limit, the present model reduces to the Yang-Gaudin model (see Eq. (3.78)), where the asymptotic behaviors of the spin gap Δ and the dispersion $\epsilon_s(k)$ near its minimum have already been obtained in the literature in the weak coupling limit [59]:

$$\frac{\Delta}{\epsilon_F} \approx \frac{8}{\pi}\sqrt{\frac{\gamma_1\xi}{\pi}}e^{-\pi^2/(2\gamma_1\xi)}, \quad \epsilon_s(k) \approx \sqrt{\Delta^2 + [v_F(k-k_F)]^2}. \tag{3.101}$$

We can see that these results are consistent with the conventional BCS mean field results.

In the BEC limit, the present model reduces to the Lieb-Liniger model with weak dimensionless coupling $\delta\gamma = \gamma_1 - \gamma_2 \to 0$. In this limit we have $c_2 \approx c_1 \gg 1$, which makes the second term on the righthand side of Eq. (3.95) for $\omega_s^{(2)}(\Lambda)$ negligible compared with the first term. As a result, we have $\omega^{(2)}(\Lambda) = \pi\sigma(\Lambda)/2$ in the leading approximation, obtained by comparing Eq. (3.95) for $\omega^{(2)}(\Lambda)$ and Eq. (3.63) for $\sigma(\Lambda)$. Then the asymptotic behaviors of the spin gap Δ and the dispersion $\epsilon_s(k)$ near its minimum can be obtained from Eq. (3.96) using Eq. (3.81) for $\sigma(\Lambda)$ in the limit $\xi \to 1$:

$$\frac{\Delta}{\epsilon_F} \approx \frac{\gamma_1^2}{\pi^2}, \quad \epsilon_s \approx \Delta + (k - k_F)^2, \tag{3.102}$$

where the leading term for the spin gap is just the binding energy for the two-strings and the dispersion reduces to free particle form near the minimum of the spectrum. These results are consistent with the usual physical picture of the BEC limit.

Since the presence of the upper bound Q^* for the Fermi momentum has no effect on the low energy excitation spectra, this completes our investigation of the present model in the context of BCS-BEC crossover.

3.3.3 Phase Diagram in Presence of External Magnetic Field

Without an external magnetic field, the ground state of the present model is a Fermi sea of two-strings. By applying external magnetic field above certain threshold depending on the density $n = N/L$, we can polarize the system. Then the ground state will be either fully polarized or mixed with both two-strings and polarized atoms. By varying the magnetic field H and the density n, we can explore the phase diagram at zero temperature and observe quantum phase transitions between three different phases: the fully paired ground state (P), the fully polarized ground state (FP) and the partially polarized ground state (PP). This kind of analysis has already been done for the Yang-Gaudin model in the literature [75, 47, 40, 41]. It is pointed out that the PP phase is gapless, and the power-law decay of the pair correlation $\langle\psi_\uparrow^\dagger(x)\psi_\downarrow^\dagger(x)\psi_\uparrow(0)\psi_\downarrow(0)\rangle \propto \cos\left(k_{\mathrm{FFLO}}|x|\right)/|x|^\alpha$ is accompanied by a spatial oscillation. The wave vector of this oscillation was numerically found to depend on the mismatch of the Fermi points $k_{\mathrm{FFLO}} \simeq \pi(n_\uparrow - n_\downarrow)$. Thus the PP phase serves as the one dimensional analog of the Fulde-Ferrell-Larkin-Ovchinnikov (FFLO) state, and it provides an ideal place to find and explore the superfluid phase with inhomogeneity.

In this section, we calculate the zero temperature phase diagram of the present model. For technical convenience, we start from the grand canonical ensemble, where the chemical potential μ is introduced

as an auxiliary parameter to establish the phase boundaries in the $H-n$ space. Also for definiteness, we choose the case $H \geqslant 0$.

We introduce two density of states, one for the unpaired atoms, which is denoted as $\rho(k)$ and one for the molecules, which is denoted as $\sigma(\Lambda)$. Then we have

$$\begin{aligned} n_\uparrow + n_\downarrow =& 2\int_{-Q}^{Q} d\Lambda\ \sigma(\Lambda) + \int_{-q}^{q} dk\ \rho(k), \\ n_\uparrow - n_\downarrow =& \int_{-q}^{q} dk\ \rho(k), \end{aligned} \tag{3.103}$$

where $m_\psi(n_\uparrow + n_\downarrow)$ is the total mass density, $(n_\uparrow - n_\downarrow)$ is the total spin density, q is the Fermi momentum of the unpaired atoms and Q is the Fermi momentum of the molecules. Following the same procedure as that in deriving Eq. (3.59), we obtain the coupled equations for the two density of statess:

$$\begin{aligned} \rho(k) =& \frac{1}{2\pi} + \frac{1}{2\pi}\int_{-q}^{q} dk'\ \theta'_{ss}(k-k')\rho(k') + \frac{1}{2\pi}\int_{-Q}^{Q} d\Lambda\ \theta'_s(k-\Lambda)\sigma(\Lambda), \\ \sigma(\Lambda) =& \frac{1}{\pi} + \frac{1}{2\pi}\int_{-q}^{q} dk\ \theta'_s(\Lambda-k)\rho(k) + \frac{1}{2\pi}\int_{-Q}^{Q} d\Lambda'\ \theta'(\Lambda-\Lambda')\sigma(\Lambda'), \end{aligned} \tag{3.104}$$

where the phase-shift functions $\theta(\Lambda-\Lambda')$ and $\theta_s(\Lambda-k)$ are defined in Eqs. (3.57) and (3.93) respectively, and the new phase-shift function

$$\theta_{ss}(k-k') = 2\arctan\left(\frac{k-k'}{c_1}\right) \tag{3.105}$$

corresponds to the scattering between two unpaired atoms with the same spin direction. The ground state energy density ϵ of the system is then

$$\epsilon = \frac{E}{L} = \int_{-Q}^{Q} d\Lambda \left(2\Lambda^2 - \frac{c_2^2}{2}\right)\sigma(\Lambda) + \int_{-q}^{q} dk\ k^2\rho(k). \tag{3.106}$$

Performing variation of ϵ with respect to $\sigma(\Lambda)$ and $\rho(k)$ under the constraint in Eq. (3.103) and making use of Eq. (3.104), we obtain

$$\begin{aligned} \epsilon^u(k) =& k^2 - \mu - h + \frac{1}{2\pi}\int_{-q}^{q} dk'\ \theta'_{ss}(k-k')\epsilon^u(k') + \frac{1}{2\pi}\int_{-Q}^{Q} d\Lambda\ \theta'_s(k-\Lambda)\epsilon^b(\Lambda), \\ \epsilon^b(\Lambda) =& 2\left(\Lambda^2 - \mu - \frac{c_2^2}{4}\right) + \frac{1}{2\pi}\int_{-q}^{q} dk\ \theta'_s(\Lambda-k)\epsilon^u(k) + \frac{1}{2\pi}\int_{-Q}^{Q} d\Lambda'\ \theta'(\Lambda-\Lambda')\epsilon^b(\Lambda'), \end{aligned} \tag{3.107}$$

where the chemical potential μ and the reduced magnetic field $h = H/2$ are the two Lagrange multi-

pliers. The two introduced functions $\epsilon^u(k)$ and $\epsilon^b(\Lambda)$ are referred to as the dressed energy functions for the unpaired atoms and molecules respectively [99, 40]. The dressed energy function is introduced in the grand canonical ensemble such that it gives out negative value when the momentum is within the Fermi sea and positive value when the momentum is outside the Fermi sea. Equivalently, we have the condition that

$$\epsilon^u(\pm q) = 0, \quad \epsilon^b(\pm Q) = 0. \tag{3.108}$$

In terms of the dressed energies, the zero temperature phase diagram can be calculated as follows. The boundary from fully polarized to partially polarized ground state is determined by the condition

$$\epsilon^u(\pm q) = 0, \quad \epsilon^b(0) \leqslant 0. \tag{3.109}$$

Then the phase boundary FP-PP can be obtained as the solution $n = n_1(h)$ to the coupled integral equations:

$$\begin{aligned}
&\epsilon^u(k) = k^2 - \mu - h + \frac{1}{2\pi}\int_{-q}^{q} dk'\ \theta'_{ss}(k-k')\epsilon^u(k'),\\
&\mu = -\frac{c_2^2}{4} + \frac{1}{4\pi}\int_{-q}^{q} dk\ \theta'_s(-k)\epsilon^u(k),\\
&\rho(k) = \frac{1}{2\pi} + \frac{1}{2\pi}\int_{-q}^{q} dk'\ \theta'_{ss}(k-k')\rho(k'),\\
&n = \int_{-q}^{q} dk\ \rho(k).
\end{aligned} \tag{3.110}$$

The boundary from fully paired to partially polarized ground state is determined by the condition

$$\epsilon^u(0) \leqslant 0, \quad \epsilon^b(\pm Q) = 0. \tag{3.111}$$

Then the phase boundary P-PP can be obtained as the solution $n = n_2(h)$ to the coupled integral equations:

$$\begin{aligned}
&\epsilon^b(\Lambda) = 2\left(\Lambda^2 - \mu - \frac{c_2^2}{4}\right) + \frac{1}{2\pi}\int_{-Q}^{Q} d\Lambda'\ \theta'(\Lambda-\Lambda')\epsilon^b(\Lambda'),\\
&\mu = -h + \frac{1}{2\pi}\int_{-Q}^{Q} d\Lambda\ \theta'_s(-\Lambda)\epsilon^b(\Lambda),\\
&\sigma(\Lambda) = \frac{1}{\pi} + \frac{1}{2\pi}\int_{-Q}^{Q} d\Lambda'\ \theta'(\Lambda-\Lambda')\sigma(\Lambda'),\\
&n = 2\int_{-Q}^{Q} d\Lambda\ \sigma(\Lambda).
\end{aligned} \tag{3.112}$$

The functions $n_1(h)$ and $n_2(h)$ cannot be expressed in closed forms, they can only be obtained by directly dealing with the corresponding coupled integral equations, generally through numerical calculations. Typical phase diagrams are presented in Fig. 3.13, where n and h are scaled by $\sqrt{\epsilon_b}$ and ϵ_b respectively, with $\epsilon_b = c_2^2/4$ being the binding energy per atom. Comparison is made between $\xi \ll 1$ and $\xi \sim 1$ - The phase diagram at small ξ is essentially the same as that in the Yang-Gaudin model. When ξ goes near 1, the phase diagram develops a new feature: there arises a critical strength h_c for the magnetic field, below which the ground state is always a Fermi sea of two-strings and cannot be polarized.

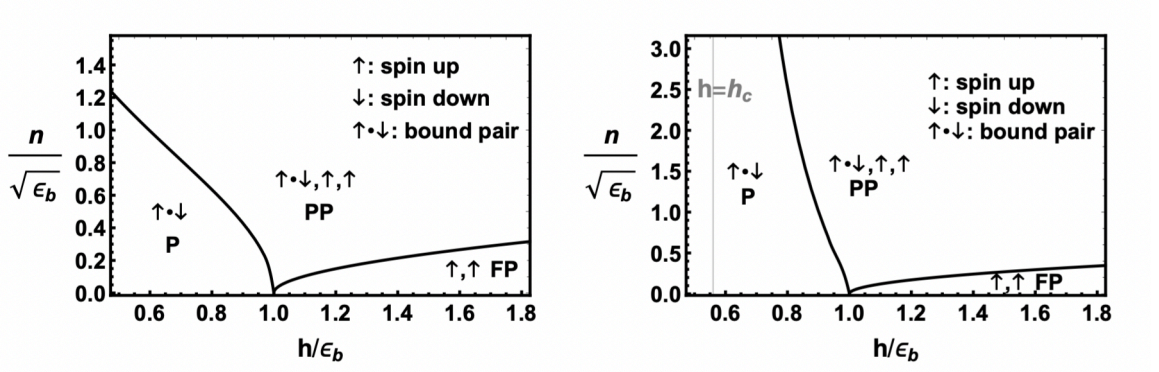

Figure 3.13: Phase diagram in the $h - n$ space at zero temperature, where n and h are scaled by $\epsilon_b = c_2^2/4$. Left panel is plotted for $\xi = 0.1$, and right panel is plotted for $\xi = 0.8$. The case with $\xi = 0.1$ is essentially the same as that in the Yang-Gaudin model, while in the case with $\xi = 0.8$, the mixed phase region (PP) is reduced. The phase boundary P-PP actually has an asymptote corresponding to the critical magnetic field $h = h_c$.

The critical magnetic field can be shown to come about due to the presence of upper bound Q^* on the Fermi momentum of the system. For fixed c_1 and c_2, when we increase the chemical potential or the mass density, we will finally get close to the upper bound Q^*. In the range $0.4 < \xi < 1$, the density of states $\sigma(x)$ is then dominated by square root singular term $\sigma^0(x)$ in Eq. (3.74). We then use it together with Eq. (3.85) to calculate the leading order contribution to the energy density $\epsilon \equiv E/L$ when Q approaches Q^* from below:

$$\begin{aligned} \epsilon = \frac{E}{L} &\approx Q^{*3} \int_{-1}^{1} dx \left(2x^2 - \frac{\xi^2 \lambda^{*2}}{2}\right) \sigma^0(x) = \frac{\pi Q^{*3} F(Q^*)(1-\xi^2\lambda^{*2})}{4(Q^*-Q)}, \\ \frac{n}{2} = \frac{N}{2L} &\approx Q^* \int_{-1}^{1} dx\, \sigma^0(x) = \frac{\pi Q^* F(Q^*)}{2(Q^*-Q)}, \end{aligned} \tag{3.113}$$

where $\xi = c_2/c_1$, $\lambda^* = c_1/Q^*$, and the relation between λ^* and ξ can be read off from Eq. (3.69) or

Fig. 3.3. This shows that the leading order contribution to the energy density is linear in $n = N/L$:

$$\epsilon(n) \approx B(\xi)n, \quad B(\xi) = \frac{1/\lambda^{*2} - \xi^2}{4} c_1^2. \tag{3.114}$$

For fixed number of particles $n = n_\uparrow + n_\downarrow$ with small varying polarization $\delta n = n_\uparrow - n_\downarrow$, the energy of the system can be expressed as

$$\epsilon(\delta n) = B(\xi)n - (h + B(\xi))\delta n. \tag{3.115}$$

When ξ is small, the coefficient $B(\xi)$ is positive, which means that an infinitesimal magnetic field will polarize the system as long as the mass density of the system is large enough, and there is no critical magnetic field h_c. When ξ goes to 1, λ^* tends to diverge, then we have $B(\xi) < 0$, which means that we need a finite strength of magnetic field $h_c = -B(\xi)$ to polarize the system. The critical ξ^* is then determined by

$$B(\xi^*) = 0 \Rightarrow \lambda^*(\xi^*)\xi^* = 1 \Rightarrow \xi^* = 0.61. \tag{3.116}$$

The value of ξ^* falls in the range $0.4 < \xi < 1$, so the usage of the square root singular form in Eq. (3.74) for the density of states when Q approaches Q^* from below is justified.

As a result, we have $h_c = 0$ for $\xi < \xi^*$ and $h_c = -B(\xi)$ for $\xi > \xi^*$. If we approach the critical value ξ^* from above, the critical magnetic field will display the following critical behavior:

$$h_c \sim (\xi - \xi^*)^{\alpha_h} \quad \text{for} \quad \xi = \xi^* + 0, \tag{3.117}$$

where the critical exponent α_h can be calculated from the functional form of $B(\xi)$ with the result $\alpha_h = 1$. This result comes from the fact that the system can be viewed as a collection of noninteracting particles in the leading approximation according to Eq. (3.114). Since Eq. (3.114) is obtained by keeping only the singular part $\sigma^0(x)$ from the density of states $\sigma(x) = \sigma_{\rm reg}(x) + \sigma^0(x)$, the interaction effect comes from the regular part $\sigma_{\rm reg}(x)$, which produces higher order corrections to the result $\alpha_h = 1$.

3.4 Bright Solitons with $c_1 < c_2$

In the previous section, we have touched the issue that a collapsing instability appears when we tune c_2 close to c_1, see Figs. (3.3), (3.6) and (3.9). In this section, we focus on the regime $0 < c_1 < c_2$, the

instability discussed in the previous section implies we would have a collapsing solution in this regime for fermionic atoms (see Eq. (3.51)). This counterintuitive result is due to the fact that the fermionic atoms are tightly bound into bosonic molecules with residual attraction before collapsing. In this section, we confirm this claim. Firstly we still make the two-string ansatz like that in Eq. (3.53)

$$k_{\alpha,1} = \Lambda_\alpha + iv, \quad k_{\alpha,2} = \Lambda_\alpha - iv, \quad v > 0, \tag{3.118}$$

where $\alpha = 1, 2, \cdots, M = N/2$. But this time we leave the reality of the center momentum Λ_α for the moment. The Bethe ansatz equations in Eq. (3.52) then implies

$$\exp(-2vL) \sim \left(\frac{v - c_2'}{v + c_2'}\right)^2. \tag{3.119}$$

For a macroscopic system where $L \to \infty$, this fixes the value $v = c_2'$, and Eq. (3.54) still follows. This time we have $c_3 = c_2 - c_1 > 0$, and we have the following Bethe equations for Λ_α:

$$\exp(i2\Lambda_\alpha L) \sim \prod_{\beta=1}^{M} \left(\frac{\Lambda_\alpha - \Lambda_\beta - ic_3}{\Lambda_\alpha - \Lambda_\beta + ic_3}\right), \tag{3.120}$$

where we have omitted other factors which have no effect on the subsequent derivations [2]. Now Eq. (3.120) has the same form as that appearing in the attractive Lieb-Liniger model, whose ground state is a single string solution encompassing all particles [67, 105]. Subsequently, unlike the uniform regime, we now have a single M-string solution for center momentum Λ_α:

$$\Lambda_\alpha = u + ic_3'(M + 1 - 2\alpha), \quad c_3' = c_3/2, \tag{3.121}$$

where u is a real number and $\alpha = 1, 2, \cdots, M = N/2$. We now have an embedded string solution of the following structure

$$\begin{aligned} &k_{\alpha,1} = \Lambda_\alpha + ic_2', \quad k_{\alpha,2} = \Lambda_\alpha - ic_2', \\ &\Lambda_\alpha = u + ic_3'(M + 1 - 2\alpha), \end{aligned} \tag{3.122}$$

where the label α runs from 1 to $M = N/2$. The physical picture of this embedded string solution is a bound state encompassing all particles: Firstly, atoms with opposite spins are bound into molecules,

[2] The second and the third terms in Eq. (3.54) cannot produce physical poles; The first term in Eq. (3.54) can produce physical poles, but it won't lead to a valid string solution, because it will lead to repeating values in original momentum k, then the exclusion principle in one dimension tells us that the wave function would vanish.

then the molecules are bound together as a single bright soliton due to the residual attraction (see Fig. 3.14).

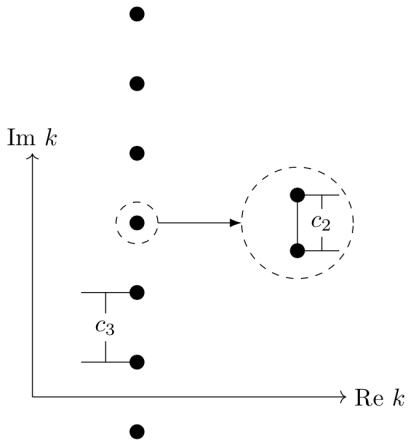

Figure 3.14: The embedded string solution. The two-string (the one in the enlarged circle) with inter-root separation c_2 is embedded in the M-string with inter-root separation $c_3 = c_2 - c_1$.

The above physical picture can be better understood by writing down the corresponding wave functions directly. This can be done through the nested coordinate Bethe ansatz:

$$\begin{aligned} \Psi_X(\sigma_1, x_1; \cdots; \sigma_N, x_N) &= \sum_{P \in S_N} [X, P] \exp\left(i \sum_{j=1}^{N} k_{P_j} x_{X_j} \right), \\ [X, P] &= \mathrm{sgn}(X)\mathrm{sgn}(P) A_{\sigma_{X_1}\sigma_{X_2}\cdots\sigma_{X_N}}(k_{P_1}, k_{P_2}, \cdots, k_{P_N}), \end{aligned} \tag{3.123}$$

where $\sigma_i = \uparrow, \downarrow$ denotes the spin directions, X denotes the ordering sector with $x_{X_1} < x_{X_2} < \cdots < x_{X_N}$ and P denotes the permutation among the wave numbers. The sign function equals 1 for even permutations and -1 for odd permutations. For M down-spins sitting at integer positions $1 \leqslant y_1 < y_2 < \cdots < y_M \leqslant N$, we denote the function $A_{\sigma_{X_1}\cdots\sigma_{X_N}}(k_{P_1}, \cdots, k_{P_N})$ as $A_P(y_1, y_2, \cdots, y_M)$. This function is obtained by generalizing the result for the Yang-Gaudin model [35, 109] from a single

coupling constant c_F to two coupling constants c_1 and c_2:

$$\begin{aligned}
A_P(y_1, y_2, \cdots, y_M) &= \sum_{R\in S_M} G_1(P)G_2(R)\prod_{i=1}^{M} F_P(y_i, \Lambda_{R_i}),\\
G_1(P) &= \prod_{j<l}(k_{P_j} - k_{P_l} + ic_1),\\
G_2(R) &= \mathrm{sgn}(R)\prod_{j<l}(\Lambda_{R_j} - \Lambda_{R_l} + ic_2),\\
F_P(y, \Lambda) &= \prod_{j=1}^{y-1}(k_{P_j} - \Lambda - ic_2') \prod_{l=y+1}^{N} (k_{P_l} - \Lambda + ic_2').
\end{aligned} \tag{3.124}$$

For a concrete illustration, we substitute Eq. (3.122) into Eqs. (3.123) and (3.124) in the case with $N = 4$, then in the basic sector $I : x_1 < x_2 < x_3 < x_4$, we have:

$$\begin{aligned}
&\Psi_I(\uparrow, x_1; \downarrow, x_2; \uparrow, x_3; \downarrow, x_4) \sim e^{-c_2'(x_2+x_4-x_1-x_3)-c_3'(x_3+x_4-x_1-x_2)},\\
&\Psi_I(\uparrow, x_1; \uparrow, x_2; \downarrow, x_3; \downarrow, x_4) = 0,\\
&\Psi_I(\uparrow, x_1; \downarrow, x_2; \downarrow, x_3; \uparrow, x_4) \sim e^{-c_2'(x_2+x_4-x_1-x_3)-c_3'(x_3+x_4-x_1-x_2)},
\end{aligned} \tag{3.125}$$

where we have set $u = 0$ for simplicity. The expression for other ordering sectors then follows from the symmetry of the system. Through the explicit wave function, the physical picture of the embedded string solution is transparent, where the exponential decay on the length scale of $1/c_2'$ represents the molecule structure and the exponential decay on the length scale of $1/c_3'$ binds all the M molecules together.

3.5 Conclusion

In this chapter, we introduced models of two-component bosons and fermions with tunable inter-species interactions in one dimension, where the Yang-Baxter equation for exact solvability can be fulfilled by fine-tuning the model parameters. The tunable interactions are realized by Feshbach resonances of two antiparallel pseudospins. The N atoms in this model can be imagined to live on hyperplanes corresponding to different ordering sectors $X : x_{X_1} < x_{X_2}, < \cdots < x_{X_N}$. Without reaction that converts atoms and molecules back and forth, we only need to require the continuity of wave function when hyperplanes intersect. With Feshbach resonances, the molecules can be viewed as living on the intersections of the hyperplanes, which play the role of the boundary conditions. Although the strict exact solvability beyond the level of two-body scatterings would require the introduction

of extra singular counterterms, the present models can still be well described by the Bethe ansatz for relatively small densities. The resulting Bethe ansatz equations admit two types of ground state solutions, depending on the relation between the two coupling constants c_1, c_2. In the regime $c_1 > c_2$, the ground state is a Fermi sea of two-strings, where the Fermi wave vector Q is under constraint: there is a limiting Q^* which Q cannot exceed, and near Q^* the distribution of the center momentum presents a square root singularity. As c_2 approach c_1 from below we come close to a diverging compressibility, which leads us into the other regime $c_2 > c_1$ with a single N particle bound state for the ground state. In the Bethe ansatz approach, this bound state reveals itself as an embedded string solution. Our model is experimentally accessible by using two hyperfine states of ^{87}Rb quantum gases with tunable couplings via Feshbach resonance. Furthermore, the uniform regime $c_1 > c_2$ provides a new scenario for investigating the physics of BCS-BEC crossover, where the system is governed by a single Hamiltonian and the behavior of the spin excitations is accessible along the whole range of the crossover. Also, we have explored the zero temperature phase diagram in presence of external magnetic field, where a critical magnetic field below which the ground state cannot be polarized is caused by the presence of the upper bound Q^* for the Fermi momentum.

Chapter 4

Solitons in One Dimensional Systems at BCS-BEC Crossover

4.1 Introduction

In the previous chapter, we constructed an exactly solvable model for BCS-BEC crossover in one dimension, where we have obtained several robust features of low energy excitation spectra along the whole crossover (see Fig. 3.7 and Fig. 3.8). In this chapter, we will explain these robust features in terms of solitons from a semiclassical point of view.

Soliton formation is an important and rich nonlinear phenomenon in various branches of physics. In many exactly solvable models, both classical and quantum mechanical ones, soliton plays a unique role. It is well known that the interacting bosons in one dimension (the Lieb-Liniger model) show an unexpected branch in its excitation spectrum, usually referred to as the type-II excitations [67, 66]. Later it was found that the interacting fermions in one dimension (the Yang-Gaudin model) have a similar phenomenon [39, 95]. The fact that they originate from solitons can be clearly seen in the semiclassical analysis, where solitons serve as an alternative solution to the semiclassical equation of motion apart from the spatially homogeneous solution [60, 25].

It is even more interesting, as we have seen in the previous chapter, that these soliton-like solutions can further affect the spin excitations in a striking way that they will fix the minimum energy of the spin excitations exactly at momentum $k_F = \pi n/2$, where nm_F (m_F is the mass of the fermionic atom) is the conserved total mass density of the system and it remains unchanged along the whole crossover.

This is in sharp contrast to the situation in higher dimensions, whereby tuning interaction along

the BCS-BEC crossover we can move this momentum from k_F on the deep BCS side to zero on the deep BEC side [76]. In this chapter, we present a comprehensive semiclassical theory of solitons in one dimensional systems at BCS-BEC crossover, where we explain the soliton interpretation of the type-II excitations and the fixing of the momentum for the minimum energy of spin excitations. Our theory gives the semiclassical interpretation of the excitation spectrum of the Yang-Gaudin model, where existing semiclassical proposals fail to reconcile with the exact solutions [25, 95]. Our theory also serves as yet another example of the dramatic effect solitons can have on low dimensional physics.

In the next section, we will review the exact solutions of the Lieb-Linger model, the Yang-Gaudin model and the model of BCS-BEC crossover in one dimension. We then further analyze them in the sections to follow. We first outline the general formalism of the semiclassical analysis in presence of solitons across the BCS-BEC crossover. We then apply it to the $S = 1/2$ and $S = 0$ excitations respectively, where we present analytic analysis on both deep BCS and deep BEC side and qualitative analysis for the crossover. Finally, we summarize the main results and make the conclusion.

4.2 Review of Exact Solutions and their Relation to Solitons

In Sec. 3.2.1, we have reviewed the Lieb-Liniger model for interacting bosons and the Yang-Gaudin model for interacting fermions, and we have constructed the exactly solvable models for BCS-BEC crossover in one dimension. The low energy excitation spectra for the latter are worked out in Sec. 3.3.2. In this section, we summarize the excitation spectra of these exactly solvable models. In the gapless $S = 0$ excitations spectrum (where S is the total spin) for all these models, there is an extra soliton-like branch apart from the usual Bogoliubov quasiparticle branch. In the gapped $S = 1/2$ excitations, one finds the minimum of the energy lying exactly at the Fermi momentum $k_F = \pi n/2$. These are the key features we would like to explain when later developing the corresponding semiclassical theory.

We start with the Lieb-Liniger model, described by the Hamiltonian in Eq. (3.2):

$$\hat{\mathcal{H}} = \int dx \left[\partial_x \hat{\varphi}^\dagger(x)\partial_x\hat{\varphi}(x) + c_B\hat{\varphi}^\dagger(x)\hat{\varphi}^\dagger(x)\hat{\varphi}(x)\hat{\varphi}(x)\right], \tag{4.1}$$

where $\hat{\varphi}$ represents the spinless bosons with mass $m_B = 1/2$, and $c_B > 0$ corresponds to the repulsion between bosons. A typical excitation spectrum of Lieb-Liniger model is shown in Fig. 4.1. It is composed of two branches, the usual Bogoliubov quasiparticle (Lieb-Liniger type-I) branch, and the Lieb-Liniger type-II branch. At long wavelength, both branches reduce to a linear dispersion as

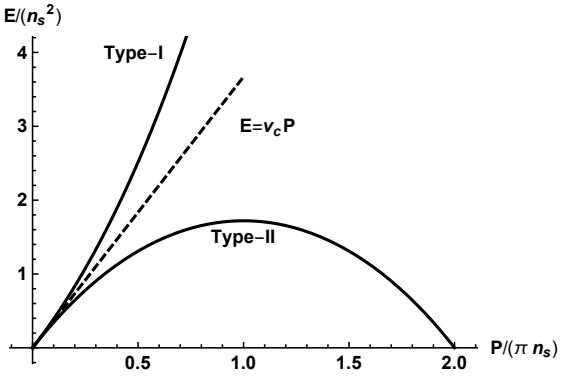

Figure 4.1: The typical excitation spectrum of the Lieb-Liniger model, calculated for coupling strength $\gamma = c_B/n_s = 0.43$. There are two branches, type-I for Bogoliubov quasiparticles and type-II for soliton-like excitations. Also shown in the figure is the sound velocity v_c, which scale as $\sqrt{c_B n}$.

phonons, with the same sound velocity $v_c = \sqrt{c_B n}$, whose magnitude decreases with the coupling strength. The key features of the type-II excitations are that it has $\epsilon(2\pi n_s) \to 0$ as the system size goes to infinity, $L \to \infty$, and it has its maximum energy achieved at momentum $k = \pi n_s$. This periodicity of the type-II branch is a consequence of the discrete translational invariance, where the shift of momentum for each boson by the amount of $2\pi/L$ costs $(n_s L)(2\pi/L)^2 \to 0$ in energy but changes the total momentum by $(n_s L)(2\pi/L) = 2\pi n_s$ [88]. Similarly, the total energy also remains invariant under the momentum reflection $k \to 2\pi/L - k$ for each boson, which means the spectrum has an additional symmetry of reflection about total momentum πn_s. As a result, the maximum of the spectrum is fixed at momentum πn_s. It is known that this point corresponds to a motionless (dark) soliton, and the entire Lieb-Liniger type-II branch has the physical interpretation as the dispersion relation $E(P)$ for the moving (grey) soliton with velocity $v_s = \partial E(P)/\partial P$ [60, 55].

Now we move on to the attractive Yang-Gaudin model, which is defined by the Hamiltonian in Eq. (3.1):

$$\hat{\mathcal{H}} = \int dx \left[\partial_x \hat{\psi}^\dagger(x) \partial_x \hat{\psi}(x) - c_F \hat{\psi}^\dagger(x) \hat{\psi}^\dagger(x) \hat{\psi}(x) \hat{\psi}(x) \right], \tag{4.2}$$

where $\hat{\psi} = \begin{pmatrix} \hat{\psi}_\uparrow \\ \hat{\psi}_\downarrow \end{pmatrix}$ represents the $S = 1/2$ fermions with mass $m_F = 1/2$, and $c_F > 0$ corresponds to the attraction between fermions. This attraction, however weak, produces bound pairs in one dimension. A typical spectrum of $S = 0$ excitations of the Yang-Gaudin model is shown in Fig. 4.2, which is pretty similar to the one we obtain in the Lieb-Liniger model. The notable differences here are the scale of the maximum energy of type-II excitations and the sound velocity. In the weak coupling limit $c_F/n \ll 1$, the maximum energy is on the scale of the Fermi energy $\epsilon_F = \pi^2 n^2/4$ and the sound velocity is on the scale of the Fermi velocity $v_F = \pi n$. Since the velocity is large when

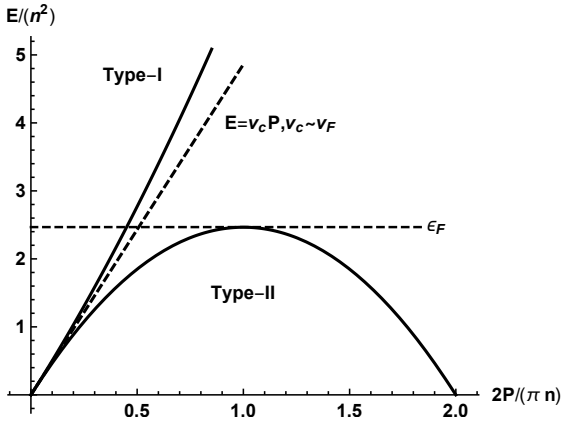

Figure 4.2: The typical $S = 0$ excitation spectrum of the Yang-Gaudin model, calculated for coupling strength $\gamma = c_F/n = 0.15$. There are also two branches, type-I for Bogoliubov quasiparticles and type-II for soliton-like excitations. Also shown in the figure is the sound velocity and the Fermi energy ϵ_F, we can see in the weak coupling limit, the dark soliton has an energy on the scale of ϵ_F and the sound velocity is on the scale of v_F.

$k \to 0$, there is no semiclassical description for the dispersion relation, but near the maximum of the spectrum where the velocity is small, a semiclassical description is still possible. The recent attempt by [25] to develop such a description led to incorrect energy scale and curvature near the maximum of the spectrum [95]. We are going to reconcile this discrepancy in this chapter.

In the strong coupling limit $c_F/n \gg 1$ where the fermions are tightly bound, instead of behaving like a system of weakly coupled bosons, the Yang-Gaudin model produces a system of hardcore bosons know as the fermionic super Tonks-Girardeau gas [39]. As a result, the sound velocity is still on the scale of the Fermi velocity, and the spectrum of Fig. 4.2 preserves qualitative shape for any value of c_F.

A typical spectrum of $S = 1/2$ excitations of the Yang-Gaudin model is shown in Fig. 4.3, where the minimum energy is achieved exactly at the Fermi momentum $k_F = \pi n/2$, irrespective of the coupling strength. This exactness is unusual, since it is without the correction on the scale of $\delta k \sim \Delta_0/v_F$ that would be introduced by the conventional BCS theory in the weak coupling limit (where Δ_0 is the gap width), and it is contrary to the usual conclusion that the minimum energy should be achieved at zero momentum in deep BEC regime in higher dimensions [76]. At first sight, this could be caused by the fact that the strong coupling limit $c_F/n \gg 1$ of Yang-Gaudin model is not a system of weakly coupled bosons, which invalidates it as a proper model for BCS-BEC crossover. To test this idea, our models proposed in the previous chapter come into play. The fermionic version

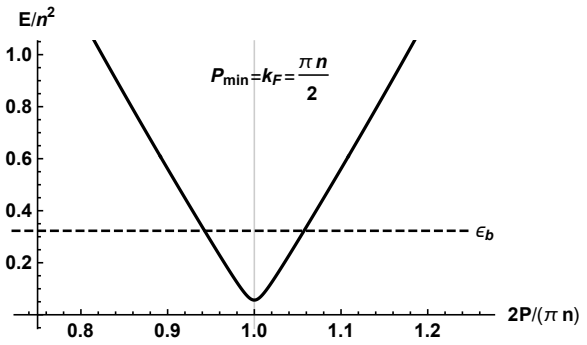

Figure 4.3: The typical $S = 1/2$ excitation spectrum of the Yang-Gaudin model, calculated for coupling strength $\gamma = c_F/n = 1.13$. The minimum energy is obtained at the Fermi momentum $k_F = \pi n/2$, with a small region of quadratic spectrum around it. Also shown in the figure is the binding energy ϵ_b for the singlet pairs, which is bigger than the spin gap.

is described by the Hamiltonian in Eq. (3.7):

$$\begin{aligned}\hat{\mathcal{H}} = \int dx \Big\{ &\partial_x\hat{\psi}^\dagger\partial_x\hat{\psi} + \frac{1}{2}\partial_x\hat{\boldsymbol{\Xi}}^\dagger\cdot\partial_x\hat{\boldsymbol{\Xi}} + \frac{1}{2}\partial_x\hat{\Pi}^\dagger\partial_x\hat{\Pi} - \epsilon_\Pi\hat{\Pi}^\dagger\hat{\Pi} + g\hat{\psi}^\dagger\hat{\psi}^\dagger\hat{\psi}\hat{\psi} \\ &+ \left[\frac{t_\Xi}{2}\left(i\partial_x\hat{\psi}^T\boldsymbol{\sigma}\sigma_y\hat{\psi}\right)\cdot\hat{\boldsymbol{\Xi}}^\dagger + h.c.\right] + \left[\frac{t_\Pi}{2}\left(i\hat{\psi}^T\sigma_y\hat{\psi}\right)\cdot\hat{\Pi}^\dagger + h.c.\right]\Big\},\end{aligned} \tag{4.3}$$

where $\hat{\psi} = \begin{pmatrix}\hat{\psi}_\uparrow \\ \hat{\psi}_\downarrow\end{pmatrix}$ represents the spin-1/2 fermions with mass $m_F = 1/2$, $\hat{\boldsymbol{\Xi}}$ represents the vector resonances with binding energy ϵ_Ξ and $\hat{\Pi}$ represents the scalar resonances with binding energy ϵ_Π. Both resonances are of mass $m_\Xi = m_\Pi = 1$. The behavior of this model is then controlled by two parameters:

$$c_1 = |t_\Xi|^2/4, \quad c_2 = c_1 + |t_\Pi|^2/(2\epsilon_\Pi). \tag{4.4}$$

This model has the Lieb-Liniger model and the Yang-Gaudin model as its two limits in the parameter range $c_1 \sim c_2$ and $c_1 \gg c_2$ respectively, thus providing a model of BCS-BEC crossover in one dimension that is subject to exact solutions. On the side where it reduces to the Yang-Gaudin model with $c_F = c_2$, the excitation spectrum is basically the same as shown in Fig. 4.2 and Fig. 4.3; On the side where it reduces to the Lieb-Liniger model with $c_B = c_1 - c_2$, the $S = 0$ spectrum is basically the same as shown in Fig. 4.1. In addition to that, we also have $S = 1/2$ excitations now, whose typical behavior is shown in Fig. 4.4. We can see that the spectrum has the same feature as that on the BCS side, with the minimum energy still obtained exactly at the Fermi momentum $k_F = \pi n/2$. even though the $S = 0$ sector corresponds to weakly interacting bosons with $v_c \ll v_F$.

In all the exactly solvable models presented above, the fixing of minimum spin excitation energy at k_F is a phenomenon robust against variations of coupling constants across the whole range, which

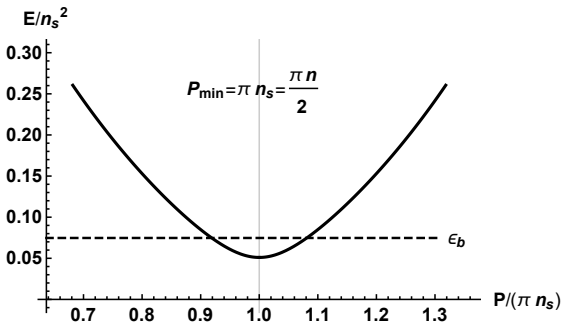

Figure 4.4: The typical $S = 1/2$ excitation spectrum on the BEC side, calculated for coupling strength $\gamma_1 = c_1/n = 0.34$ and $\gamma_2 = c_2/n = 0.27$. In the plotting scale we have used $n_s = n/2$. The minimum energy is again obtained at the Fermi momentum $k_F = \pi n/2$. Also shown in the figure is the binding energy ϵ_b for the singlet pair, which is bigger than the spin gap.

is in sharp contrast to the situation in higher dimensions [76]. It leads us to the conclusion that this is most probably a general feature not limited to exact solvability. One may suspect that the fixing is a consequence of the Luttinger theorem, but this is not true due to the fact that the system here is gapped and there is no conservation of the number of fermions (since there is tunneling between atoms and molecules back and forth). On the other hand, the maximum of the $S = 0$ excitations can be interpreted as a dark soliton, with the spectrum near it as a moving grey soliton. We propose that the minimum of the $S = 1/2$ excitations is also a dark soliton with one extra fermion bounded on it and k_F is just the momentum of this dark soliton, whereas the fermion sitting bounded on top of it doesn't bring any new momentum. This will be done in the next sections.

4.3 General Formalism

For the purpose of semiclassical analysis, let's consider the following simplified model of BCS-BEC crossover at the mean field level:

$$\begin{aligned}\hat{\mathcal{H}} &= \int dx\ \left\{\partial_x\hat{\psi}^\dagger\partial_x\hat{\psi} + \frac{1}{2}\partial_x\hat{b}^\dagger\partial_x\hat{b} - \epsilon_b\hat{b}^\dagger\hat{b} + \left[\frac{t_b}{2}\left(i\hat{\psi}^T\sigma_y\hat{\psi}\right)\hat{b}^\dagger + h.c.\right]\right\} - \mu\hat{\mathcal{N}},\\ \hat{\mathcal{N}} &= \int dx\left(\hat{\psi}^\dagger\hat{\psi} + 2\hat{b}^\dagger\hat{b}\right), \quad \hat{\mathcal{P}} = \frac{1}{2i}\int dx\left(\hat{\psi}^\dagger\partial_x\hat{\psi} + \hat{b}^\dagger\partial_x\hat{b} - h.c.\right),\end{aligned} \tag{4.5}$$

where $\hat{\psi} = \begin{pmatrix}\hat{\psi}_\uparrow\\ \hat{\psi}_\downarrow\end{pmatrix}$ represents the $S = 1/2$ fermions with mass $m_F = 1/2$, $\hat{b}$ with mass $m_b = 1$ represents a scalar resonance with resonant energy $-\epsilon_b$ when $\epsilon_b < 0$ or a molecule with binding energy ϵ_b when $\epsilon_b > 0$. The coupling constant t_b is chosen to be real. Operator $\hat{\mathcal{N}}$ is a conserved quantity and the expectation value of $m_F\hat{\mathcal{N}} = \hat{\mathcal{N}}/2$ gives the total mass of the system. Although not subject

to exact solutions, this model grasps the essence of the BCS-BEC crossover and is more friendly to semiclassical analysis.

A conventional way to analyze the semiclassical origin of the excitations is to treat the operators as classical fields and to solve the semiclassical equations of motion for them. Its validity can be justified in the narrow resonance limit and via the saddle point approximation in the path integral formalism. The symmetry-broken ground state of the system is then represented by the expectation value $\left\langle \hat{b} \right\rangle = b_0$, where b_0 is a constant, and the excitations are represented by a space-time varying expectation value $b(x,t) \equiv \left\langle \hat{b} \right\rangle$, where we use the periodic boundary condition such that $b(x,t) = b(x+L,t)$. As we treat the operator $\hat{b}$ as a classical field $b(x,t)$, the part of $\hat{\mathcal{H}}$ that involves fermionic operators can be diagonalized via the Bogoliubov-Valatin transformation

$$\begin{pmatrix} \hat{\psi}_\uparrow \\ \hat{\psi}^\dagger_\downarrow \end{pmatrix} = \sum_n \begin{pmatrix} u_n(x,t) & -v_n^*(x,t) \\ v_n(x,t) & u_n^*(x,t) \end{pmatrix} \begin{pmatrix} \hat{\gamma}_{n\uparrow} \\ \hat{\gamma}^\dagger_{n\downarrow} \end{pmatrix} \tag{4.6}$$

to the following Hamiltonian

$$\hat{\mathcal{H}}_\psi = \sum_{\epsilon_n>0} \left[-\epsilon_n(\Delta,\Delta^*) + \epsilon_n \Big|_{t_b=0} \right] + \sum_{\epsilon_n>0,\sigma} \epsilon_n \hat{\gamma}^\dagger_{n\sigma} \hat{\gamma}_{n\sigma}, \tag{4.7}$$

where we have defined $\Delta(x,t) \equiv t_b b(x,t)$ and the classical fields $u_n(x,t), v_n(x,t)$ satisfy the Bogoliubov-de Gennes equation [94] with periodic boundary conditions:

$$\begin{gathered} \begin{pmatrix} -\partial_x^2 - \mu & \Delta \\ \Delta^* & \partial_x^2 + \mu \end{pmatrix} \begin{pmatrix} u_n \\ v_n \end{pmatrix} = \epsilon_n \begin{pmatrix} u_n \\ v_n \end{pmatrix}, \\ \begin{cases} u_n(x+L,t) = u_n(x,t) \\ v_n(x+L,t) = v_n(x,t) \end{cases}. \end{gathered} \tag{4.8}$$

Using these classical fields $b(x,t)$, $u_n(x,t)$ and $v_n(x,t)$, the energy and momentum of the system under a particular filling configuration of Eq. (4.7) can then be expressed as

$$\begin{aligned} E &= \int dx \left(\frac{1}{2} |\partial_x b|^2 - (2\mu + \epsilon_b)|b|^2 \right) + E_\psi, \\ E_\psi &= \sum_{\epsilon_n>0} \left[-\epsilon_n(\Delta,\Delta^*) + \epsilon_n \Big|_{t_b=0} \right] + \sum_{\epsilon_n>0,\sigma} \epsilon_n \left\langle \hat{\gamma}^\dagger_{n\sigma} \hat{\gamma}_{n\sigma} \right\rangle, \\ P &= \int dx \left(\sum_{\epsilon_n>0} \frac{u_n^* \overleftrightarrow{\partial_x} u_n + v_n^* \overleftrightarrow{\partial_x} v_n}{2i} \sum_\sigma \left\langle \hat{\gamma}^\dagger_{n\sigma} \hat{\gamma}_{n\sigma} \right\rangle \right) + \int dx \left(\sum_{\epsilon_n>0} (-i) v_n \overleftrightarrow{\partial_x} v_n^* + \frac{b^* \overleftrightarrow{\partial_x} b}{2i} \right), \end{aligned} \tag{4.9}$$

where E_ψ is the eigenvalue of the mean field Hamiltonian $\hat{\mathcal{H}}_\psi$ in Eq. (4.7) under this particular filling configuration, and the double arrow derivative is defined as

$$f \overleftrightarrow{\partial_x} g \equiv f(\partial_x g) - (\partial_x f) g. \tag{4.10}$$

The solutions to Eq. (4.8) have a special particle-hole symmetry that if $(u_n, v_n)^{\mathrm{T}}$ is a solution with eigenvalue ϵ_n, then $(-v_n^*, u_n^*)^{\mathrm{T}}$ must be a solution with eigenvalue $-\epsilon_n$. As a result, nonzero eigenvalues appear in pairs. Moreover, if Eq. (4.8) possesses zero eigenvalue, it must be degenerate, otherwise we would have

$$\begin{pmatrix} u_0 \\ v_0 \end{pmatrix} = c \begin{pmatrix} -v_0^* \\ u_0^* \end{pmatrix}, \tag{4.11}$$

where $(u_0, v_0)^{\mathrm{T}}$ is the solution to Eq. (4.8) for $\epsilon = 0$ and c is constant complex number of modulus one $|c| = 1$. Equation (4.11) would then lead to $|c|^2 u_0 = -u_0$, which cannot be true unless u_0 is trivially zero (This argument is analogous to that for Kramers degeneracy). In later sections where $\Delta(x, t)$ is identified as a soliton, we find that the degenerate zero modes appear only in the deep BCS limit, where the spectrum is linearized around the Fermi points. But this turns out to be an artifact of the linearization, and there will be no zero mode when the nonlinear effect of the spectrum is taken into account.

It is clear from the above analysis that the solutions to Eq. (4.8) always appear in pairs, the state $S = 0$ then corresponds to a zero (or even) occupation of Bogoliubov fermions $\hat{\gamma}_{n\sigma}$ and the state $S = 1/2$ is made out of odd occupation. Also as we will see in later sections, the state of the $S = 0$ soliton corresponding to the exact solution is not necessarily a ground state of $\hat{\mathcal{H}}_\psi$.

4.3.1 Dark Soliton

The dark soliton is characterized by a twist in the configuration of $b(x)$ where its value changes sign rapidly from $x < 0$ to $x > 0$. Taking into consideration the periodic boundary condition, $b(x)$ then has the following asymptotic behavior at spatial boundaries:

$$b(x \to \pm L/2) \sim e^{i\pi x/L}, \tag{4.12}$$

where we are taking the infinite system limit that $L \to \infty$. It would be helpful to perform the following gauge transformation:

$$b(x) = e^{i\pi x/L} \tilde{b}(x), \tag{4.13}$$

then the dark soliton can be presented as

$$\tilde{b}(x) = -ib_0 f\left(\frac{x}{l_s}\right), \tag{4.14}$$

where $l_s \ll L$ is the size of the soliton sitting at $x = 0$, the constant number b_0 is chosen to be real, and the shape function $f(x)$ has the asymptotic behavior that $f(x \to \pm\infty) = \pm 1$. Under this gauge transformation, the periodic boundary condition of $b(x)$ becomes $\tilde{b}(x + L) = -\tilde{b}(x)$. As a result, $\tilde{b}(x)$ can be chosen purely imaginary, or equivalently, $f(x)$ can be chosen purely real.

To get rid of the phase in Eq. (4.13), we perform the following gauge transformation on the classical fields $u_n(x), v_n(x)$:

$$\begin{cases} u_n(x) = e^{i\pi x/L}\tilde{u}(x) \\ v_n(x) = \tilde{v}_n \end{cases}, \tag{4.15}$$

then Eq. (4.8) is transformed into

$$\begin{pmatrix} -\partial_x^2 - \mu & t_b\tilde{b} \\ (t_b\tilde{b})^* & \partial_x^2 + \mu \end{pmatrix} \begin{pmatrix} \tilde{u}_n \\ \tilde{v}_n \end{pmatrix} = \epsilon_n \begin{pmatrix} \tilde{u}_n \\ \tilde{v}_n \end{pmatrix}, \quad \begin{cases} \tilde{u}_n(x + L, t) = -\tilde{u}_n(x, t) \\ \tilde{v}_n(x + L, t) = \tilde{v}_n(x, t) \end{cases}, \tag{4.16}$$

where we have neglected both L^{-1} and L^{-2} correction to the eigenenergy ϵ_n. The former can be neglected because it contributes to the total energy in Eq. (4.9) a term proportional to P/L, which goes to zero in the limit $L \to \infty$ for finite momentum P. The latter can be neglected because it contributes to the total energy a term proportional to NL^{-2}, which also goes to zero in the limit $L \to \infty$. Using these gauge transformed classical fields, the energy E, the momentum P and the conserved quantity N of the system can be expressed as:

$$\begin{aligned} E &= \int dx \left(\frac{1}{2}|\partial_x\tilde{b}|^2 - (2\mu + \epsilon_b)|\tilde{b}|^2\right) + E_\psi, \\ P &= \int dx \left(\sum_{\epsilon_n>0} \frac{\tilde{u}_n^* \overleftrightarrow{\partial_x} \tilde{u}_n + \tilde{v}_n^* \overleftrightarrow{\partial_x} \tilde{v}_n}{2i} \sum_\sigma \langle \hat{\gamma}_{n\sigma}^\dagger \hat{\gamma}_{n\sigma} \rangle\right) + \int dx \left(\sum_{\epsilon_n>0} (-i)\tilde{v}_n \overleftrightarrow{\partial_x} \tilde{v}_n^* + \frac{\tilde{b}^* \overleftrightarrow{\partial_x} \tilde{b}}{2i}\right) + \frac{N}{2L}\pi, \\ N &= \int dx \sum_{\epsilon_n>0} \left[(\tilde{u}_n^*\tilde{u}_n - \tilde{v}_n^*\tilde{v}_n) \sum_\sigma \langle \hat{\gamma}_{n\sigma}^\dagger \hat{\gamma}_{n\sigma} \rangle\right] + \int dx \left(\sum_{\epsilon_n>0} 2\tilde{v}_n^*\tilde{v}_n + 2\tilde{b}^*\tilde{b}\right), \end{aligned} \tag{4.17}$$

where the effect of gauge transformation is taken into account in the limit $L \to \infty$. The contribution to the energy is vanishingly small ($\sim NL^{-2}$) while the contribution to the momentum remains finite, which appears in the expression for P as the last term proportional to $n = N/L$.

To be consistent with the choice that $\tilde{b}(x)$ is purely imaginary, $\tilde{u}_n(x)$ and $\tilde{v}_n(x)$ can be chosen purely real and purely imaginary respectively. Since the classical fields $\tilde{b}(x)$, $\tilde{u}_n(x)$ and $\tilde{v}_n(x)$ are chosen to be either purely real or purely imaginary, the contribution from the integral for the momentum P in Eq. (4.17) is zero, then we arrive at the result that the momentum of the dark soliton is exactly the Fermi momentum:

$$P = k_F = \pi n/2, \tag{4.18}$$

whether it is for a $S = 0$ state or a $S = 1/2$ state.

Now we have to determine the actual form of the dark soliton profile $f(x)$. It is obtained by solving the equation of motion for the classical field $\tilde{b}(x)$. Because the dark soliton corresponds to a local minimum or a local maximum of the energy for $S = 0$ or $S = 1/2$ spectrum respectively, the desired equation of motion for $\tilde{b}(x)$ can be derived by extremizing the energy E in Eq. (4.17):

$$-\frac{1}{2}\partial_x^2\tilde{b} - (2\mu + \epsilon_b)\,\tilde{b} + \frac{\delta E_\psi}{\delta \tilde{b}^*} = 0. \tag{4.19}$$

Together with Eq. (4.16), we now have a complete set of equations to determine all the relevant classical fields.

As mentioned at the end of Sec. 4.2, our proposal for $S = 1/2$ excitations is based upon the assumption that one extra fermion can be bounded on the dark soliton, which is equivalent to the assumption that there is at least one localized state solution to Eq. (4.16), so we present below a simple one-parameter variational approach to verify this assumption.

The Hamiltonian operator corresponding to Eq. (4.16) is as follows:

$$\hat{\mathcal{H}}_b = \begin{pmatrix} -\partial_x^2 - \mu & t_b\tilde{b} \\ (t_b\tilde{b})^* & \partial_x^2 + \mu \end{pmatrix}, \tag{4.20}$$

and it has a positive as well as a negative sector, due to the particle-hole symmetry discussed after Eq. (4.8). Accordingly, the existence of the localized state can be proved by the fact that the expectation value $I(\kappa)$ of $\hat{\mathcal{H}}_b^2$ on a normalized trial wave function $\psi_\kappa(x)$ is below the boundary of the continuous spectrum for $\hat{\mathcal{H}}_b^2$, where κ is the variational parameter:

$$I(\kappa) = \int dx\,(\mathcal{H}\psi_\kappa(x))^*\,\mathcal{H}\psi_\kappa(x), \qquad \int dx\;\psi_\kappa^*(x)\psi_\kappa(x) = 1. \tag{4.21}$$

Here we make the choice that $I(0)$ corresponds to the boundary of the continuous spectrum and $\kappa > 0$

corresponds to the localized state. Then the existence of localized state corresponds to $I'(0) < 0$.

For $\mu > 0$, the boundary of the continuous spectrum for $\hat{\mathcal{H}}_b^2$ is $\Delta_0^2 = (t_b b_0)^2$, and the normalized trial wave function can be chosen as

$$\psi_\kappa = \sqrt{\kappa} e^{-\kappa|x|} \begin{pmatrix} \cos k_F x \\ \sin k_F x \end{pmatrix}, \tag{4.22}$$

where $k_F^2 = \mu$. Then we have

$$I(\kappa) = \Delta_0^2 + \kappa^4 + 4\kappa^2 k_F^2 - \Delta_0^2 \kappa l_s \int e^{-2\kappa l_s |y|} f^2(y) dy, \tag{4.23}$$

which has the required property that

$$I(0) = \Delta_0^2, \quad I'(0) < 0. \tag{4.24}$$

For $\mu \leqslant 0$, the boundary of the continuous spectrum for $\hat{\mathcal{H}}_b^2$ is $\Delta_0^2 + \mu^2$, and the following normalized trial wave function is chosen:

$$\psi_\kappa = \sqrt{\kappa} e^{-\kappa|x|} \begin{pmatrix} 1 \\ 0 \end{pmatrix}, \tag{4.25}$$

Then we have

$$I(\kappa) = (-\kappa^2 + |\mu|)^2 + \Delta_0^2 - \Delta_0^2 \kappa l_s \int e^{-2\kappa l_s |y|} f^2(y) dy, \tag{4.26}$$

which again has the required property that

$$I(0) = \Delta_0^2 + \mu^2, \quad I'(0) < 0. \tag{4.27}$$

Taking also into consideration that the solutions to Eq. (4.16) always appear in pairs and belong to the negative and positive sectors respectively, we then proved here that there is at least one localized state for each sector for the whole range of μ across the BCS-BEC crossover.

In later sections, we will show that the number of localized states is exactly one for each sector in both the deep BCS and the deep BEC limit, and we didn't find any evidence for the existence of a second localized state (though appearance of such state would not violate any further consideration).

4.3.2 Grey Soliton

In order to transform the dark soliton into a moving grey soliton, we need to generalize the above construction to the following asymptotic behavior at spatial boundaries:

$$b(x \to \pm L/2, t) \sim e^{i\theta_s x/L}, \tag{4.28}$$

where the phase parameter $\theta_s \in [0, 2\pi)$ and we take the limit $L \to \infty$. We will show in later sections that the moving grey soliton can be presented in the following form:

$$b(x,t) = b_0 \left[\cos\frac{\theta_s}{2} - i\sin\frac{\theta_s}{2} f\left(\frac{x - v_s t}{l_s}\right)\right] e^{i\theta_s x/L}, \tag{4.29}$$

where v_s is the velocity of the grey soliton. The velocity v_s and phase parameter θ_s are not independent variational variables. As we will show now, they are related to each other via the semiclassical velocity formula $v_s = \partial E(\theta_s)/\partial P(\theta_s)$.

Considering the transformation of the variables from (x,t) to (z,t) such that $z = x - v_s t$, we will have

$$\begin{aligned}
\hat{\mathcal{H}} \to \hat{\Omega} &= \hat{\mathcal{H}} + \frac{i v_s}{2}\int dz \left(\hat{\psi}^\dagger \overleftrightarrow{\partial_z} \hat{\psi} + \hat{b}^\dagger \overleftrightarrow{\partial_z} \hat{b}\right), \\
\hat{\mathcal{P}} \to \hat{\mathcal{P}} &= \frac{(-i)}{2}\int dz \left(\hat{\psi}^\dagger \overleftrightarrow{\partial_z} \hat{\psi} + \hat{b}^\dagger \overleftrightarrow{\partial_z} \hat{b}\right),
\end{aligned} \tag{4.30}$$

where we have variable x on the lefthand side and variable z on the righthand side. We can see that in Eq. (4.30) new terms are added to the Hamiltonian operator, while the momentum operator remains unchanged. This implies that the variable transformation introduced here is not a Galilean transformation, for which the momentum would have been changed by the amount proportional to $v_s N \to \infty$. From Eq. (4.30) we obtain the following operator relations:

$$\frac{\partial\hat{\Omega}}{\partial v_s} = -\hat{\mathcal{P}}, \quad \hat{\Omega} = \hat{\mathcal{H}} - v_s\hat{\mathcal{P}}. \tag{4.31}$$

By taking the expectation values of both sides on the soliton with phase parameter θ_s, we can see that the change of variables from x to z is equivalent to a Legendre transformation:

$$\frac{\partial\Omega(\theta_s)}{\partial v_s} = -P(\theta_s), \quad \Omega(\theta_s) = E(\theta_s) - v_s P(\theta_s). \tag{4.32}$$

By taking derivative with respect to θ_s of both sides of the second equation in (4.32), we obtain

$$\frac{\partial \Omega}{\partial \theta_s} = \frac{\partial E}{\partial \theta_s} - \frac{\partial v_s}{\partial \theta_s} P - v_s \frac{\partial P}{\partial \theta_s}. \tag{4.33}$$

Then using the first equation in (4.32) we also obtain

$$\frac{\partial \Omega}{\partial \theta_s} = \frac{\partial \Omega}{\partial v_s} \frac{\partial v_s}{\partial \theta_s} = -\frac{\partial v_s}{\partial \theta_s} P. \tag{4.34}$$

Combining Eq. (4.33) and Eq. (4.34), we arrive at the following equation

$$v_s = \frac{\partial E/\partial \theta_s}{\partial P/\partial \theta_s} = \frac{\partial E}{\partial P}. \tag{4.35}$$

When the soliton is interpreted as a proper excitation, Eq. (4.35) is just the semiclassical velocity formula mentioned above, which determines the soliton velocity v_s as a function of θ_s. Then the fact that the dark soliton corresponds to either the maximum ($S = 0$) or minimum energy ($S = 1/2$) follows from the condition that $v_s(\theta_s = \pi) = 0$.

As in derivation for the dark soliton, it would be helpful to do the following gauge transformation of the classical fields:

$$\begin{cases} b(x,t) = e^{i\frac{\theta_s x}{L}} \tilde{b}(z), \\ u_n(x,t) = e^{i\frac{\theta_s x}{L}} \tilde{u}_n(z), \\ v_n(x,t) = \tilde{v}_n(z), \end{cases} \tag{4.36}$$

where $z = x - v_s t$. This leaves us with the analysis of classical fields $\tilde{b}(z)$ or $\tilde{\Delta}(z) = t_b \tilde{b}(z)$, $\tilde{u}_n(z)$ and $\tilde{v}_n(z)$, for which we will omit the tilde in the following whenever there is no confusion. Also, the gauge transformation modifies the boundary conditions of the classical fields:

$$\begin{cases} b(z+L) = e^{-i\theta_s} b(z), \\ u_n(z+L) = e^{-i\theta_s} u_n(z), \\ v_n(z+L) = v_n(z). \end{cases} \tag{4.37}$$

Using these classical fields, again we can write down the expressions for the energy E, momentum P

and the conserved quantity N:

$$
\begin{aligned}
E &= \int dz \left(\frac{1}{2}|\partial_z b|^2 - (2\mu + \epsilon_b)|b|^2 \right) + E_\psi, \\
P &= \int dz \left(\sum_{\epsilon_n > 0} \frac{u_n^* \overleftrightarrow{\partial_z} u_n + v_n^* \overleftrightarrow{\partial_z} v_n}{2i} \sum_\sigma \langle \hat{\gamma}_{n\sigma}^\dagger \hat{\gamma}_{n\sigma} \rangle \right) + \int dz \left(\sum_{\epsilon_n > 0} (-i) v_n \overleftrightarrow{\partial_z} v_n^* + \frac{b^* \overleftrightarrow{\partial_z} b}{2i} \right) + \frac{N}{2L}\theta_s, \\
N &= \int dz \sum_{\epsilon_n > 0} \left[(u_n^* u_n - v_n^* v_n) \sum_\sigma \langle \hat{\gamma}_{n\sigma}^\dagger \hat{\gamma}_{n\sigma} \rangle \right] + \int dz \left(\sum_{\epsilon_n > 0} 2 v_n^* v_n + 2 b^* b \right),
\end{aligned}
\tag{4.38}
$$

where the energy and momentum are understood by taking the reference point that $E(\theta_s = 0) = 0$ and $P(\theta_s = 0) = 0$. Also, the chemical potential is determined by the usual thermodynamic relation that $\mu = \partial E / \partial N$.

For a particular filling configuration of the mean field Hamiltonian $\hat{\mathcal{H}}_\psi$ in Eq. (4.7), we now derive the semiclassical equations of motion for the classical fields $b(z), u_n(z)$ and $v_n(z)$. Unlike the dark soliton, the grey soliton only extremizes the energy E under certain constraints. Usually we would extremize the energy E under the constraint of fixed momentum P, but this approach may not respect the desired boundary condition in Eq. (4.37). To overcome this difficulty, we use a modified extremization process. Firstly, we partition the momentum P in Eq. (4.38) into two parts: the contribution P_ψ from the fermion fields and the contribution P_b from the b field:

$$
P_b = \int dz \left(\frac{(-i)}{2} b^* \overleftrightarrow{\partial_z} b + \frac{b^* b}{L} \theta_s \right), \quad P_\psi = P - P_b \tag{4.39}
$$

Then instead of keeping P fixed, we keep both P_ψ and P_b fixed, and this introduces two Lagrangian multiplier v_ψ and v_b into the free energy F we want to extremize:

$$
E \to F = E - v_\psi P_\psi - v_b P_b. \tag{4.40}
$$

We can visualize this modified extremization in the functional space spanned by P_ψ and P_b (see Fig. 4.5). Each point on the hyperline $P_\psi + P_b = P$ corresponds to an extreme of the free energy F, and one point among them (the starred point in Fig. 4.5) is picked out by adjusting the Lagrangian multiplier pair (v_ψ, v_b) to satisfy the boundary condition in Eq. (4.37). This modified extremization process is morally equivalent to the method of constrained instanton used in field theories [2]. Also,

following the derivation from Eq. (4.32) to Eq. (4.35), we obtain

$$dE = v_\psi dP_\psi + v_b dP_b = v_s(dP_\psi + dP_b). \tag{4.41}$$

This allows a trivial solution that $v_\psi = v_b = v_s$ or a nontrivial solution such that

$$\frac{v_s - v_\psi}{v_b - v_s} = \frac{\partial P_b}{\partial P_\psi}. \tag{4.42}$$

We will see in later sections that the nontrivial solution is crucial on the deep BCS side.

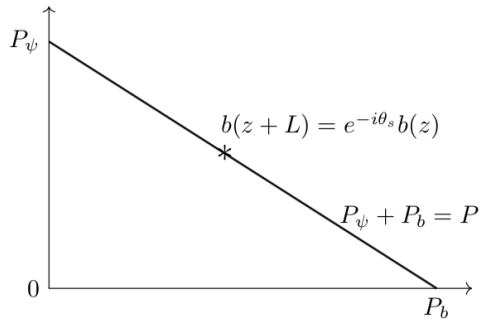

Figure 4.5: The functional space for the extremization spanned by P_ψ and P_b. The thick line is the collection of extreme points and the starred point is the one that satisfies the required boundary condition in Eq. (4.37).

Applying the modified extremization process, we obtain the following equations of motion for the classical fields in the limit $L \to \infty$:

$$-\frac{1}{2}\partial_z^2 b + iv_b \partial_z b - (2\mu + \epsilon_b)\, b + \frac{\delta E_\psi}{\delta b^*} = 0, \tag{4.43}$$

$$\begin{pmatrix} -\partial_z^2 - \mu + iv_\psi \partial_z & \Delta(z) \\ \Delta^*(z) & \partial_z^2 + \mu + iv_\psi \partial_z \end{pmatrix} \begin{pmatrix} u_n \\ v_n \end{pmatrix} = \bar{\epsilon}_n \begin{pmatrix} u_n \\ v_n \end{pmatrix}, \tag{4.44}$$

where $\Delta(z)$ field is related to $b(z)$ field through the definition $\Delta(z) = t_b b(z)$ and the eigenvalue $\bar{\epsilon}_n$ differs from ϵ_n in Eq. (4.7) and Eq. (4.8) in that $\bar{\epsilon}_n$ contributes to the free energy F in Eq. (4.40) while ϵ_n contributes to the energy E in Eq. (4.9). We should keep this in mind when later calculating the energy E. Also, the proof of the existence of the localized state for a dark soliton can be easily generalized here to Eq. (4.44) for a grey soliton.

4.4 Theory of $S = 1/2$ Soliton

In this section, we apply the general formalism outlined above to the $S = 1/2$ soliton, which turns out to be simpler than the $S = 0$ soliton. The two weak coupling limits - the deep BCS side and the deep BEC side - permit analytical treatment, because on either side, one of the degrees of freedom lies high in energy compared to the other such that we are left with a decoupled theory with weak interaction.

4.4.1 Deep BCS Side

On the deep BCS side, we tune the resonant level of b field far above the Fermi sea such that $\epsilon_b < 0, |\epsilon_b| \gg \mu$. Since the b field now only acts as a virtual state to effect the low energy physics, we can ignore its dynamics, and the equation of motion for it reduces to a self-consistent equation:

$$\Delta = \lambda \sum_{\epsilon_n > 0} u_n v_n^* \left(1 - \sum_\sigma \left\langle \hat{\gamma}_{n\sigma}^\dagger \hat{\gamma}_{n\sigma} \right\rangle \right) + \tau (i\partial_z \Delta), \tag{4.45}$$

where $\lambda = \frac{|t_b|^2}{-(2\mu + \epsilon_b)} > 0$ serves as the effective coupling constant and $\tau = v_b/(2\mu + \epsilon_b)$. Also for the dark soliton, we should bear in mind that we need to set $v_\psi = v_b = 0$ and $\tau = 0$. Combined with the equation of motion for the fermion fields, we can reconstruct the Hamiltonian as

$$\hat{\mathcal{H}} = \int dz \left(\sum_\sigma \hat{\psi}_\sigma^\dagger \left(-\partial_z^2 - \mu \right) \hat{\psi}_\sigma \right) + \int dz \left(\Delta^* \hat{\psi}_\downarrow \hat{\psi}_\uparrow + \Delta \hat{\psi}_\uparrow^\dagger \hat{\psi}_\downarrow^\dagger + \frac{|\Delta|^2}{\lambda} \right). \tag{4.46}$$

This is just the BCS mean field Hamiltonian for the conventional superconductivity and the Δ field is just the gap parameter. Thus, our semiclassical analysis on the deep BCS side can be equally well applied to the Yang-Gaudin model in the weak coupling limit. The system is made out of loosely bounded Cooper pairs, and we have a large chemical potential $\mu = k_F^2$, where $k_F = \pi n/2$ and $n = N/L$. Since the low energy physics happens only near the two Fermi points, we can linearize the spectrum around them:

$$\begin{pmatrix} u_n \\ v_n \end{pmatrix} = \sum_\alpha \begin{pmatrix} u_n^\alpha \\ v_n^\alpha \end{pmatrix} e^{i\alpha k_F z}, \tag{4.47}$$

where $\alpha = -1$ and $\alpha = 1$ denotes the left and right moving modes respectively. Correspondingly, Eq. (4.44) can be linearized to the following form:

$$\begin{pmatrix} -i\alpha v_F \partial_z - \alpha v_\psi k_F & \Delta(z) \\ \Delta^*(z) & i\alpha v_F \partial_z - \alpha v_\psi k_F \end{pmatrix} \begin{pmatrix} u_n^\alpha \\ v_n^\alpha \end{pmatrix} = \bar{\epsilon}_n^\alpha \begin{pmatrix} u_n^\alpha \\ v_n^\alpha \end{pmatrix}, \tag{4.48}$$

where the bar notation of the eigenvalue again reminds us that $\bar{\epsilon}_n^\alpha$ contributes to the free energy F instead of the energy E. Moreover, due to the linearization made here, we can further determine the eigenvalue ϵ_n^α that contributes to energy E as $\epsilon_n^\alpha = \bar{\epsilon}_n^\alpha + \alpha v_\psi k_F$.

The solution to this linearized Bogoliubov-de Gennes equation under soliton profile in the context of polyacetylene and charge density waves is well established in the literature [97, 100, 10, 11]. Essentially, the solvability comes from the fact that Eq. (4.48) has the form of Dirac equation in one dimension and it can be associated with a nonlinear Schrödinger equation for the $\Delta(z)$ field via the inverse scattering method [30]. There then exists the following soliton solution:

$$\Delta(z) = \Delta_0 \left[\cos\frac{\theta_s}{2} - i \sin\frac{\theta_s}{2} \tanh\left(\frac{z}{l_s}\right) \right], \tag{4.49}$$

where the size of the soliton is $l_s^{-1} = \left(\Delta_0 \sin\frac{\theta_s}{2}\right)/v_F$. The eigenmodes of Eq. (4.48) can be classified into two categories. The first category includes the delocalized states labelled by left-right moving index $\alpha = \pm$, band index $\iota = \pm$ and momentum k:

$$\begin{cases} u_{\iota k}^\alpha = \frac{1}{2}\frac{1}{\sqrt{N_{\iota k}^\alpha L}} \left[1 + \alpha \frac{v_F k + i\Delta_2 \tanh\left(\frac{\Delta_2}{v_F} z\right)}{\epsilon_{\iota k} - \alpha\Delta_1} \right] e^{ikz} \\ v_{\iota k}^\alpha = \frac{1}{2}\frac{1}{\sqrt{N_{\iota k}^\alpha L}} \left[-\alpha + \frac{v_F k + i\Delta_2 \tanh\left(\frac{\Delta_2}{v_F} z\right)}{\epsilon_{\iota k} - \alpha\Delta_1} \right] e^{ikz} \end{cases}, \tag{4.50}$$
$$\Delta_1 = \Delta_0 \cos\frac{\theta_s}{2}, \quad \Delta_2 = \Delta_0 \sin\frac{\theta_s}{2}, \quad N_{\iota k}^\alpha = \frac{\epsilon_{\iota k}}{\epsilon_{\iota k} - \alpha\Delta_1}.$$

The corresponding eigenvalues are

$$\bar{\epsilon}_{\iota k}^\alpha = \epsilon_{\iota k} - \alpha v_\psi k_F, \ \epsilon_{\iota k} = \iota \epsilon_k, \ \epsilon_k = \sqrt{\Delta_0^2 + v_F^2 k^2}. \tag{4.51}$$

so the band $\iota = +$ corresponds to the excitations defined in Eq. (4.7). The second category is the localized states on the soliton core, labelled only by the left-right moving index α:

$$\begin{pmatrix} u_0^\alpha \\ v_0^\alpha \end{pmatrix} = \frac{1}{2}\sqrt{\frac{\Delta_2}{v_F}} \operatorname{sech}\left(\frac{\Delta_2 z}{v_F}\right) \begin{pmatrix} 1 \\ \alpha \end{pmatrix}, \tag{4.52}$$

and the corresponding eigenvalues are:

$$\bar{\epsilon}_0^\alpha = \epsilon_0^\alpha - \alpha v_\psi k_F, \quad \epsilon_0^\alpha = \alpha \Delta_0 \cos\frac{\theta_s}{2}. \tag{4.53}$$

According to the above expression for the eigenvalues, the localized states corresponding to the dark soliton ($\theta_s = \pi, v_\psi = 0$) are degenerate zero modes, but this degeneracy is an artifact of the linearization in Eq. (4.47), while the correction from the quadratic spectrum up to leading order will lift this degeneracy:

$$\epsilon_0^\alpha = \alpha \sqrt{\Delta_0^2 - \left[\Delta_0 \sin\frac{\theta_s}{2} - \frac{\pi v_F k_F}{2} \operatorname{csch}\left(\frac{\pi l_s k_F}{2}\right)\right]^2}. \tag{4.54}$$

The actual localized states are linear combinations of the left and right moving localized states, so the superscript $\alpha = \pm$ in Eq. (4.54) labels positive and negative modes instead of left and right moving modes.

To complete the construction of the soliton, we still need to satisfy the self-consistent requirement in Eq. (4.45). In the present classification of the eigenmodes, it is expressed as

$$\Delta = \lambda \sum_{\alpha,k} u_{+,k}^\alpha {v_{+,k}^\alpha}^* \left(1 - \sum_\sigma \left\langle \hat{\gamma}_{+,k,\sigma}^{\alpha\dagger} \hat{\gamma}_{+,k,\sigma}^\alpha \right\rangle\right) + \lambda u_0^+ {v_0^+}^* \left(1 - \sum_\sigma \left\langle \hat{\gamma}_{0,\sigma}^{+\dagger} \hat{\gamma}_{0,\sigma}^+ \right\rangle\right) + \tau(i\partial_z \Delta). \tag{4.55}$$

The $S = 1/2$ soliton is obtained by setting $\sum_\sigma \left\langle \hat{\gamma}_{+,k,\sigma}^{\alpha\dagger} \hat{\gamma}_{+,k,\sigma}^\alpha \right\rangle = 0$ and $\sum_\sigma \left\langle \hat{\gamma}_{0,\sigma}^{+\dagger} \hat{\gamma}_{0,\sigma}^+ \right\rangle = 1$, then the above equation reduces to

$$\Delta = \lambda \int \frac{dk}{2\pi} \frac{\Delta}{\epsilon_k} + \frac{\lambda}{4} \frac{\Delta_0}{v_F} \frac{\theta_s - \pi}{\pi} \frac{\sin\frac{\theta_s}{2}}{\cosh^2\left(\frac{\Delta_2}{v_F} z\right)} + \tau(i\partial_z \Delta). \tag{4.56}$$

For the dark soliton, the second part on the righthand side vanishes and we need to set $\tau = 0$, then the resulting equation is exactly the one we have in conventional BCS theory with a homogenous gap parameter:

$$1 = \lambda \int \frac{dk}{2\pi} \frac{1}{\epsilon_k} \Rightarrow \Delta_0 \propto \exp\left(-\frac{1}{\lambda \nu(\epsilon_F)}\right), \tag{4.57}$$

where $\nu(\epsilon_F)$ is the density of states on the Fermi level.

For the moving grey soliton, the second part on the righthand side of Eq. (4.56) has a finite value, but it can be canceled by the third term under the choice that

$$\tau = \frac{\lambda}{4\Delta_0} \frac{\pi - \theta_s}{\pi} \sin^{-1}\frac{\theta_s}{2}, \tag{4.58}$$

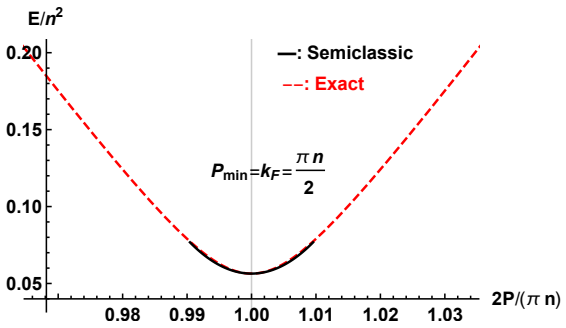

Figure 4.6: The typical $S = 1/2$ excitation spectrum in the semiclassical result and exact solution. The latter is plotted for $\gamma = c_F/n = 1.13$, and correspondingly the former is plotted taking the spin gap at the same coupling strength as the input parameter.

which then determines v_b as

$$v_b = \frac{|t_b|^2}{4\Delta_0}\frac{\theta_s - \pi}{\pi}\sin^{-1}\frac{\theta_s}{2}. \tag{4.59}$$

We can see that determination of parameters τ, v_b in the above equation is consistent with $\tau = 0, v_b = 0$ for $\theta_s = \pi$ in the case of dark soliton.

Having specified the $S = 1/2$ soliton, we can proceed to calculate its energy and momentum near the dark soliton up to leading order in $\xi = \theta_s - \pi$ using the formula in Eq. (4.38) and Eq. (4.7). The calculation consists of first determining the phase shift $\delta(k)$ for the continuous spectrum from the boundary conditions in Eq. (4.37) and then changing the summations over k into integrations while taking into account the correction due to the phase shift $\delta(k)$ in the limit $L \to \infty$ [100, 25]. Also, we need to keep in mind that we should use ϵ_n^α instead of $\bar{\epsilon}_n^\alpha$ in the calculation of energy E. The final result is:

$$E_{1/2}^{\mathrm{BCS}}(\theta_s) = \frac{2\Delta_0}{\pi}\left(1 + \frac{1}{8}\xi^2\right), \quad P_{1/2}^{\mathrm{BCS}}(\theta_s) = k_F - \frac{\Delta_0}{2v_F}\xi. \tag{4.60}$$

This translates into the following dispersion relation and soliton velocity up to leading order in ξ:

$$E_{1/2} = \frac{2\Delta_0}{\pi}\left(1 + \frac{v_F^2(P_{1/2} - k_F)^2}{2\Delta_0^2}\right), \quad v_s^{\mathrm{BCS}} = \frac{\partial E_{1/2}}{\partial P_{1/2}} = -\frac{\xi}{\pi}v_F. \tag{4.61}$$

It is clear that the minimum energy is achieved exactly at the Fermi momentum $k_F = \pi n/2$, as observed in the exact solutions. Also, the soliton velocity now is characterized by the Fermi velocity v_F, which is also consistent with the exact solutions. A comparison of the current semiclassical result with the exact solution is shown in Fig. 4.6, where the agreement is good in the vicinity of the dark soliton.

To complete the analysis, we still need to determine v_ψ and v_b from Eq. (4.42). In order to do that, we need the expressions for P_ψ and P_b respectively:

$$P_b = \frac{\Delta_0^2}{|t_b|^2}(\pi + 2\xi), \quad P_\psi = P_{1/2}^{\mathrm{BCS}}(\theta_s) - P_b. \tag{4.62}$$

Substituting them into Eq. (4.42) and using Eq. (4.59), we obtain up to leading order:

$$v_b = \frac{|t_b|^2}{4\pi\Delta_0}\xi, \quad v_\psi = v_s^{\mathrm{BCS}} - \frac{v_s^{\mathrm{BCS}} - v_b}{1 + |t_b|^2/(4\Delta_0 v_F)} \approx v_s^{\mathrm{BCS}}, \tag{4.63}$$

where the expression for v_ψ will be of use in later section when we analyze the $S = 0$ soliton. This closes our analysis of the $S = 1/2$ soliton on the deep BCS side.

4.4.2 Deep BEC Side

On the BEC side, we tune the resonant level to a tightly bounded molecule with binding energy $\epsilon_b > 0$. Then we have a negative chemical potential $\mu < 0$ characterizing the absence of a Fermi sea, and we need to consider the quadratic Bogoliubov-de Gennes equation in Eq. (4.44). For delocalized states characterized by momentum k, we formally obtain the spectrum of Bogoliubov quasiparticles as:

$$\epsilon_k = \sqrt{(k^2 - \mu)^2 + |\Delta|^2}. \tag{4.64}$$

For large negative chemical potential μ, we can expand the spectrum as

$$\epsilon_k = (k^2 - \mu) + \frac{|\Delta|^2}{2(k^2 - \mu)} - \frac{|\Delta|^4}{8(k^2 - \mu)^3} + \cdots. \tag{4.65}$$

Substituting this into Eq. (4.43), we can bring the equation of motion for $b = \Delta/t_b$ to the following form known as the Gross-Pitaevskii equation:

$$-\frac{1}{2}\partial_z^2 b + iv_b\partial_z b + 2g(|b|^2 - n_s)b = 0, \tag{4.66}$$

where the parameters are defined via

$$g = \frac{3|t_b|^4}{128|\mu|^{5/2}}, \quad n_s = \frac{\frac{|t_b|^2}{4|\mu|^{1/2}} + 2\mu + \epsilon_b}{\frac{3|t_b|^4}{64|\mu|^{5/2}}}. \tag{4.67}$$

The Gross-Pitaevskii equation as a nonlinear Schrödinger equation has been extensively studied

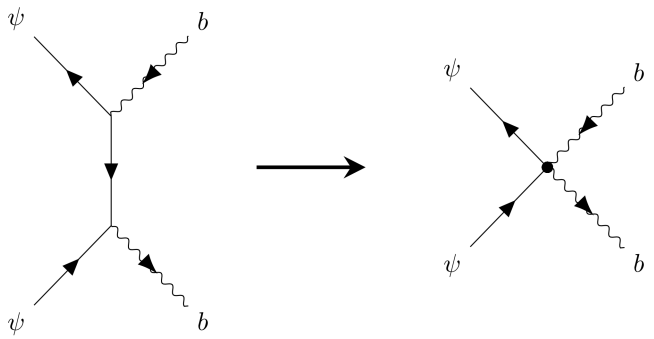

Figure 4.7: The Feynman diagrams (left) for leading contribution to the scattering process $\psi b \to \psi b$ (right), where the solid line denotes the fermion propagator, the wiggled line denotes the boson propagator, the fermion-boson vertex denotes the resonant coupling t_b, and the dotted vertex on the right denotes the effective coupling g'.

in the literature [104, 111, 112, 60, 55]. It also supports a soliton solution:

$$b(z) = \sqrt{n_s}\left(\cos\frac{\theta_s}{2} - i\sin\frac{\theta_s}{2}\tanh\frac{z}{l_s}\right), \tag{4.68}$$

where the size of the soliton is $l_s = [v_c \sin(\theta_s/2)]^{-1}$, the Lagrangian multiplier is $v_b = v_c\cos(\theta_s/2)$ and $v_c = \sqrt{gn}$ is the sound velocity. By calculating the total mass of the system we can also determine $n_s = n/2$.

The $S = 1/2$ soliton is constructed by adding an extra fermion into the system, then we can effectively describe the system as follows: There is a weakly interacting background (the bound pairs) with the effective coupling constant g. The extra fermion added into the system interacts with the background locally by an effective coupling constant g', which can be calculated perturbatively from Eq. (4.5) in the narrow resonance limit. For this purpose, we consider the scattering process $\psi b \to \psi b$, whose Feynman diagrams are shown in Fig. 4.7. The scattering amplitude up to leading order is then

$$g'(\omega, k) = -\frac{|t_b|^2}{\omega - \epsilon_k} \approx \frac{|t_b|^2}{-2\mu} > 0. \tag{4.69}$$

As a result, the added fermion ψ can be described as a quantum particle moving in the potential created by the background:

$$(-\partial_z^2 - \mu + iv_\psi\partial_z)\psi + g'(|b|^2 - n_s)\psi = \bar{\epsilon}\psi, \tag{4.70}$$

where in the second term on the lefthand side, we have adjusted for the interaction of the fermion with the uniform background (the constant term $g'n_s$), since it can be incorporated into the chemical

potential. Performing the gauge transformation $\psi \to \psi e^{iv_\psi z/2}$ which shifts the momentum by $v_\psi/2$, and substituting Eq. (4.68) into Eq. (4.70), we end up with a Schrödinger equation for a particle moving in the Pöschl-Teller potential [84]:

$$-\partial_z^2\psi - \alpha^2\frac{\zeta(\zeta-1)}{\cosh^2\alpha z}\psi = \left(\bar{\epsilon} + \mu + \frac{v_\psi^2}{4}\right)\psi, \tag{4.71}$$

where the two parameter α and $\zeta > 1$ are determined by

$$\alpha = v_c \sin(\theta_s/2), \quad \alpha^2\zeta(\zeta-1) = g' n_s \sin^2(\theta_s/2). \tag{4.72}$$

The Pöschl-Teller potential produces a bound state with the following energy:

$$\bar{\epsilon}_0 = -\alpha^2(\zeta-1)^2 - \frac{v_\psi^2}{4} - \mu = -v_c^2\sin^2\frac{\theta_2}{2}\left(\frac{\sqrt{1+2g'/g}-1}{2}\right)^2 - \frac{v_\psi^2}{4} + |\mu|. \tag{4.73}$$

Also the momentum of this bound state is simply $k_0 = v_\psi/2$, and we can determine the eigenvalue ϵ_0 that contributes to the energy E as

$$\epsilon_0 = \bar{\epsilon}_0 + v_\psi k_0. \tag{4.74}$$

Then the total energy $E_{1/2}(\theta_s)$ and momentum $P_{1/2}(\theta_s)$ of the system can be determined according to Eq. (4.38):

$$\begin{aligned} E_{1/2}^{\mathrm{BEC}}(\theta_s) &= \int dz\ \left(\frac{1}{2}|\partial_z b|^2 + g(|b|^2 - n_s)^2\right) + \epsilon_0 = n_s v_c\left[\frac{4}{3}\sin^3\frac{\theta_s}{2} - 2u\sin^2\frac{\theta_s}{2}\right] + \frac{1}{4}v_\psi^2 + |\mu|, \\ P_{1/2}^{\mathrm{BEC}}(\theta_s) &= \int dz\ \frac{1}{2i}(b^*\partial_z b - b\partial_z b^*) + n_s\theta_s + k_0 = n_s(\theta_s - \sin\theta_s) + \frac{1}{2}v_\psi, \end{aligned} \tag{4.75}$$

where $u = \sqrt{\frac{g}{n}}\left(\frac{\sqrt{1+2g'/g}-1}{2}\right)^2 \gg 1$ in the narrow resonance limit. Thus the minimum of $E_{1/2}^{\mathrm{BEC}}(\theta_s)$ is at $\theta_s = \pi$ with the following minimum energy:

$$E_{1/2}^{\mathrm{BEC}}(\theta_s = \pi) - |\mu| = n_s v_c\left(\frac{4}{3} - 2u\right) < 0, \tag{4.76}$$

so $E_{1/2}^{\mathrm{BEC}}(\theta_s = \pi)$ is lower than the energy of adding one particle with zero momentum to the uniform background of bound pairs. Again, we arrive at the conclusion that the minimum energy is achieved exactly at the Fermi momentum $k_F = \pi n_s = \pi n/2$.

We are then left with the determination of the velocities v_ψ, v_s in addition to $v_b = v_c\cos(\theta_s/2)$,

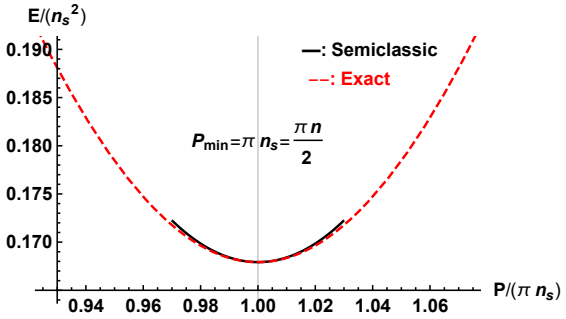

Figure 4.8: The typical $S = 1/2$ excitation spectrum in the semiclassical result and the exact solution. The former is plotted for $\gamma = g/n = 0.07$, and correspondingly the latter is plotted for $\delta\gamma = \gamma_1 - \gamma_2 = 0.07$.

which should be obtained by solving Eq. (4.41). Here the trivial solution will do the work:

$$v_\psi = v_b = v_s^{\rm BEC} = v_c \cos\frac{\theta_s}{2}. \tag{4.77}$$

A comparison of the current semiclassical result and the exact solution is shown in Fig. 4.8, they agree well in the vicinity of $P = k_F$.

In between the deep BCS and BEC sides, the physical picture of the $S = 1/2$ excitations remain the same - they are moving solitons with one extra fermion bounded on the soliton core (see Fig. 4.9). This explains what we observed in exact solutions: instead of adding one particle on the uniform background, the more energy-favorable excitation is the addition of one particle on the dark soliton. The energy cost in the creation of the dark soliton is offset by the energy gain of trapping the particle inside the dip of the density profile. The fact that the minimum energy is achieved exactly at the Fermi momentum is then a consequence of the soliton formation.

Figure 4.9: The physical picture of the $S = 1/2$ excitations along the BCS-BEC crossover - they are one extra spin trapped in the density dip produced by the dark or grey soliton configuration.

4.5 Theory of $S = 0$ Soliton

In this section, we apply the general formalism to the $S = 0$ soliton, where we will find a crossover between the two weak coupling limits of the soliton structure.

4.5.1 Deep BEC Side

The analysis on the deep BEC side is simpler, since we have only the Gross-Pitaevskii equation for the classic field $b(z)$ presented in Eq. (4.66), and we don't need to worry about the self-consistency requirement as in Eq. (4.45). In fact, from Eq. (4.66) we can reconstruct the low energy effective Hamiltonian as

$$\hat{\mathcal{H}} = \int dz \left[\frac{1}{2} \partial_z \hat{b}^\dagger \partial_z \hat{b} + g \hat{b}^\dagger \hat{b}^\dagger \hat{b} \hat{b} \right], \tag{4.78}$$

with is just the Lieb-Liniger model defined in Eq. (3.2) but with the mass $m_b = 1$. As mentioned previously, the fact that $S = 0$ (type-II) excitations of the Lieb-Liniger model have the physical interpretation as moving solitons is well understood [60, 55]. The energy and momentum can be calculated directly using the soliton profile in Eq. (4.68):

$$\begin{aligned} E_0^{\mathrm{BEC}}(\theta_s) &= \int dz \ \left(\frac{1}{2} |\partial_z b|^2 + g(|b|^2 - n_s)^2 \right) = \frac{4}{3} n_s v_c \sin^3 \frac{\theta_s}{2} \\ P_0^{\mathrm{BEC}}(\theta_s) &= \int dz \ \frac{1}{2i} (b^* \partial_z b - b \partial_z b^*) + n_s \theta_s = n_s (\theta_s - \sin \theta_s), \end{aligned} \tag{4.79}$$

then the soliton velocity is determined as $v_s^{\mathrm{BEC}} = \partial E_0 / \partial P_0 = v_c \cos(\theta_s/2)$, which is consistent with the result in Eq. (4.77). A comparison of the semiclassical result with the exact solution is shown in Fig. 4.10, where in the weak coupling limit, we will obtain a next to perfect match [60].

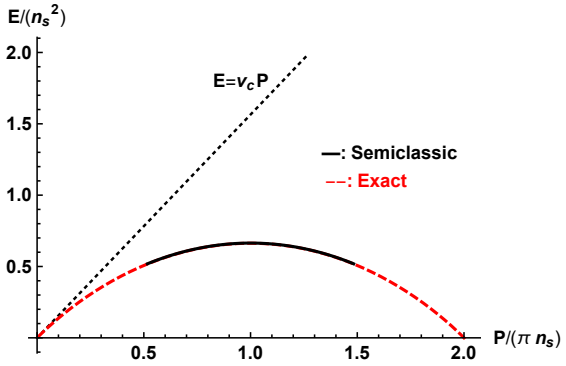

Figure 4.10: The typical $S = 0$ excitation spectrum in the semiclassical result and the exact solution, The former is plotted for $\gamma = g/n = 0.06$, and correspondingly the latter is plotted for $\delta\gamma = \gamma_1 - \gamma_2 = 0.06$.

4.5.2 Deep BCS Side

Now we move on to the deep BCS side, where the situation is complicated by the requirement of the self-consistent condition in Eq. (4.55). The $S = 0$ soliton is obtained by setting $\sum_\sigma \left\langle \hat{\gamma}^{\alpha\dagger}_{+,k,\sigma} \hat{\gamma}^{\alpha}_{+,k,\sigma} \right\rangle = 0$

and $\sum_\sigma \left\langle \hat{\gamma}^{+\dagger}_{0,\sigma}\gamma^{+}_{0,\sigma}\right\rangle = 0$, then Eq. (4.55) reduces to

$$\Delta = \lambda \int \frac{dk}{2\pi}\frac{\Delta}{\epsilon_k} + \frac{\lambda}{4}\frac{\Delta_0}{v_F}\frac{\theta_s}{\pi}\frac{\sin\frac{\theta_s}{2}}{\cosh^2\left(\frac{\Delta_2}{v_F}z\right)} + \tau(i\partial_z\Delta). \tag{4.80}$$

Compared with Eq. (4.56) for the $S = 1/2$ soliton, the self-consistent equation here differs in the second term on the righthand side: it is now proportional to θ_s instead of $(\theta_s - \pi)$ as in Eq. (4.56). Since the dark soliton corresponds to the parameterization that $\theta_s = \pi$ and $\tau = 0$, this means that we cannot fulfill the self-consistent equation for the $S = 0$ soliton thus constructed, and the ground state of $\hat{\mathcal{H}}_\psi$ in Eq. (4.7) does not correspond to a proper $S = 0$ excitation, as mentioned in Sec. 4.3.

A solution of the above problem was conjectured by [25] and consisted in the assumption that both negative and positive energy localized states are occupied with fractional occupation number. We found this solution to be incorrect for the following reasons: (1) Only positive energy states of the BCS Hamiltonian are meaningful and including the negative energy ones, in fact, describes the same states by different variables; (2) Even if this mistake is rectified, the fractional occupation of the localized state is forbidden on the mean field level as this state is not connected to the continuum (unlike Fano resonance); (3) It gives the value of the energy and of the curvature at $P = k_F$ inconsistent with the exact solution [95].

Here, inspired by the fact that the maximum energy is on the scale of the Fermi energy, we propose that the proper construction of a $S = 0$ soliton is as follows. We break the weakly bounded pair at the bottom of the Fermi sea, which leaves us with two fermions. We then put one of them on the localized level to produce a $S = 1/2$ soliton. This is possible because the breaking of the bound pair at the bottom of the Fermi sea has no effect on the linearized spectrum. After that, we can form a singlet from the other fermion and the $S = 1/2$ soliton, which gives us the desired $S = 0$ soliton. To carry out such a construction, we need to go beyond the present mean field analysis and include the Fock potential produced by the spin density on fermion of the opposite spin (see Fig. 4.11). Hartree potential is not considered here since it is not sensitive to spin.

By including the Fock potential, the equation of motion for the fermionic fields is modified as:

$$\begin{pmatrix} -i\alpha v_F\partial_z - \alpha v_\psi k_F & \Delta(z) \\ \Delta^*(z) & i\alpha v_F\partial_z - \alpha v_\psi k_F \end{pmatrix}\begin{pmatrix} u^\alpha_n \\ v^\alpha_n \end{pmatrix} + \begin{pmatrix} -V_{\rm F} & 0 \\ 0 & V_{\rm F} \end{pmatrix}\begin{pmatrix} u^\alpha_n \\ v^\alpha_n \end{pmatrix} = \bar{\epsilon}^\alpha_n \begin{pmatrix} u^\alpha_n \\ v^\alpha_n \end{pmatrix}. \tag{4.81}$$

The Fock potential is $V_{\rm F} = \frac{\lambda}{2}\frac{\Delta_2}{v_F}\mathrm{sech}^2\left(\frac{\Delta_2}{v_F}\right)$, where we have incorporated the constant part $\lambda n/2$ of V_F into the chemical potential. Also from Eq. (4.63) we have $v_\psi \approx v_s^{\rm BCS}$. The first term in $V_{\rm F}$

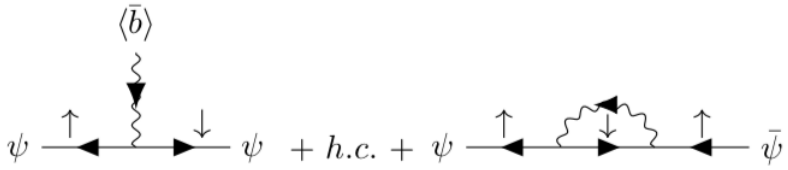

Figure 4.11: The diagrammatic representation of the mean field potential (left) and the Fock potential (right) experienced by fermions. The solid line denotes the fermion propagator, the wiggled line denotes the boson propagator, and the fermion-boson vertex denotes the resonant coupling t_b. The thin arrow on the fermion propagator denotes the spin direction of the fermion.

comes from the fermions in the continuous spectrum and the second term comes from the fermion in the localized state. For states with momentum near k_F, the Fock potential $V_{\rm F}$ only acts as a small correction to the chemical potential, while for states near zero momentum, $V_{\rm F}$ has a more dramatic effect of producing an extra localized state. In the latter case, we can ignore the small off-diagonal components in Eq. (4.81), and the hole excitation near zero momentum is described by the Schrödinger equation without linearization:

$$\left(\partial_z^2 + \mu + iv_\psi \partial_z\right)\psi(z) + V_{\rm F}\psi(z) = \bar{\epsilon}\psi(z). \tag{4.82}$$

As usual, we perform the gauge transformation that $\psi(z) \to \psi(z)e^{-iv_\psi z/2}$ with a shift in momentum as $-v_\psi/2$, and again we are led to the Schrödinger equation for a particle moving in Pöschl-Teller potential:

$$-\partial_z^2\psi - \alpha^2\zeta(\zeta-1)\mathrm{sech}^2\left(\alpha z\right)\psi = \left(-\bar{\epsilon} + \mu + \frac{v_\psi^2}{4}\right)\psi, \tag{4.83}$$

where $\alpha = \frac{\Delta_2}{v_F}$, $\alpha^2\zeta(\zeta-1) = \frac{\lambda\Delta_2}{2v_F}$. This produces a bound hole state with energy

$$\bar{\epsilon}_1 = \frac{\Delta_0^3}{32\lambda v_F^3}\left(1 - \frac{3}{8}\xi^2\right) + \mu + \frac{v_\psi^2}{4}. \tag{4.84}$$

Also the momentum of this bound hole state is simply $k_1 = -v_\psi/2$, and we can determine the eigenvalue ϵ_1 that contributes to the energy E as

$$\epsilon_1 = \bar{\epsilon}_1 + v_\psi k_1. \tag{4.85}$$

This localized state then combines with the $S = 1/2$ soliton to form a singlet, which is the desired $S = 0$ soliton (see Fig. 4.12).

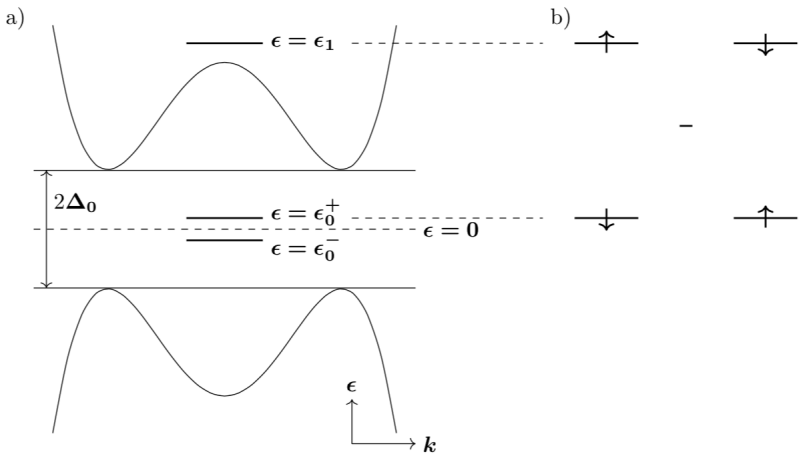

Figure 4.12: a) The spectrum in the Fock approximation, where $\epsilon_0^{\pm}$ represents the two localized states in Eq. (4.54). They are linear combinations of the left and right moving localized states in Eq. (4.52) and Eq. (4.53) once nonlinear effects are taken into consideration. ϵ_1 represents the extra localized state produced by the Fock potential. b) The configuration of the $S = 0$ soliton, which is formed as a singlet of the two localized states with energies ϵ_1 and ϵ_0^+.

We can now determine the energy and the momentum of the $S = 0$ soliton as

$$\begin{aligned} E_0^{\rm BCS}(\theta_s) &= E_{1/2}^{\rm BCS}(\theta_s) + \epsilon_1 = E_0 + \left(\frac{\Delta_0}{4\pi} - \frac{3}{8}\frac{\Delta_0^3}{32\lambda v_F^3} - \frac{v_F^2}{4\pi^2}\right)\xi^2, \\ E_0 &= \frac{2\Delta_0}{\pi} + \mu + \frac{\Delta_0^3}{32\lambda v_F^3}, \\ P_0^{\rm BCS}(\theta_s) &= P_{1/2}^{\rm BCS}(\theta_s) + k_1 = k_F + \left(\frac{v_F}{2\pi} - \frac{\Delta_0}{2v_F}\right)\xi \end{aligned} \tag{4.86}$$

where we have used the expression for $v_\psi \approx v_s^{\rm BCS}$ in Eq. (4.61). In the weak coupling limit, we have $v_F^2 \gg \Delta_0$, then the energy does conform to what we observed in exact solutions that it is on the scale of the Fermi energy $\mu = \epsilon_F$, and the dispersion of the $S = 0$ soliton can be approximated as

$$E_0(P_0) \approx E_0 - (P_0 - k_F)^2. \tag{4.87}$$

which agrees with the exact solutions and reduces to the noninteracting fermion result. A comparison of the current semiclassical result with the exact solution is shown in Fig. 4.13, where the former grasps the basic features of the latter.

4.5.3 Crossover Problem

Here we argue that the crossover region of the $S = 0$ soliton is not described by a simple mean field configuration but rather by the linear combination of the states considered in Sec. 4.5.1 and Sec.

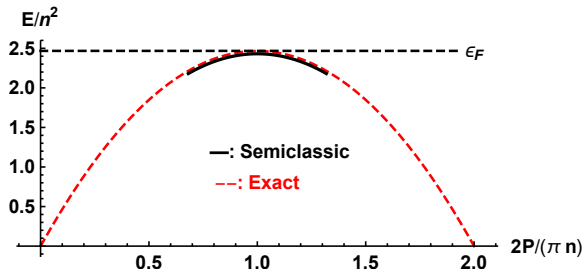

Figure 4.13: The typical $S = 0$ excitation spectrum in the semiclassical result and the exact solution. The latter is plotted for $\gamma = c_F/n = 0.15$, and correspondingly the former is plotted taking the spin gap at the same coupling strength as the input parameter.

4.5.2.

Unlike the $S = 1/2$ soliton, the $S = 0$ soliton on the BEC side and BCS side have different natures. The former is just the usual soliton formed in the condensed bound pairs, while the latter is a singlet formed by two localized spins (one is trapped by the Fock potential of the other, see Fig. 4.14 for an illustration). We refer to the latter as a dressed soliton. The dressed soliton can tunnel into the usual soliton configuration since the state localized by the Fock potential lies in the continuous spectrum (see Fig. 4.12). On the deep BCS side, the tunneling is negligible. When we tune the resonant level to leave the deep BCS side, the tunneling between the dressed soliton and the usual soliton becomes stronger, and the physical soliton will be a linear combination of them. Till on the deep BEC side, the usual soliton dominates. The two localized spins we have on the BCS side then bound together to become one of the bound pairs on the BEC side. There is no abrupt change happening in the soliton formation along the crossover, just as what we have observed in the excitation spectra of the exactly solvable models.

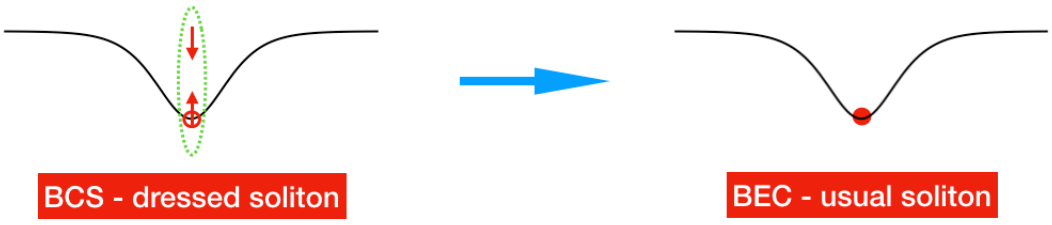

Figure 4.14: The physical picture of the $S = 0$ excitations on the BCS side and BEC side. They have different natures on different sides - on the BCS side, it is a singlet formed by two localized spins; on the BEC side, it is the usual soliton formed in the condensed bound pairs. Along the crossover from BCS side to the BEC side, the singlet becomes more and more tightly bounded, and eventually evolves into the condensate.

The above qualitative argument can be made more rigorous by analyzing the tunneling of the state localized by the Fock potential into the quasiparticle continuum. The desired analysis is performed

for Eq. (4.81) in the regime where the chemical potential μ is the largest energy scale near the BCS side, so the off-diagonal part can be treated perturbatively. We have both electron-like eigenstate $|\Psi^e\rangle$ and hole-like eigenstates $\left|\Psi^h\right\rangle$ at zeroth-order, and in each sector we will get a localized state $\left|\Psi_0^{e,h}\right\rangle$. Here we focus on the state $\left|\Psi_0^h\right\rangle$ with energy ϵ_0^h on the scale of μ, which will tunnel into the continuum of the electron-like state $|\Psi_k^e\rangle$ as the off-diagonal perturbation sets in. The resonance width due to this tunneling can be calculated using the Fermi golden rule:

$$\Gamma = 2\pi\nu_{\uparrow,\downarrow}(2\epsilon_F)|\mathcal{M}|^2 = \frac{1}{\sqrt{2}v_F}|\mathcal{M}|^2, \tag{4.88}$$

where we have taken the density of states $\nu_{\uparrow,\downarrow}(\epsilon) = \nu(\epsilon)/2$ for each spin to be the one at $2\epsilon_F$ since the localized level is close to the chemical potential μ, and $\mathcal{M} = \langle\Psi_k^e| \begin{pmatrix} 0 & \Delta \\ \Delta^* & 0 \end{pmatrix} \left|\Psi_0^h\right\rangle$ is the matrix element between the continuum and the localized state. It can be estimated by the Fourier component $\tilde{\Delta}(\sqrt{2}k_F)$ of the soliton profile, normalized by the size of the soliton:

$$|\mathcal{M}|^2 = \frac{1}{l_s}|\tilde{\Delta}(\sqrt{2}k_F)|^2 = \frac{\Delta_0^2 l_s \pi^2 \sin^2\frac{\theta_s}{2}}{\sinh^2\left(\frac{l_s\pi k_F}{\sqrt{2}}\right)}. \tag{4.89}$$

In the end we obtain the following result for the resonance width near the BCS side:

$$\Gamma = \frac{\Delta_0^2 l_s \pi^2 \sin^2\frac{\theta_s}{2}}{\sqrt{2}v_F \sinh^2\left(\frac{l_s\pi k_F}{\sqrt{2}}\right)}. \tag{4.90}$$

For the large chemical potential near the BCS side, the ratio between the resonance width Γ and the energy ϵ_0^h is exponentially small and the localized state remains well-defined. This is equivalent to the statement that the tunneling to the usual soliton is negligible. As we tune the system away from the BCS side, up to the point where the chemical potential is comparable to the gap parameter Δ_0, the velocity of the particle and the Fermi momentum are also tuned to be on the order of magnitude comparable to Δ_0. At that point, the resonance width Γ becomes comparable to the energy ϵ_0^h. With further tuning toward the BEC side, we then encounter a large resonance width $\Gamma \gg \epsilon_0^h$, and the localized state ceases to be well defined and merges into the quasiparticle continuum. Correspondingly, we have the spin-singlet described on the BCS side develop into a normal bound pair on the BEC side. As a result, we have a smooth crossover from the soliton of BCS type into the one of BEC type.

4.6 Conclusion

In this chapter, we developed a semiclassical theory of moving solitons in one dimensional BCS-BEC crossover, where on both the deep BCS and deep BEC side, our results grasp the essential features of the exact solutions. Our theory also resolves the inconsistency between the semiclassical analysis and the exact solutions in the attractive Yang-Gaudin model. In the meantime, we revealed the mechanism of a striking phenomenon discussed in the previous chapter that the minimum energy of the spin excitation is fixed at the Fermi momentum along the whole range of BCS-BEC crossover in one dimension. Conventionally in higher dimensions, we would expect this momentum to be shifted from k_F on the BCS side to zero somewhere on the way to the BEC side, and it is believed that this is the only sharp change that could happen in a BCS-BEC crossover [76]. We then show that the counterintuitive fixing comes about as a special feature of the one dimensional systems, that the conventional quasiparticle is not stable with respect to soliton formation. Our theory serves as yet another example of the important role solitons can play in low dimensional physical systems, in addition to those well established in one dimensional lattice models [97, 100] and charge density waves [10, 11].

Bibliography

[1] S. K. Adhikari. Quantum scattering in two dimensions. *American Journal of Physics*, 54(4):362–367, 1986. 6

[2] I. Affleck. On constrained instantons. *Nuclear Physics B*, 191(2):429 – 444, 1981. 82

[3] R. P. Anderson, C. Ticknor, A. I. Sidorov, and B. V. Hall. Spatially inhomogeneous phase evolution of a two-component bose-einstein condensate. *Phys. Rev. A*, 80:023603, Aug 2009. 30

[4] N. Andrei and C. Destri. Solution of the multichannel kondo problem. *Phys. Rev. Lett.*, 52:364–367, Jan 1984. 41

[5] P. Bedaque, H.-W. Hammer, and U. van Kolck. The three-boson system with short-range interactions. *Nuclear Physics A*, 646(4):444 – 466, 1999. 5

[6] F. F. Bellotti, T. Frederico, M. T. Yamashita, D. V. Fedorov, A. S. Jensen, and N. T. Zinner. Scaling and universality in two dimensions: three-body bound states with short-ranged interactions. *Journal of Physics B: Atomic, Molecular and Optical Physics*, 44(20):205302, 2011. 5, 23, 28

[7] F. F. Bellotti, T. Frederico, M. T. Yamashita, D. V. Fedorov, A. S. Jensen, and N. T. Zinner. Supercircle description of universal three-body states in two dimensions. *Phys. Rev. A*, 85:025601, Feb 2012. 5, 23, 28

[8] F. F. Bellotti, T. Frederico, M. T. Yamashita, D. V. Fedorov, A. S. Jensen, and N. T. Zinner. Mass-imbalanced three-body systems in two dimensions. *Journal of Physics B: Atomic, Molecular and Optical Physics*, 46(5):055301, 2013. 5, 23, 28

[9] E. Braaten and H.-W. Hammer. Universality in few-body systems with large scattering length. *Physics Reports*, 428(56):259 – 390, 2006. 5

[10] S. Brazovskii. *Solitons in Crystals of Charge Density Waves*, pages 425–446. North-Holland, Dec. 1989. 85, 98

[11] S. A. Brazovskiĭ. Self-localized excitations in the Peierls-Fröhlich state. *Soviet Journal of Experimental and Theoretical Physics*, 51:342, Feb. 1980. 85, 98

[12] I. V. Brodsky, M. Y. Kagan, A. V. Klaptsov, R. Combescot, and X. Leyronas. Exact diagrammatic approach for dimer-dimer scattering and bound states of three and four resonantly interacting particles. *Phys. Rev. A*, 73:032724, Mar 2006. 5, 23, 28

[13] L. W. Bruch and J. A. Tjon. Binding of three identical bosons in two dimensions. *Phys. Rev. A*, 19:425–432, Feb 1979. 5, 28

[14] F. Cabral and L. W. Bruch. Trimer binding in two dimensions. *The Journal of Chemical Physics*, 70(10):4669–4672, 1979. 5

[15] S. Charbonneau, T. Steiner, M. L. W. Thewalt, E. S. Koteles, J. Y. Chi, and B. Elman. Optical investigation of biexcitons and bound excitons in gaas quantum wells. *Phys. Rev. B*, 38:3583–3586, Aug 1988. 5

[16] C. Chin, R. Grimm, P. Julienne, and E. Tiesinga. Feshbach resonances in ultracold gases. *Rev. Mod. Phys.*, 82:1225–1286, Apr 2010. 30

[17] G. S. Danilov. On the three-body problem with short-range forces. *Sov. Phys. JETP*, 13:349, 1961. 4

[18] H. Deng, H. Haug, and Y. Yamamoto. Exciton-polariton bose-einstein condensation. *Rev. Mod. Phys.*, 82:1489–1537, May 2010. 5

[19] H. Deng, G. Weihs, C. Santori, J. Bloch, and Y. Yamamoto. Condensation of semiconductor microcavity exciton polaritons. *Science*, 298(5591):199–202, 2002. 5

[20] J. P. D'Incao, F. Anis, and B. D. Esry. Ultracold three-body recombination in two dimensions. *Phys. Rev. A*, 91:062710, Jun 2015. 7

[21] J. P. D'Incao and B. D. Esry. Adiabatic hyperspherical representation for the three-body problem in two dimensions. *Phys. Rev. A*, 90:042707, Oct 2014. 7, 16

[22] S.-H. Dong. *Wave Equations in Higher Dimensions*. Springer, 1 edition, 2011. 7

[23] L.-M. Duan, E. Demler, and M. D. Lukin. Controlling spin exchange interactions of ultracold atoms in optical lattices. *Phys. Rev. Lett.*, 91:090402, Aug 2003. 30

[24] A. R. Edmonds. *Angular Momentum in Quantum Mechanics*. Princeton University Press, 1996. 7

[25] D. K. Efimkin and V. Galitski. Moving solitons in a one-dimensional fermionic superfluid. *Phys. Rev. A*, 91:023616, Feb 2015. 69, 70, 72, 87, 93

[26] V. Efimov. Energy levels arising from resonant two-body forces in a three-body system. *Physics Letters B*, 33(8):563 – 564, 1970. 1, 4

[27] V. Efimov. Weakly-bound states of three resonantly interacting particles. *Sov.J.Nucl.Phys.*, 12, May 1971. 1, 4

[28] M. Erhard, H. Schmaljohann, J. Kronjäger, K. Bongs, and K. Sengstock. Measurement of a mixed-spin-channel feshbach resonance in ^{87}Rb. *Phys. Rev. A*, 69:032705, Mar 2004. 30

[29] L. D. Faddeev. *Mathematical Aspects of the Three-Body Problem in the Quantum Scattering Theory*. Israel Program for Scientific Translations, 1965. 7

[30] L. D. Faddeev and L. Takhtajan. *Hamiltonian Methods in the Theory of Solitons*. Springer-Verlag, Berlin, 1987. 85

[31] H. S. Friedrich. *Theoretical Atomic Physics*. Springer Science and Business Media, 3 edition, 2005. 14, 22

[32] J. N. Fuchs, A. Recati, and W. Zwerger. Exactly solvable model of the bcs-bec crossover. *Phys. Rev. Lett.*, 93:090408, Aug 2004. 32, 52, 55

[33] P. Fulde and R. A. Ferrell. Superconductivity in a strong spin-exchange field. *Phys. Rev.*, 135:A550–A563, Aug 1964. 31

[34] B. Ganchev, N. Drummond, I. Aleiner, and V. Fal'ko. Three-particle complexes in two-dimensional semiconductors. *Phys. Rev. Lett.*, 114:107401, Mar 2015. 5, 11

[35] M. Gaudin. Un systeme a une dimension de fermions en interaction. *Physics Letters A*, 24(1):55 – 56, 1967. 31, 32, 66

[36] M. Gaudin. *The Bethe Wavefunction*. Cambridge University Press, 2014. 49

[37] L. S. Gradstein and I. M. Ryzhik. *Tables of Integrals, Series and Products.* Academic Press, 6 edition, 2000. 17, 24, 26, 27

[38] S.-J. Gu, Y.-Q. Li, Z.-J. Ying, and X.-A. Zhao. Thermodynamics of two component bosons in one dimension. *International Journal of Modern Physics B*, 16(14n15):2137–2143, 2002. 31

[39] X. W. Guan, M. T. Batchelor, and C. Lee. Fermi gases in one dimension: From bethe ansatz to experiments. *Rev. Mod. Phys.*, 85:1633–1691, Nov 2013. 32, 69, 72

[40] X. W. Guan, M. T. Batchelor, C. Lee, and M. Bortz. Phase transitions and pairing signature in strongly attractive fermi atomic gases. *Phys. Rev. B*, 76:085120, Aug 2007. 60, 62

[41] X. W. Guan and T. L. Ho. Quantum criticality of a one-dimensional attractive fermi gas. *Phys. Rev. A*, 84:023616, Aug 2011. 60

[42] V. Gurarie. One-dimensional gas of bosons with feshbach-resonant interactions. *Phys. Rev. A*, 73:033612, Mar 2006. 31, 33, 41

[43] F. D. M. Haldane. Luttinger liquid theory of one-dimensional quantum fluids. i. properties of the luttinger model and their extension to the general 1d interacting spinless fermi gas. *Journal of Physics C: Solid State Physics*, 14(19):2585–2609, Jul 1981. 1

[44] E. Haller, M. Gustavsson, M. J. Mark, J. G. Danzl, R. Hart, G. Pupillo, and H.-C. Nägerl. Realization of an excited, strongly correlated quantum gas phase. *Science*, 325(5945):1224–1227, 2009. 30

[45] H.-W. Hammer and L. Platter. Efimov physics from a renormalization group perspective. *Phil. Trans. Roy. Soc. Lond.*, A369:2679, 2011. 5

[46] P. C. Hohenberg. Existence of long-range order in one and two dimensions. *Phys. Rev.*, 158:383–386, Jun 1967. 1

[47] H. Hu, X.-J. Liu, and P. D. Drummond. Phase diagram of a strongly interacting polarized fermi gas in one dimension. *Phys. Rev. Lett.*, 98:070403, Feb 2007. 60

[48] L. Hultén. *Ark. Mat. Astron. Fys. B.*, 26A:1, 1938. 38

[49] V. Hutson. The circular plate condenser at small separations. *Mathematical Proceedings of the Cambridge Philosophical Society*, 59(1):211–224, 1963. 49

[50] T. Iida and M. Wadati. Exact analysis of δ-function attractive fermions and repulsive bosons in one-dimension. *Journal of the Physical Society of Japan*, 74(6):1724–1736, 2005. 49

[51] A. Imambekov, A. A. Lukyanov, L. I. Glazman, and V. Gritsev. Exact solution for 1d spin-polarized fermions with resonant interactions. *Phys. Rev. Lett.*, 104:040402, Jan 2010. 33, 41

[52] M. Iskin. Dimer-atom scattering between two identical fermions and a third particle. *Phys. Rev. A*, 81:043634, Apr 2010. 28

[53] O. I. Kartavtsev and A. V. Malykh. Universal low-energy properties of three two-dimensional bosons. *Phys. Rev. A*, 74:042506, Oct 2006. 7

[54] J. Kasprzak et al. *Nature*, 443:409–414, Sep 2006. 5

[55] M. Khodas, A. Kamenev, and L. I. Glazman. Photosolitonic effect. *Phys. Rev. A*, 78:053630, Nov 2008. 71, 89, 92

[56] T. Kinoshita, T. Wenger, and D. S. Weiss. Observation of a one-dimensional tonks-girardeau gas. *Science*, 305(5687):1125–1128, 2004. 30

[57] A. Klauser and J.-S. Caux. Equilibrium thermodynamic properties of interacting two-component bosons in one dimension. *Phys. Rev. A*, 84:033604, Sep 2011. 31

[58] V. E. Korepin, N. M. Bogoliubov, and A. G. Izergin. *Quantum Inverse Scattering Method and Correlation Functions*. Cambridge University Press, UK, 1993. 31, 35, 36, 37, 39, 46, 53

[59] V. Y. Krivnov and A. A. Ovchinnikov. One-dimensional Fermi gas with attraction between the electrons. *Soviet Journal of Experimental and Theoretical Physics*, 40:781, Oct. 1975. 52, 55, 59

[60] P. P. Kulish, S. V. Manakov, and L. D. Faddeev. Comparison of the Exact Quantum and Quasiclassical Results for the Nonlinear Schrodinger Equation. *Theor. Math. Phys.*, 28:615–620, 1976. [Teor. Mat. Fiz.28,38(1976)]. 69, 71, 89, 92

[61] L. D. Landau and L. M. Lifshitz. *Quantum Mechanics: Non-Relativistic Theory*, volume 3. Butterworth-Heinemann, 3 edition, 1981. 6

[62] A. I. Larkin and Y. N. Ovchinnikov. Nonuniform state of superconductors. *Zh. Eksp. Teor. Fiz.*, 47:1136–1146, Sep 1964. 31

[63] J. Levinsen and V. Gurarie. Properties of strongly paired fermionic condensates. *Phys. Rev. A*, 73:053607, May 2006. 28

[64] J. Levinsen, P. Massignan, and M. M. Parish. Efimov trimers under strong confinement. *Phys. Rev. X*, 4:031020, Jul 2014. 28

[65] Y.-A. Liao, A. S. C. Rittner, T. Paprotta, W. Li, G. B. Partridge, R. G. Hulet, S. K. Baur, and E. J. Mueller. Spin-imbalance in a one-dimensional fermi gas. *Nature*, 467(7315):567–569, 09 2010. 30

[66] E. H. Lieb. Exact analysis of an interacting bose gas. ii. the excitation spectrum. *Phys. Rev.*, 130:1616–1624, May 1963. 30, 32, 53, 55, 69

[67] E. H. Lieb and W. Liniger. Exact analysis of an interacting bose gas. i. the general solution and the ground state. *Phys. Rev.*, 130:1605–1616, May 1963. 30, 32, 49, 52, 65, 69

[68] Q.-G. Lin. Levinson theorem in two-dimensions. *Phys. Rev.*, A56:1938–1944, 1997. 14, 22

[69] MATLAB. *version 9.0.0 (R2016a)*. The MathWorks Inc., Natick, Massachusetts, 2016. 22

[70] N. D. Mermin and H. Wagner. Absence of ferromagnetism or antiferromagnetism in one- or two-dimensional isotropic heisenberg models. *Phys. Rev. Lett.*, 17:1133–1136, Nov 1966. 1

[71] K. M. Mertes, J. W. Merrill, R. Carretero-González, D. J. Frantzeskakis, P. G. Kevrekidis, and D. S. Hall. Nonequilibrium dynamics and superfluid ring excitations in binary bose-einstein condensates. *Phys. Rev. Lett.*, 99:190402, Nov 2007. 30

[72] R. Miller and D. Kleinman. Excitons in gaas quantum wells. *Journal of Luminescence*, 30(1):520 – 540, 1985. 5

[73] R. C. Miller, D. A. Kleinman, A. C. Gossard, and O. Munteanu. Biexcitons in gaas quantum wells. *Phys. Rev. B*, 25:6545–6547, May 1982. 5

[74] H. Moritz, T. Stöferle, M. Köhl, and T. Esslinger. Exciting collective oscillations in a trapped 1d gas. *Phys. Rev. Lett.*, 91:250402, Dec 2003. 30

[75] G. Orso. Attractive fermi gases with unequal spin populations in highly elongated traps. *Phys. Rev. Lett.*, 98:070402, Feb 2007. 60

[76] M. M. Parish. *The BCS-BEC Crossover*, pages 179–197. World Scientific Publishing Co, Sept. 2015. 53, 70, 72, 74, 98

[77] F. M. Pen'kov and W. Sandhas. Differential form of the skornyakov ter-martirosyan equations. *Phys. Rev. A*, 72:060702, Dec 2005. 29

[78] D. S. Petrov. Three-body problem in fermi gases with short-range interparticle interaction. *Phys. Rev. A*, 67:010703, Jan 2003. 28

[79] D. S. Petrov. Quantum mechanical stabilization of a collapsing bose-bose mixture. *Phys. Rev. Lett.*, 115:155302, Oct 2015. 6

[80] D. S. Petrov and G. E. Astrakharchik. Ultradilute low-dimensional liquids. *Phys. Rev. Lett.*, 117:100401, Sep 2016. 6

[81] D. S. Petrov, C. Salomon, and G. V. Shlyapnikov. Weakly bound dimers of fermionic atoms. *Phys. Rev. Lett.*, 93:090404, Aug 2004. 28

[82] D. S. Petrov and G. V. Shlyapnikov. Interatomic collisions in a tightly confined bose gas. *Phys. Rev. A*, 64:012706, Jun 2001. 6

[83] L. Pollet, S. M. A. Rombouts, and P. J. H. Denteneer. Ultracold atoms in one-dimensional optical lattices approaching the tonks-girardeau regime. *Phys. Rev. Lett.*, 93:210401, Nov 2004. 30

[84] G. Pöschl and E. Teller. Bemerkungen zur quantenmechanik des anharmonischen oszillators. *Zeitschrift für Physik*, 83(3):143–151, Mar 1933. 90

[85] A. Prem and V. Gurarie. One-dimensional model of chiral fermions with feshbach resonant interactions. *Journal of Statistical Mechanics: Theory and Experiment*, 2018(2):023111, 2018. 33

[86] S. Rahbar and E. Hashemizadeh. A computational approach to the fredholm integral equation of the second kind. *Proceedings of the World Congress on Engineering*, 2, 2008. 46

[87] T. Ren and I. Aleiner. Three-boson bound states in two dimensions. *Phys. Rev. B*, 95:045401, Jan 2017. 6

[88] T. Ren and I. Aleiner. Bethe-ansatz analysis of near-resonant two-component systems in one dimension. *Phys. Rev. A*, 99:023611, Feb 2019. 30, 71

[89] T. Ren and I. Aleiner. Solitons in one-dimensional systems at the bcs-bec crossover. *Phys. Rev. A*, 99:013626, Jan 2019. 59

[90] S. T. Rittenhouse, N. P. Mehta, and C. H. Greene. Green's functions and the adiabatic hyperspherical method. *Phys. Rev. A*, 82:022706, Aug 2010. 7, 16

[91] S. Rudin. One-dimensional backward-scattering fermion model with built-in cutoff. *Phys. Rev. B*, 28:4825–4828, Oct 1983. 41

[92] P. Schlottmann. Thermodynamics of the one-dimensional multicomponent fermi gas with a delta -function interaction. *Journal of Physics: Condensed Matter*, 5(32):5869, 1993. 31

[93] P. Schlottmann. Ground-state and elemental excitations of the one-dimensional multicomponent fermi gas with delta -function interaction. *Journal of Physics: Condensed Matter*, 6(7):1359, 1994. 31

[94] J. R. Schrieffer. *Theory of Superconductivity, Section 2.5.* Westview Press, 1983. 75

[95] S. S. Shamailov and J. Brand. Dark-soliton-like excitations in the yang-gaudin gas of attractively interacting fermions. *New Journal of Physics*, 18(7):075004, 2016. 69, 70, 72, 93

[96] G. V. Skorniakov and K. A. Ter-Martirosian. *Sov. Phys. JETP*, 4:648, 1957. 4

[97] W. P. Su, J. R. Schrieffer, and A. J. Heeger. Soliton excitations in polyacetylene. *Phys. Rev. B*, 22:2099–2111, Aug 1980. 85, 98

[98] B. Sutherland. *Beautiful Models: 70 Years of Exactly Solved Quantum Many-Body Problems.* World Scientific, June 2004. 31, 41

[99] M. Takahashi. *Thermodynamics of One-Dimensional Solvable Models.* Cambridge University Press, UK, 1999. 62

[100] H. Takayama, Y. R. Lin-Liu, and K. Maki. Continuum model for solitons in polyacetylene. *Phys. Rev. B*, 21:2388–2393, Mar 1980. 85, 87, 98

[101] F. Tassone and Y. Yamamoto. Exciton-exciton scattering dynamics in a semiconductor microcavity and stimulated scattering into polaritons. *Phys. Rev. B*, 59:10830–10842, Apr 1999. 6

[102] N. Y. K. Tim Byrnes and Y. Yamamoto. Exciton-polariton condensates. *Nat. Phys.*, 10, Nov 2014. 5

[103] I. V. Tokatly. Dilute fermi gas in quasi-one-dimensional traps: From weakly interacting fermions via hard core bosons to a weakly interacting bose gas. *Phys. Rev. Lett.*, 93:090405, Aug 2004. 32

[104] T. Tsuzuki. Nonlinear waves in the pitaevskii-gross equation. *Journal of Low Temperature Physics*, 4(4):441–457, Apr 1971. 89

[105] L. Å. Šamaj and Z. Bajnok. *Introduction to the Statistical Physics of Integrable Many-body Systems*. Cambridge University Press, UK, May 2013. 31, 35, 36, 37, 53, 65, 114

[106] A. H. van Amerongen, J. J. P. van Es, P. Wicke, K. V. Kheruntsyan, and N. J. van Druten. Yang-yang thermodynamics on an atom chip. *Phys. Rev. Lett.*, 100:090402, Mar 2008. 30

[107] M. Wadati and K. Ohkuma. Bethe states for the quantum three wave interaction equation. *Journal of the Physical Society of Japan*, 53(4):1229–1237, 1984. 33

[108] A. Widera, S. Trotzky, P. Cheinet, S. Fölling, F. Gerbier, I. Bloch, V. Gritsev, M. D. Lukin, and E. Demler. Quantum spin dynamics of mode-squeezed luttinger liquids in two-component atomic gases. *Phys. Rev. Lett.*, 100:140401, Apr 2008. 30

[109] C. N. Yang. Some exact results for the many-body problem in one dimension with repulsive delta-function interaction. *Phys. Rev. Lett.*, 19:1312–1315, Dec 1967. 31, 32, 66

[110] C. N. Yang. s matrix for the one-dimensional n-body problem with repulsive or attractive δ-function interaction. *Phys. Rev.*, 168:1920–1923, Apr 1968. 31, 32

[111] V. E. Zakharov and A. B. Shabat. Exact Theory of Two-dimensional Self-focusing and One-dimensional Self-modulation of Waves in Nonlinear Media. *Soviet Journal of Experimental and Theoretical Physics*, 34:62, 1972. 89

[112] V. E. Zakharov and A. B. Shabat. Interaction between solitons in a stable medium. *Soviet Journal of Experimental and Theoretical Physics*, 37:823, Nov. 1973. 89

Appendix A

Calculation of the Matrix Elements of the Berry Connection

Here we calculate the matrix elements of the Berry connection for the case with zero angular momentum $m = 0$. Firstly we verify the orthogonality of the eigenstates $\chi_i(\boldsymbol{n})$ in Eq. (2.50) and calculate the normalization factor N_i in Eq. (2.62) via the overlap integral:

$$\langle \chi_i |\, \chi_j \rangle = \frac{1}{8\pi^2} \int_{-1}^{1} dx \int_{0}^{2\pi} d\phi_1 d\phi_2 \; \chi_i(\boldsymbol{n}) \chi_j(\boldsymbol{n}). \tag{A.1}$$

Substituting the expression in Eq. (2.50) into the above integral, we will get

$$\langle \chi_i |\, \chi_j \rangle = (\alpha_i \alpha_j + 2\beta_i \beta_j) I_1 + 2(\alpha_i \beta_j + \alpha_j \beta_i + \beta_i \beta_j) I_2, \tag{A.2}$$

where the two integral $I_{1,2}$ are

$$\begin{aligned} I_1 &\equiv \frac{1}{8\pi^2} \int_{-1}^{1} dx \int_{0}^{2\pi} d\phi_1 d\phi_2 \; G_{\nu_i}(\boldsymbol{n} \cdot \boldsymbol{n}_1) G_{\nu_j}(\boldsymbol{n} \cdot \boldsymbol{n}_1), \\ I_2 &\equiv \frac{1}{8\pi^2} \int_{-1}^{1} dx \int_{0}^{2\pi} d\phi_1 \phi_2 \; G_{\nu_i}(\boldsymbol{n} \cdot \boldsymbol{n}_1) G_{\nu_j}(\boldsymbol{n} \cdot \boldsymbol{n}_2). \end{aligned} \tag{A.3}$$

Substituting Eq. (2.48) into Eq. (A.3) and performing the integration, we will get

$$\begin{aligned} I_1 &= \frac{1}{4\pi} \frac{1}{(\nu_i - \nu_j)(\nu_i + \nu_j + 1)} \left[G_{\nu_i}(x) - G_{\nu_j}(x) \right]_{x \to 1}, \\ I_2 &= \frac{1}{4\pi} \frac{1}{(\nu_i - \nu_j)(\nu_i + \nu_j + 1)} \left[G_{\nu_i}(x) - G_{\nu_j}(x) \right]_{x = -\frac{1}{2}}. \end{aligned} \tag{A.4}$$

Substitute these back into the overlap integral in Eq. (A.1), and apply the constraint on coefficients (α_i, β_i) in Eq. (2.51), we finally arrived at

$$\langle \chi_i |\, \chi_j \rangle = \begin{cases} 0 & (i \neq j) \\ \frac{\left[(\alpha_i^2+2\beta_i^2)\partial_{\nu_i} G_{\nu_i}(1)+[2\beta_i^2+4\alpha_i\beta_i]\partial_{\nu_i} G_{\nu_i}\left(-\frac{1}{2}\right)\right]}{(4\pi)(2\nu_i+1)} & (i = j) \end{cases} . \tag{A.5}$$

Secondly we try to calculate the matrix element of the Berry connection in Eq. (2.37). The scale dependence only appears in the regularized Green's function $G_{\nu_i}(1)$, thus the relevant quantity that contributes to the derivative with respect to $\ln r$ is inside integral I_1:

$$I_1 = \frac{1}{4\pi} \frac{1}{(\nu_i - \nu_j)((\nu_i + \nu_j + 1)} \frac{1}{2\pi} \ln \frac{r_i}{r_j} + (\cdots), \tag{A.6}$$

where we have used the expression for $G_{\nu_i}(1)$ in Eq. (2.49), and the scale r is equipped with subscript to differentiate between $|\chi_i\rangle$ and $|\chi_j\rangle$. The derivative involved in Eq. (2.37) is then performed with respect to r_i and we finally get the expression for the matrix element D_{ij} as

$$D_{ij} = \frac{(\alpha_i \alpha_j + 2\beta_i \beta_j)}{8\pi^2 \sqrt{N_i N_j}(\nu_i - \nu_j)(\nu_i + \nu_j + 1)}, \tag{A.7}$$

with the normalization factor N_i given by $\langle \chi_i |\, \chi_i \rangle$.

Appendix B

First Order Correction to Adiabatics

In this section we present the detail of calculation of the first order correction to the effective potential u_0 in Eq. (2.63) and obtain the result in Eq. (2.69). Using the matrix Hamiltonian $\hat{H}(\nu)$ in Eq. (2.65) and normalization condition in Eq. (2.68), together with the expression for the first order correction in Eq. (2.61), we arrive at the following expression:

$$\begin{aligned} |D_{0j}|^2 &= \frac{(2\nu_0+1)(2\nu_j+1)}{[\nu_0(\nu_0+1)-\nu_j(\nu_j+1)]^2} \frac{\mathrm{Tr}[\vec{\alpha}_0 \cdot \vec{\alpha}_0^T \cdot \vec{\alpha}_j \cdot \vec{\alpha}_j^T]}{\partial_{\nu_0} \det \hat{H}\ \partial_{\nu_j} \det \hat{H}} \\ &= \frac{(2\nu_0+1)(2\nu_j+1)}{[\nu_0(\nu_0+1)-\nu_j(\nu_j+1)]^2} \frac{\mathrm{Tr}[\det \hat{H}_0 \cdot \hat{H}_0^{-1} \det \hat{H}_j \cdot \hat{H}_j^{-1}]}{\partial_{\nu_0} \det \hat{H}\ \partial_{\nu_j} \det \hat{H}}. \end{aligned} \tag{B.1}$$

The last line can be further simplified to the following form using the residuals of $\hat{K} = \hat{H}^{-1}$:

$$|D_{0j}|^2 = \frac{(2\nu_0+1)(2\nu_j+1)}{[\nu_0(\nu_0+1)-\nu_j(\nu_j+1)]^2} \mathrm{Tr}[\mathrm{Res}\ \hat{K}(\nu_0) \cdot \mathrm{Res}\ \hat{K}(\nu_j)]. \tag{B.2}$$

The total correction Δu_0 in Eq. (2.63) can then be converted into a contour integration on the complex plane of variable ν, where the integration contour is along the real axis. On that complex plane, each ν_j is a first-order pole along the positive real axis, and each have its counterpart on the negative real axis. There are four extra poles off real axis, corresponding to true bound state (ν_0) and spurious

bound state (ν_s) respectively (see Fig. 2.7). Finally the expression for Δu_0 are as follows:

$$\begin{aligned}\sum_{j\neq 0}|D_{0j}|^2 =&\sum_{j\neq 0}\frac{(2\nu_0+1)(2\nu_j+1)}{[\nu_0(\nu_0+1)-\nu_j(\nu_j+1)]^2}\mathrm{Tr}[\mathrm{Res}\ \hat{K}(\nu_0)\cdot\mathrm{Res}\ \hat{K}(\nu_j)]\\ =&\sum_{j\neq 0}\frac{\partial}{\partial\nu_0}\Big[-\frac{1}{\nu_0-\nu_j}+\frac{1}{\nu_0+\nu_j+1}\Big]\mathrm{Tr}[\mathrm{Res}\ \hat{K}(\nu_0)\cdot\mathrm{Res}\ \hat{K}(\nu_j)]\\ =&\frac{1}{2}\left\{\frac{1}{2\pi i}\oint_{\mathcal{C}}d\nu\frac{\mathrm{Tr}[\mathrm{Res}\ \hat{K}(\nu_0)\cdot\hat{K}(\nu)]}{(\nu_0-\nu)^2}-\frac{1}{2\pi i}\oint_{\mathcal{C}}d\nu\frac{\mathrm{Tr}[\mathrm{Res}\ \hat{K}(\nu_0)\cdot\hat{K}(\nu)]}{(\nu_0+\nu+1)^2}\right\}\\ =&\frac{1}{2}\left\{\frac{1}{2\pi i}\oint_{\mathcal{C}}d\nu\frac{\mathrm{Tr}[\mathrm{Res}\ \hat{K}(\nu_0)\cdot\hat{K}(\nu)]}{(\nu_0-\nu)^2}+\frac{1}{2\pi i}\oint_{\mathcal{C}}d\nu\frac{\mathrm{Tr}[\mathrm{Res}\ \hat{K}(\nu_0^*)\cdot\hat{K}(\nu)]}{(\nu_0^*-\nu)^2}\right\},\end{aligned}\tag{B.3}$$

where we have used the fact that Res $\hat{K}(\nu_0)=-$Res $\hat{K}(\nu_0^*)$ and the factor $1/2$ appears because we are only summing over positive real poles. This is nothing but Eq. (2.69) in the main text.

To evaluate the resulting contour integrals in Eq. (2.69), we only care about the behavior of the integrand around the poles far off the real axis. The large ν behavior is

$$\begin{aligned}&\hat{H}(\nu)\Big|_{|\nu|\gg 1}=\begin{pmatrix}A(\nu)&0\\0&B(\nu)\end{pmatrix},\quad \hat{K}(\nu)=(\nu)=\begin{pmatrix}\frac{1}{A(\nu)}&0\\0&\frac{1}{B(\nu)}\end{pmatrix},\\ &A(\nu)=\ln\frac{r}{\alpha_<}-\frac{1}{2}[\psi(-\nu)+\psi(\nu+1)],\quad B(\nu)=\ln\frac{r}{\alpha_>}-\frac{1}{2}[\psi(-\nu)+\psi(\nu+1)].\end{aligned}\tag{B.4}$$

The poles off the real axis are given by zeros of the diagonal functions $A(\nu)$ and $B(\nu)$. Near the poles, taking ν_0 as an example, we have $A(\nu_0)\neq 0$ and

$$\begin{aligned}&B(\nu)=B'(\nu-\nu_0)+\frac{1}{2}B''(\nu-\nu_0)^2+\frac{1}{6}B'''(\nu-\nu_0)^3+\cdots,\\ &\frac{1}{B(\nu)}=\frac{1}{B'(\nu-\nu_0)}-\frac{1}{2}\frac{B''}{B'^2}-\Big[\frac{B'''}{6B'^2}-\frac{B''^2}{4B'^3}\Big](\nu-\nu_0)+\cdots,\end{aligned}\tag{B.5}$$

where the coefficients B',B'',B''' are

$$B'=\frac{2i}{(|u_0|-1)^{1/2}},\quad B''=-\frac{4}{|u_0|-1},\quad B'''=-\frac{16i}{(|u_0|-1)^{3/2}}.\tag{B.6}$$

The the residual and the regular part of $\hat{K}(\nu)$ near $\nu=\nu_0$ is

$$\mathrm{Res}\ \hat{K}(\nu_0)=\begin{pmatrix}0&0\\0&\frac{1}{B'}\end{pmatrix},\quad \hat{K}^{\mathrm{reg},\nu_0}(\nu)=\begin{pmatrix}\frac{1}{A(\nu)}&0\\0&-\frac{1}{2}\frac{B''}{B'^2}-\Big[\frac{B'''}{6B'^2}-\frac{B''^2}{4B'^3}\Big](\nu-\nu_0)+\cdots\end{pmatrix}.\tag{B.7}$$

Substituting the above expression into the contour integral in Eq. (2.69), we obtain

$$\begin{aligned}
&\frac{1}{2\pi i}\oint_C d\nu \frac{\mathrm{Tr}[\mathrm{Res}\ \hat{K}(\nu_0)\cdot\hat{K}(\nu)]}{(\nu_0-\nu)^2}+\frac{1}{2\pi i}\oint_C d\nu \frac{\mathrm{Tr}[\mathrm{Res}\ \hat{K}(\nu_0^*)\cdot\hat{K}(\nu)]}{(\nu_0^*-\nu)^2}\\
=&-\frac{\partial}{\partial\nu}\mathrm{Tr}[\mathrm{Res}\ \hat{K}(\nu_0)\cdot\hat{K}^{\mathrm{reg},\nu_0}(\nu)]\Big|_{\nu=\nu_0}-\frac{\mathrm{Tr}[\mathrm{Res}\ \hat{K}(\nu_0)\cdot\mathrm{Res}\ \hat{K}(\nu_0^*)]}{(\nu_0-\nu_0^*)^2}\\
&-\frac{\mathrm{Tr}[\mathrm{Res}\ \hat{K}(\nu_0^*)\cdot\mathrm{Res}\ \hat{K}(\nu_0)]}{(\nu_0^*-\nu_0)^2}-\frac{\partial}{\partial\nu}\mathrm{Tr}[\mathrm{Res}\ \hat{K}(\nu_0^*)\cdot\hat{K}^{\mathrm{reg},\nu_0^*}(\nu)]\Big|_{\nu=\nu_0^*},
\end{aligned}\tag{B.8}$$

where the contribution from the unphysical poles $\nu=\nu_s,\nu_s^*$ is zero because they reside at different corner along the diagonal, which makes the trace of the matrix product zero. Finally, the first order correction to the adiabatic approximation is evaluated to be

$$\sum_j |D_{0j}|^2=\left[\frac{B'''}{6B'^3}-\frac{B''^2}{4B'^4}+\frac{1}{B'^2(\nu_0-\nu_0^*)^2}\right]=\frac{1}{3},\tag{B.9}$$

which combined with Eq. (2.59) gives us the marginal result $\gamma=1$.

Similarly we can calculate the same first order correction to adiabatics for the case of non-zero angular momentum m. By direct calculation similar to the case of zero angular momentum we obtain the following result for the Berry connection D_{ij}:

$$\begin{aligned}
D_{ij}&=\frac{1}{8\pi^2\sqrt{N_iN_j}}\int_{-1}^{1}dx\int_0^{2\pi}d\phi_1d\phi_2\ \frac{d\chi_i^{(m)}(\boldsymbol{n})}{d\ln r}\chi_j^{(m)}(\boldsymbol{n})\\
&=\frac{1}{8\pi^2\sqrt{N_iN_j}}(\alpha_i\alpha_j+2\beta_i\beta_j)\frac{1}{2^m}\frac{1}{(\nu_i-\nu_j)(\nu_i+\nu_j+m+1)},
\end{aligned}\tag{B.10}$$

where the normalization factor N_i of the angular eigenfunctions is calculated to be

$$N_i=\frac{\left[(\alpha_i^2+2\beta_i^2)\partial_{\nu_i}G_{\nu_i}^{(m)}(1)+[2(-)^m\beta_i^2+4\alpha_i\beta_i]\partial_{\nu_i}G_{\nu_i}^{(m)}(-\frac{1}{2})\right]}{2^m(4\pi)(2\nu_i+m+1)},\tag{B.11}$$

and the single-argument Green's function is defined as

$$G_\nu^{(m)}(x)=\left(\frac{1+x}{2}\right)^{m/2}f(\nu,m)R_\nu^{(m)}\left(\frac{1+x}{2}\right),\tag{B.12}$$

where the functions $f(\nu,m)$ and $R_\nu^{(m)}(x)$ are defined in Eq. (2.82) and Eq. (2.72). For the correction to the effective potential of the lowest level, we still have

$$\Delta u_0^{(m)}(r\to\infty)=\sum_{j\neq0}|D_{0j}|^2.\tag{B.13}$$

This can be calculated exactly the same way as the case $m = 0$. The only change is the expression for the matrix Hamiltonian $\hat{H}(\nu)$:

$$\hat{H}(\nu) = 2\pi \begin{pmatrix} \frac{1}{\lambda_1} + G_\nu^{(m)}(1); & \sqrt{2}G_\nu^{(m)}\left(-\frac{1}{2}\right) \\ \sqrt{2}G_\nu^{(m)}\left(-\frac{1}{2}\right); & G_\nu^{(m)}(1) + (-)^m G_\nu^{(m)}\left(-\frac{1}{2}\right) - \frac{1}{\lambda_2} \end{pmatrix}. \tag{B.14}$$

The rest of the calculation is essentially the same as the case $m = 0$, and the contour integration trick eventually gives us the following result:

$$\begin{aligned} &\Delta u_0^{(m)}(r \to \infty) = 1/3, \\ &u_0^{(m)}(r \to \infty) = -r^2\epsilon_b^{(2)} + (m^2 - 1) + O(r^{-2}). \end{aligned} \tag{B.15}$$

This shows that the marginal value $\gamma = 1$ is only realized when $m = 0$; for non-zero angular momentum, no bound state is guaranteed for the system.

Appendix C

Algebraic Bethe Ansatz for Two-Component Systems

This appendix closely follows the derivation presented in [105]. For a time inversion and space inversion invariant and species-conserving model in free space, the two-body S-matrix in pseudospin subspace $\{\uparrow,\downarrow\}$ assumes the general form in Eq. (3.11), which is repeated here:

$$S(k) = \begin{pmatrix} a(k) & 0 & 0 & 0 \\ 0 & b(k) & c(k) & 0 \\ 0 & c(k) & b(k) & 0 \\ 0 & 0 & 0 & a(k) \end{pmatrix}, \tag{C.1}$$

where the relative momentum $k = k_2 - k_1$ is the difference in momentum between the two scattering particles. The wave functions of the eigenstates then assumes the general form of the nested coordinate Bethe ansatz in Eq. (3.123), which is also repeated here:

$$\begin{aligned} \Psi_X(\sigma_1, x_1; \cdots; \sigma_N, x_N) &= \sum_{P\in S_N} [X,P] \exp\left(i \sum_{j=1}^{N} k_{P_j} x_{X_j} \right), \\ [X,P] &= \mathrm{sgn}(X)\mathrm{sgn}(P) A_{\sigma_{X_1}\sigma_{X_2}\cdots\sigma_{X_N}}(k_{P_1}, k_{P_2}, \cdots, k_{P_N}), \end{aligned} \tag{C.2}$$

where X denotes the ordering sector with $x_{X_1} < x_{X_2} < \cdots < x_{X_N}$ and P denotes the permutation among the wave numbers. The sign function equals 1 for even permutations and -1 for odd permutations. We impose the periodic boundary condition for the wave functions, so the wave functions are

invariant under the following shift of coordinates:

$$\tilde{x}_{X_1} = x_{X_1} + L, \quad \tilde{x}_{X_2} = x_{X_2}, \quad \ldots, \quad \tilde{x}_{X_N} = x_{X_N}. \tag{C.3}$$

This shift brings the ordering sector $X : x_{X_1} < x_{X_2} < \cdots < x_{X_N}$ to $\tilde{X} : \tilde{x}_{X_2} < \tilde{x}_{X_3} < \cdots < \tilde{x}_{X_N} < \tilde{X}_{X_1}$, and the invariance of the wave functions is equivalent to the relation

$$A_{\sigma_{X_2}\cdots\sigma_{X_N}\sigma_{X_1}}\left(k_{P_2}, \cdots, k_{P_N}, k_{P_1}\right) = (\mp 1)^{N-1} \exp\left(-\mathrm{i}k_{P1}L\right) A_{\sigma_{X_1}\cdots\sigma_{X_N}}\left(k_{P_1}, \cdots, k_{P_N}\right), \tag{C.4}$$

where the upper minus sign is for bosons, and the lower plus sign is for fermions. The A-coefficients can be related to each other via the two-body S-matrix:

$$A_{\cdots\sigma_j\sigma_i\cdots}\left(\cdots, k_v, k_u, \cdots\right) = \sum_{\sigma_i'\sigma_j'} S^{\sigma_i\sigma_j}_{\sigma_i'\sigma_j'}\left(k_u, k_v\right) A_{\cdots\sigma_i'\sigma_j'\cdots}\left(\cdots, k_u, k_v, \cdots\right). \tag{C.5}$$

Using Eq. (C.5), we can transform the condition in Eq. (C.4) into an eigenvalue problem:

$$T_j A = (\mp 1)^{N-1} \exp\left(-\mathrm{i}k_j L\right) A, \tag{C.6}$$

where the transfer matrix T_j is defined as

$$\begin{aligned} &T_j = T\left(k = k_j; k_1, \cdots, k_N\right), \\ &T\left(k; k_1, \cdots, k_N\right)^{\sigma_1\cdots\sigma_N}_{\sigma_1'\cdots\sigma_N'} = \sum_{\gamma_1,\ldots,\gamma_N} S^{\sigma_N\gamma_1}_{\sigma_N'\gamma_2}\left(k - k_N\right) S^{\sigma_{N-1}\gamma_2}_{\sigma_{N-1}'\gamma_3}\left(k - k_{N-1}\right) \cdots S^{\sigma_2\gamma_{N-1}}_{\sigma_2'\gamma_N}\left(k - k_2\right) S^{\sigma_1\gamma_N}_{\sigma_1'\gamma_1}\left(k - k_1\right). \end{aligned} \tag{C.7}$$

The transfer matrix $T(k; k_1, \cdots, k_N)$ is usually referred to as the inhomogeneous transfer matrix, and it can be obtained as the trace of the monodromy matrix $\mathscr{T}$ in the auxiliary ξ-space:

$$T\left(k; k_1, \cdots, k_N\right) = \mathrm{Tr}_\xi\, \mathscr{T}_\xi\left(k; k_1, \cdots, k_N\right), \tag{C.8}$$

where the monodromy matrix $\mathscr{T}$ is the product of Lax matrices $L_{\xi n}$:

$$\begin{aligned} &\mathscr{T}_\xi\left(k; k_1, \cdots, k_N\right) = L_{\xi N}\left(k - k_N\right) L_{\xi(N-1)}\left(k - k_{N-1}\right) \cdots L_{\xi 1}\left(k - k_1\right), \\ &L_{\xi n}(k)^{\gamma_\xi\sigma_1\ldots\sigma_N}_{\gamma_\xi'\sigma_1'\ldots\sigma_N'} = S^{\gamma_\xi\sigma_n}_{\gamma_\xi'\sigma_n'}(k)\delta_{\sigma_1\sigma_1'}\cdots\delta_{\sigma_{n-1}\sigma_{n-1}'}\delta_{\sigma_{n+1}\sigma_{n+1}'}\cdots\delta_{\sigma_N\sigma_N'}. \end{aligned} \tag{C.9}$$

Using the above definitions, we can express the monodromy matrix in the auxiliary ξ-space:

$$\mathscr{T}\left(k;k_1,\cdots,k_N\right)=\begin{pmatrix} A\left(k;k_1,\cdots,k_N\right) & B\left(k;k_1,\cdots,k_N\right) \\ C\left(k;k_1,\cdots,k_N\right) & D\left(k;k_1,\ldots,k_N\right) \end{pmatrix}. \tag{C.10}$$

The matrices A, B, C and D fulfills the following commutation relations as a result of the Yang-Baxter equation:

$$\begin{aligned} &[A(k),A(k')]=[B(k),B(k')]=[C(k),C(k')]=[D(k),D(k')]=0, \\ &A(k)B(k')=\frac{a(k'-k)}{b(k'-k)}B(k')A(k)-\frac{c(k'-k)}{b(k'-k)}B(k)A(k'), \\ &D(k)B(k')=\frac{a(k-k')}{b(k-k')}B(k')D(k)-\frac{c(k-k')}{b(k-k')}B(k)D(k'), \end{aligned} \tag{C.11}$$

where a, b and c are the matrix elements of the two-body S-matrix. The inhomogeneous transfer matrix can be expressed as the trace of $\mathscr{T}$ in the auxiliary ξ-space:

$$T\left(k;k_1,\cdots,k_N\right)=A\left(k;k_1,\cdots,k_N\right)+D\left(k;k_1,\cdots,k_N\right). \tag{C.12}$$

Next, we want to diagonalize the inhomogeneous matrix T. We first construct a generating vector of the 2^N-dimensional Hilbert space as the tensor product of spin-up vectors on the chain of N sites:

$$\Omega=\underbrace{e^+}_{1}\otimes\underbrace{e^+}_{2}\otimes\cdots\otimes\underbrace{e^+}_{N-1}\otimes\underbrace{e^+}_{N},\quad e^+=\begin{pmatrix}1\\0\end{pmatrix}. \tag{C.13}$$

The actions of the matrix elements of the monodromy matrix on this generating vector give us the following results:

$$A\Omega=\prod_{n=1}^{N}a\left(\lambda-\lambda_n\right)\Omega,\quad C\Omega=0,\quad D\Omega=\prod_{n=1}^{N}b\left(\lambda-\lambda_n\right)\Omega. \tag{C.14}$$

The eigenvectors of the inhomogeneous transfer matrix with M spins down are assumed to be in the following form:

$$\psi\left(k_1,\cdots,k_N;\Lambda_1,\cdots,\Lambda_M\right)=\prod_{\alpha=1}^{M}B\left(\Lambda_\alpha;k_1,\cdots,k_N\right)\Omega, \tag{C.15}$$

where the parameters $\Lambda_1,\cdots,\Lambda_M$ are yet to be determined. Using the commutation relations in Eq. (C.11) and the results in Eq. (C.14), we can obtain the conditions for the ansatz in Eq. (C.15) to

be eigenvectors of the inhomogeneous transfer matrix $T = A + D$:

$$\prod_{n=1}^{N} \frac{a(\Lambda_\alpha - k_n)}{b(\Lambda_\alpha - k_n)} = \prod_{\substack{\beta=1 \\ \beta\neq\alpha}}^{M} \frac{a(\Lambda_\alpha - \Lambda_\beta) b(\Lambda_\beta - \Lambda_\alpha)}{a(\Lambda_\beta - \Lambda_\alpha) b(\Lambda_\alpha - \Lambda_\beta)}, \quad \alpha = 1, 2 \cdots, M. \tag{C.16}$$

In the meantime, the periodic boundary conditions as specified in Eq. (C.6) take the following form:

$$(\mp)^{N-1} \exp(-ik_j L) = \prod_{n=1}^{N} a(k_j - k_n) \prod_{\alpha=1}^{M} \frac{a(\Lambda_\alpha - k_j)}{b(\Lambda_\alpha - k_j)}, \quad j = 1, 2, \cdots, N. \tag{C.17}$$

The $M + N$ coupled equations in Eq. (C.16) and Eq. (C.17) are those specified in Eq. (3.15) of the main text, which are referred to as the Bethe ansatz equations.